BREAKDOWN MEASUREMENTS IN ARGON AND XENON APPLICABLE TO METAL HALIDE HIGH INTENSITY DISCHARGE LAMPS

BY

RICHARD SHANE MOSS

B.S., University of Illinois at Urbana-Champaign, 2000

THESIS

Submitted in partial fulfillment of the requirements
for the degree of Master of Science in Mechanical Engineering
in the Graduate College of the
University of Illinois at Urbana-Champaign, 2002

Urbana, Illinois

Signature Page

BREAKDOWN MEASUREMENTS IN ARGON AND XENON APPLICABLE TO METAL HALIDE HIGH INTENSITY DISCHARGE LAMPS

Richard Shane Moss, M.S.
Department of Mechanical and Industrial Engineering
University of Illinois at Urbana-Champaign, 2002
Mark J. Kushner, Adviser

Metal halide high intensity discharge (HID) lamps typically operate as multi-atmosphere thermal arcs in the steady state, but during the starting phase the lamps are moderate pressure glow discharges. This starting phase is of considerable interest because of the large required voltages inducing sputtering and other detrimental effects. The goal of this thesis was to investigate basic processes using rare gas mixtures so that optimum starting strategies can be developed for metal halide HID lamps. Breakdown measurements on a test lamp were conducted at various pulse repetition frequencies (0.005-1000 Hz), voltage pulses (up to 2000 V), pressures (0.5 – 110 Torr), and argon/xenon compositions, and with various ground planes. Photographs of discharges in argon, xenon, and a 10% xenon in argon mixture were also taken at various pressures to provide additional insight.

It was found that the mean breakdown time reflects the rate at which electrons are being created, and is dependent upon E/N (electric field)/(gas number density) and capacitive effects. Lower breakdown times are achieved by lowering pressure, increasing voltage and pulse repetition frequencies, and by closer placement of ground planes. Small percentages (5-10%) of xenon in argon also lower breakdown times. Lower breakdown times enable lowering the necessary applied voltage and in being able to break down at higher pressures leading to reduced sputtering and shorter warm restart periods.

ACKNOWLEDGMENTS

First and foremost, I would like to thank my adviser, Professor Mark J. Kushner. He has given me so many opportunities for growth and learning. I would not have accomplished many of the things I have without his help and this I truly appreciate. I also appreciate the time, patience, and wisdom he has given to me.

I would like to acknowledge the support provided for this project by the General Electric (GE) Research and Development Center, the Electric Power Research Institute (EPRI), and the National Science Foundation (NSF).

I would also like to thank people in the Computational Optical and Discharge Physics Group: Kapil Rajaraman, Ananth Bhoj, Alex Vasenkov, Pramod Subramonium, Rajesh Dorai, Vivek Vyas, and Arvind Sankaran, all of whom have given me lots and lots of help, advice, and friendship. I would also like to thank Kelly Collier for her smiles and assistance too. I would like to thank some people from "across the street" too, from the "Gas house," where these experiments took place; mostly Clark Wagner, Scott McCain, Nels Ostrom, Cy Herring, and Gary Eden. All of them provided me invaluable assistance that was greatly needed.

I would like to thank Professor David Ruzic for his helpful conversations about glow discharges. I would also like to thank Moshe Shapiro for peaking my curiosity about plasmas while I was an undergraduate and started me down this path. I would also like to give special thanks to a close friend Martin Nieto for help and advice, both professionally and otherwise.

Most importantly, I would like to thank my parents, Gary and Debbi Moss, for their support and love throughout this endeavor. I would also like to thank my sister,

Kristi, for her support and friendship too. My brother-in-law, Andy Theis, has been an amazing friend too, from whom I have got a lot of support. Last, I would like to thank my nephews and niece, Devyn, Megyn, and Prestyn, for all their love and for keeping me in place by beating me in several games.

TABLE OF CONTENTS

Page

1. INTRODUCTION……. 1

   1.1 Introduction……. 1
   1.2 Applications and Specifications…….. 2
   1.3 Starting Metal Halide Lamps …..…….. 3
   1.4 Research Involving Metal Halide Lamps……... 5
   1.5 Figures…… 7
   1.6 References……... 9

2. EXPERIMENTAL SETUP…… 11

   2.1 Overview……. 11
   2.2 Pulsing Circuit…… 11
   2.3 Lamp Geometry…….. 13
   2.4 Vacuum and Gas Handling System…… 15
   2.5 Experimental Procedures…… 17
   2.6 Recommendations……... 19
   2.7 Figures…… 20
   2.8 References……... 37

3. BREAKDOWN IN PURE ARGON…….. 38

   3.1 Theory of Breakdown……. 38
   3.2 Pulse Repetition Frequency (PRF) Effects……. 40
   3.3 Ground Plane Effects……. 41
   3.4 Figures……..... 43
   3.5 References……... 47

4. BREAKDOWN IN ARGON/XENON MIXTURES……. 48

   4.1 Overview……. 48
   4.2 Xenon Compositional Effects……. 49
   4.3 Figures…….…... 52
   4.4 References…….…… 72

5. ARGON/XENON DISCHARGE PHOTOGRAPHS……. 73

   5.1 Overview…….. 73
   5.2 Visual Characteristics of Discharge in Argon and Xenon……..…. 73
   5.3 Figures……. 78
   5.4 References……108

6. CONCLUSIONS……..……... 109

APPENDIX A: ARGON CROSS SECTIONS…..……..110

A.1 References……...111

APPENDIX B: XENON CROSS SECTIONS…….…….. 112

B.1 References……. 113

APPENDIX C: KINETICS OF ARGON/XENON MIXTURES……...114

C.1 Argon Reaction Mechanisms……. …… 114
C.2 Xenon Reaction Mechanisms…….……116
C.3 Additional Reactions for Argon/Xenon Mixtures…….……..… 119
C.4 Figures…….……121
C.5 References……... 125

1. INTRODUCTION

1.1 Introduction

Electric incandescent lighting was invented in 1879 simultaneously by Thomas Edison in the United States and Sir Joseph Wilson Swan in England. Electric discharge lamps are now the most efficient lighting sources produced in large part due to a deeper understanding of plasma physics. Metal halide plasma lighting sources are the lamps of interest here. Surprisingly, the principles of metal halide lamps were established as early as 1900 by Charles Steinmetz when he applied for a patent which was awarded in 1911.[1] It was not until the 1960s, however, that metal iodide lamps were offered by most major lamp companies.[2] Today there are primarily four major producers of metal halide high intensity discharge (HID) lamps: General Electric, Philips, Osram/Sylvania, and Venture.

Lighting plasmas are extensively used. "In terms of total quantities of plasma being continuously generated, lighting plasmas are far and away the predominant practical application of plasma science."[3] Lighting dissipates about 40% of the energy used in the United States. To regulate this energy use, the Energy Policy Act (EPACT) of 1992[4] established minimum efficiency standards for incandescent lamps and fluorescent lamps and banned the production of certain types of lamps. The Energy Policy Act of 2002[5] created the Next Generation Lighting Initiative establishing a government-industry partnership to develop ultra-efficient lighting, mostly for semiconductor-based lighting. The Department of Energy also has the goal to reduce lighting energy consumption by 50% by the year 2010. EPACT has also forced

compliance with ASHRAE (American Society of Heating, Refrigerating, and Air-Conditioning Engineers), particularly ASHRAE/IES (Illuminating Engineering Society) Standard 90.1 that mandates a 20% reduction in energy usage in a given building's envelope.[6] Similar statewide regulations have been enacted in California, Wisconsin, and Minnesota.

1.2 Applications and Specifications

Metal halide lamps are popular choices for many indoor and outdoor applications. They are used in streetlights, sporting complexes, factories, gymnasiums, billboards, storefronts, TV and film, stage, concerts, photographic and large screen presentations, projectors, and automotive headlights. Metal halide HID lamps are favored for these applications because of their relatively high efficiency, large color rendering indices (CRI), and long lifetimes. A typical metal halide HID lamp is shown in Figure 1.1.

Efficiencies are compared as the light output divided by the electrical power supplied to the lamp, or lumens/W. Incandescent bulbs are typically 10-20 lumens/W and a mercury lamp yields 55-60 lumens/W. Metal halide lamps can reach over 125 lumens/W.

The colors of lamps are primarily compared by the CRI and the correlated color temperature (CCT). The CRI is rated on a scale from 1 to 100, with 100 being natural daylight. Northern sky daylight has a CCT of 6774 K. Having a high CRI is not always important and depends on the application and the desired lighting effects. Mercury vapor lamps typically have CRIs in the range of 15 to 55. Sylvania's Tru-Color Metalarc

Ceramic has one of the highest color renditions currently available for HID applications with a CRI of 94.[7]

Metal halide HID lamps also have considerably longer lifetimes than other commercial bulbs. Under continuous operation, these lamps can operate for 15 000 to 20 000 hours. Repeated starting of the lamp can reduce this lifetime due to the damage incurred during startup. In comparison, incandescent bulbs only last for 1000 to 2000 hours.

1.3 Starting Metal Halide Lamps

Metal halide lamps typically operate as multiatmosphere thermal arcs in the steady state; however, during their starting phase the lamps are moderate pressure glow discharges.[8-15] Commercial metal halide lamps are usually filled with a rare gas such as argon at 10's to a few hundred Torr and with a metal halide and/or mercury dose. The electrode spacings are generally 1 to 5 cm depending on the lamp wattage and application. The lamp is usually constructed from fused silica (quartz) in larger lamps or polycrystalline alumina in smaller, higher temperature lamps, such as the one shown in Figure 1.2. At startup, the metal dose at best provides a few to 10's mTorr of vapor at room temperature. However, during warm restarts of a lamp, the metal halide vapor pressure may be 100's of Torr to many atmospheres. It is this high metal (or metal halide) vapor pressure which makes it difficult to restart warm lamps as the voltage available from the lamp ballast is typically insufficient to produce breakdown while the cathode temperature is too low for thermal emission.[16,17]

The starting processes of metal halide lamps have been studied with the intent of improving reliability and restart capability.[9-13] The ignition process is typically separated into five stages: two breakdown phases, cold cathode, glow-to-arc transition, and thermionic arc. The breakdown consists of two phases, the statistical and formative time lag which will be discussed in Chapter 3. The initial seed electrons are typically generated by cosmic rays, photoionization from artificial sources such as ultraviolet (UV) flashlamps, or electric emission from microscopic roughness on the tips of the cathode. Following breakdown, the lamp either enters a cold cathode or a glow discharge phase depending on whether mercury has condensed on the electrodes. If it has, then the lamp first enters a cold cathode phase. During this phase, ions accelerated by the large electric fields near the electrodes vaporize the mercury, which is then rapidly ionized by electrons. This "prompt" ionization decreases the impedance of the lamp, possibly only temporarily because the source of mercury is quickly depleted. A conventional glow discharge, at this time, is thus established.[13]

After the mercury from the electrodes is depleted, a further increase in current requires an increase in the impedance of the lamp. This is to facilitate a larger E/N (electric field) / (gas number density) to sustain an avalanche in the higher ionization potential buffer gas. The primary source of electrons during this period is secondary emission from the electrodes by ion bombardment. The relatively high operating voltage produces energetic ions, which both sputter and heat the cathode. This heating eventually raises the cathode temperature sufficiently high for thermionic emission to occur, which is the beginning of the glow-to-arc transition.[14,15] The thermionic source dominates all other source terms during this phase of lamp ignition, and an arc develops the conductive

path between the electrodes causing the lamp impedance to fall again. The arc usually takes between a half minute and four minutes to fully develop. The impedance curve for the lamp from breakdown to thermionic emission is shown in Figure 1.3.

1.4 Research Involving Metal Halide Lamps

The evolution of modern lamps has been motivated primarily by the need for more efficient and brighter lighting, better color, longer lifetimes, environmental issues, time, and government regulations. Time is an issue primarily due to the long periods necessary for restarting warm metal halide lamps, which can be on the order of a few to 20 minutes, until the lamp cools enough for the metals to condense.

Research has been devoted to improving the "environmental friendliness." Small amounts of radioactive isotopes, such as ^{85}Kr, are used to provide background ionization to aid in the initiation of breakdown for many commercial lamps. There is obviously a good deal of motivation for eliminating the radioactive isotopes. Finding other methods for providing the initial electrons has been intensive. Researchers have also been interested in finding alternatives to mercury. For example, Born has investigated one such possibility by replacement with metallic zinc.[21]

However, more research in the HID field has been involved with improving the reliability and reducing the breakdown voltage for starting metal halide lamps. Large starting voltages result in higher rates of sputtering of the cathode, which reduces the lifetime of the lamp and results in darkening of the arc tube.[11,16] This darkening of the arc tube further reduces the amount of the light output and reduces the efficiency and usefulness of the lamp. Therefore, lowering the starting voltages would increase the

lifetime and visibility, and also translate into simpler power supply ballasts. Current electronic ballasts need control methods due to the complex starting mechanisms.[17,20,22,23] Optimizing the starting waveform will minimize sputtering.

Other strategies to reduce the required starting voltage include providing auxiliary sources of ionization. To this end some metal halide lamps include a trigger electrode adjacent to the cathode. By applying a smaller voltage between the main electrode and the trigger electrode to create a local plasma, preionization is achieved with minimal sputtering. This in turn permits smaller voltages to be applied between the two main electrodes and still ensure breakdown. For a given available voltage from a power supply or lamp ballast, lowering the E/N required for breakdown increases the largest gas density for which breakdown can be achieved, thereby improving the restart capabilities of warm lamps.

Several approaches for restarting warm, high-pressure arc-tubes have been investigated.[12] Some electronic ballasts have the ability to detect the hot reignition phase and thus apply a larger voltage to the lamp, ensuring breakdown. This may not be possible depending on the gas pressure. Lamps that require in excess of 20 to 30 kV for reignition pose the risk of external arcing and need special sockets that can withstand these higher voltages. Another approach is to turn the lamp off slowly and maintain a small current through the lamp. Thus, the impedance of the lamp can be maintained in a low state, and a full discharge can then be restored quickly by simply increasing the ballast to full power.[18,19]

In this thesis, experiments will be described and their results discussed for breakdown in an idealized metal halide lamp. The goal is to investigate basic processes using rare gas mixtures so that more optimum starting strategies can be developed.

1.5 Figures

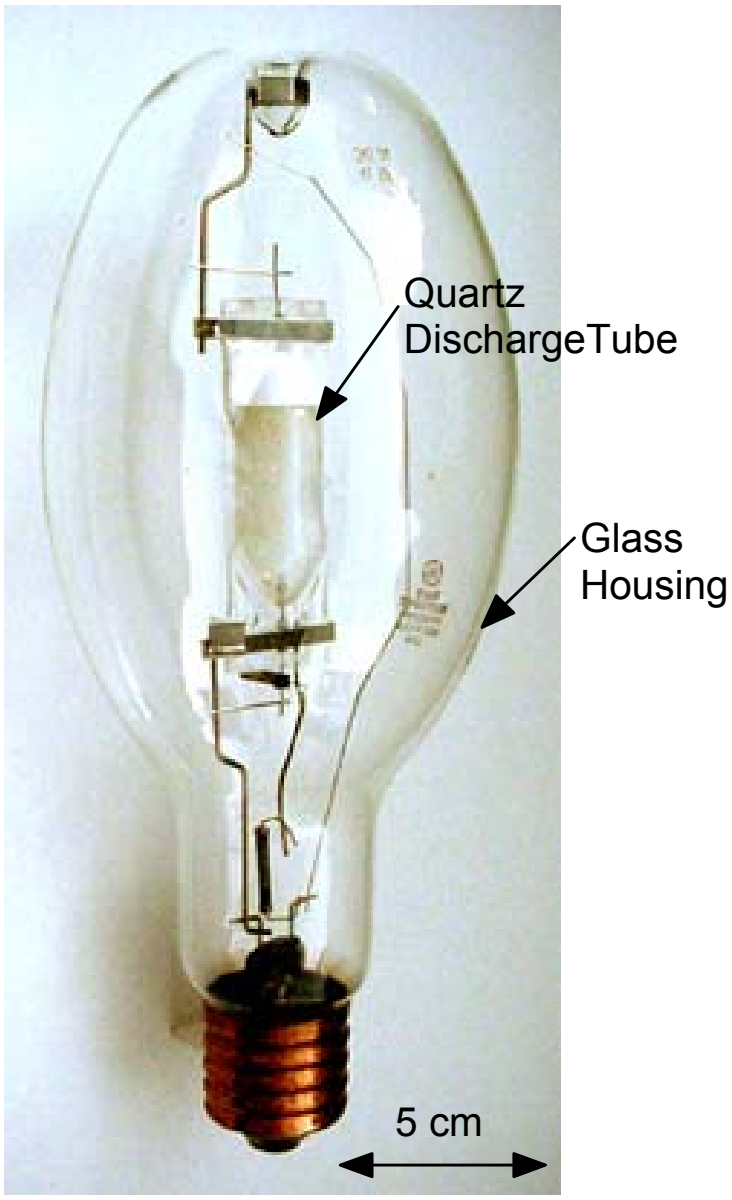

Figure 1.1 A typical metal halide HID lamp, the GE R400.

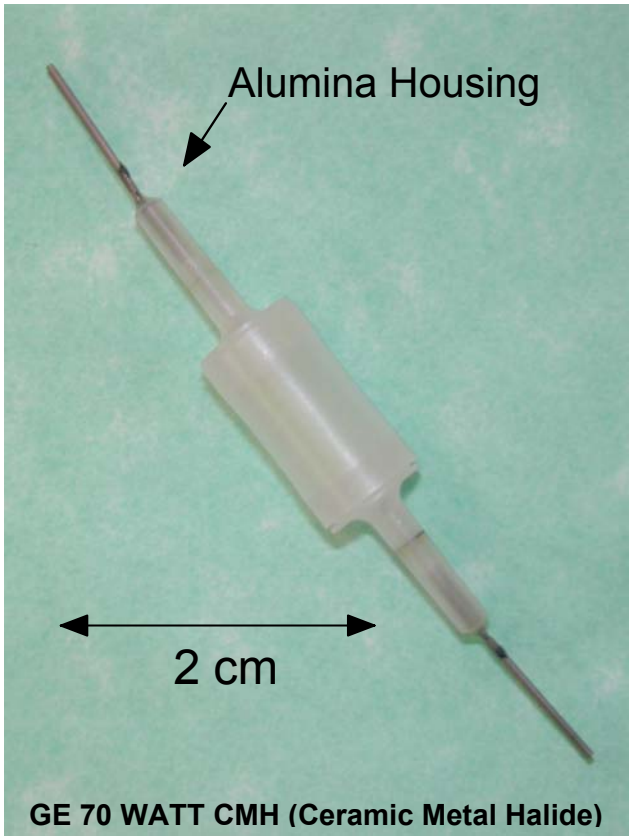

Figure 1.2 Metal halide lamp that the experimental geometry is based on.

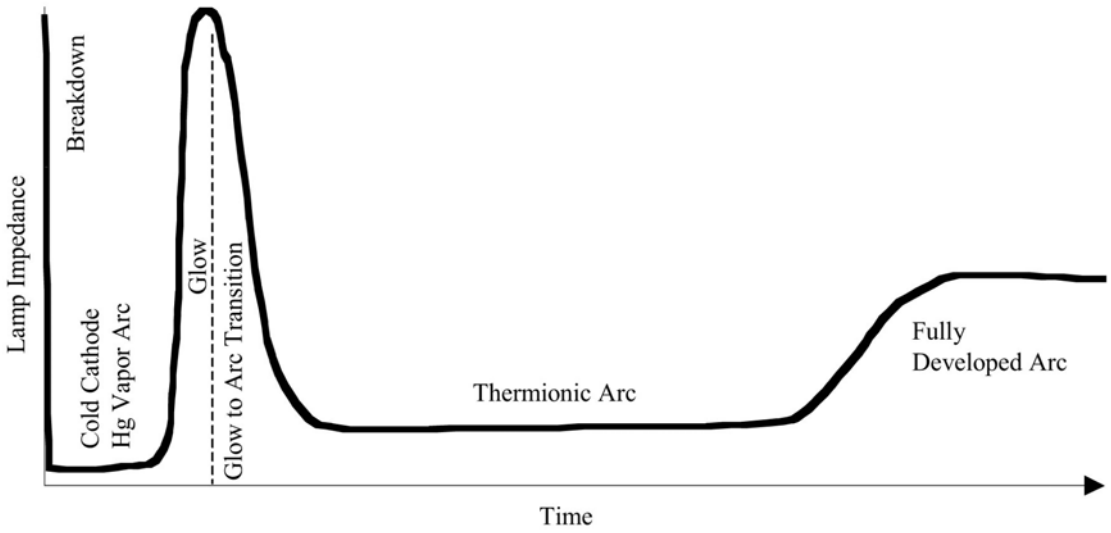

Figure 1.3 Metal halide HID lamp impedance as a function of time.[12]

1.6 References

1. C. P. Steinmetz, "Electric Lighting," United States Patent 1,006,021. Filed April 30, 1900; granted October 17, 1911.

2. J. F. Waymouth, *Electric Discharge Lamps*. (MIT Press, Cambridge, 1971).

3. J. F. Waymouth, "LTE and Near-LTE Lighting Plasmas," Invited Review Paper in Special Issue on Applications of Partially Ionized Plasma, GL. Rogoff, Guest Editor, IEEE Transactions on Plasma Science **19**, 1003 (1991).

4. Energy Policy Act of 1992

5. Energy Policy Act of 2002

6. J. R. Knisley, "Addressing lighting efficiency per ASHRAE and IES," Electrical Construction and Maintenance **96** (4), 33 (1997).

7. Sylvania - http://www.sylvania.com/business/hot/hid/metcer.htm.

8. G. Zaslavsky, S. Cohen, and W. Keeffe, "Improved starting of the 100-W metal halide lamp," Journal of the Illuminating Engineering Society **19** (2), 76 (1990).

9. W. W. Byszewski and A. B. Budinger, "Enhanced starting of HID lamps," Journal of the Illuminating Engineering Society **19** (2), 70 (1990).

10. S. Cohen, G. Zaslavsky, and J. N. Lester, "Pulse starting the 100-W metal halide lamp," Journal of the Illuminating Engineering Society **18** (2), 3 (1989).

11. P. D. Gregor, Y. M. Li, A. B. Budinger, and W. W. Byszewski, "Arc tube transparency loss due to starting of HID lamps," Journal of the Illuminating Engineering Society **25** (2), 150 (1996).

12. W. W. Byszewski, Y. M. Li, A. B. Budinger, and P. D. Gregor, "Advances in starting high intensity discharge lamps," Plasma Sources Science and Technology **5**, 720 (1996).

13. L. C. Pitchford, I. Peres, K. B. Liland, J. P. Boeuf, and H. Gielen, "The breakdown and glow phases during the initiation of discharges for lamps," Journal of Applied Physics **82** (1), 112 (1997).

14. J. F. Waymouth, "The glow-to-thermionic-arc transition," Journal of the Illuminating Engineering Society **16** (2), 166 (1987).

15. G. M. J. F. Luijks and J. A. J. M. van Vliet, "Glow-to-arc transitions in gas discharge lamps," Lighting Research Technology **20** (3), 87 (1988).

16. L. Cifuentes, G. M. Forsdyke, and N. W. O'Brien, "The corrosion of tungsten in metal halide lamps: A review," Corrosion Science **33** (10), 1581 (1992).

17. N. Fukumori, H. Nishimura, K. Uchihashi, and M. Fukuhara, "A study of HID lamp life when operated by electronic ballasts," Journal of the Illuminating Engineering Society **24** (1), 41 (1995).

18. D. Smith and H. Zhu, "Properties of high intensity discharge lamps operating on reduced power lighting systems," Journal of the Illuminating Engineering Society **22** (2), 27 (1993).

19. R. G. Gibson, "Dimming of metal halide lamps," Journal of the Illuminating Engineering Society **23** (2), 19 (1994).

20. N. Aoike, M. Hoshino, and A. Iwabuchi, "Automotive HID headlamps, producing compact electronic ballasts using power ICs," Industry Applications Magazine **8** (1), 37 (2002).

21. M. Born, "Investigations on the replacement of mercury in high-pressure discharge lamps by metallic zinc," Journal of Physics D: Applied Physics **34**, 909 (2001).

22. I. Oota, N. Hara, F. Ueno, "A high efficiency power control circuit for metal halide lamp," *in Conference Proceedings - IEEE Applied Power Electronics Conference and Exposition – APEC* vol. 2**,** 1998, p. 1168.

23. H. J. Faehnrich and E. Rasch, "Electronic ballasts for metal halide lamps," Journal of the Illuminating Engineering Society **17** (2), 131 (1988).

2. EXPERIMENTAL SETUP

2.1 Overview

The experimental setup was designed to closely emulate commercial high intensity discharge lamps to provide data to validate the code LAMPSIM. For this purpose, the parameters varied in the experiment were pressure, voltage, location of ground planes, argon/xenon composition, and, indirectly, the pulse repetition frequency.

The general block diagrams of the experiments are shown in Figures 2.1 and 2.2. The apparatus consists of the pulsing circuit, the lamp housing, and the vacuum and gas handling. Data was taken with a digitizing oscilloscope. The experimental setups are fundamentally the same except for a few modifications to allow for controlling the gas composition and the addition of a UV light to provide seed electrons to reduce statistical variation in the breakdown times. Photographs of the experimental setups are in Figures 2.3 to 2.6. The setup with a ground plane in close proximity is shown in Figure 2.4. The setup with the mercury lamp supported by high-temperature foam to insulate from direct heat conduction is shown in Figure 2.6.

2.2 Pulsing Circuit

The purpose of the circuit was to provide high-voltage pulses with fast rise times at variable frequencies. The pulsing circuit involved two IGBTs (insulated gate bipolar transistors) in series driven by optoisolators via a digital pulse generator. Pulse widths of approximately 20 μs were used at various repetition rates. This circuit was originally designed by Clark Wagner and Scott McCain.[1] The layout of the circuit is shown in

Figure 2.7, and the actual device, implemented on a Global Specialties Solderless PB-103 breadboard, can be seen in Figure 2.8.

A Stanford Research Systems DG535 digital delay / pulse generator was used for producing the initial pulses. The DG535 is a precise delay and pulse generator providing four precision delays or two independent pulses with 5-ps resolution, with the trigger to output jitter being less than 50 ps. The signal from the pulse generator switched on the 2N2222 NPN transistor to trigger the optoisolator. The NTE3090, an optoisolator from NTE electronics, has a 6-lead DIP type package and contains a GaAs IRED (infrared emitting diode) optically coupled to a high-speed integrated detector with a Schmitt trigger output. The NTE3090 is designed for applications requiring electrical isolation and fast response times. A KEPCO ATE 36-1.5 M 50 W supply powered the optoisolators.

The signal from the optoisolator needed to be amplified in order to drive the insulated gate bipolar transistors (IGBT). This was accomplished using three 2N3906 small signal transistors in parallel, driven by two 9-V batteries in series regulated by a 1N4743A zener diode to operate at 13 V. As long as the batteries had at least 13 V across them, the circuit would exhibit the same behavior. Three transistors were used to obtain fast rise times. Only two 9-V batteries were used because the maximum gate-to-emitter voltage for the IGBT was ± 20 V.

The IGBTs, International Rectifier IRG4PH40U, were chosen because they can handle a collector-to-emitter breakdown potential of 1200 V, which is relatively high for transistors. The device has a rise time of 24 ns. Since HID lamps typically need several kV to breakdown, two transistors were used in series to handle up to 2 kV. The high

voltage was provided by a Bertan Associates Model 215 supply, with specifications of 0 to ± 3000 V and current from 0 to 5 mA.

Since the IGBTs had to be driven in series, two identical circuits were used, driven by the DG535 pulse generator as it could supply two independent pulses which could be referenced to each other. In order for the IGBTs not to be overvoltaged they had to be turned on and off as closely as possible to each other to prevent damage. There are four pulse output BNCs: AB, -AB, CD, and -CD. The AB output provides a pulse for the interval between the time set for channel A and channel B. The CD output provides a pulse for the interval between the time set for channel C and channel D. These outputs allow the DG535 to generate two precisely timed complementary pulses.

Since the IGBTs are in series, they are prone to failure from being overvoltaged if they were both not turned on and off at the same time. Several IGBTs were destroyed during the first few months of experiments while timing issues were resolved. Typical voltage pulses are shown in Figure 2.9 having a rise time of ≈ 150 ns. The voltage of the pulse was defined as the amplitude to which the pulse asymptotically approached for an open circuit.

2.3 Lamp Geometry

The lamp geometry was designed to be similar to a commercial high intensity discharge lamp, with adjustability built in for experimentation. The design used o-rings to allow for relatively quick replacement of the glass pieces if necessary. The geometry allowed for various electrode spacings and lamp diameters. The electrode spacings could

be achieved by replacing the same diameter glass tubing with various lengths. To change the diameter of the tube required the housing to be remachined.

A 3-D perspective of the lamp geometry is in Figure 2.10 with an exploded assembly view in Figure 2.11. Machine drawings of the individual components are in Figures 2.12(a)-(g). Since the performance of the lamp is sensitive to ground planes, the lamp was placed away from the stainless steel vacuum components by being mounted on a Pyrex tube with o-ring adapters. A seal was achieved with component G with a size 217 o-ring. A size 217 o-ring has a 1 7/16-in. outer diameter, 1 3/16-in. inner diameter, and a width of 1/8 in. All o-rings were Buna-N, a Nitrile elastomer. The lamp was mounted onto the Pyrex tubing with components A and B being bolted together horizontally and tightened vertically until the tapers of the Pyrex and machined parts wedged together. The whole assembly was held together by tightening the hex head nuts on the ¼-20 threaded rod until all of the o-rings formed seals.

O-ring grooves were machined into components F and G to allow for sealing the glass tubing of the lamp. This was accomplished with size 012 o-rings which have an outer diameter of ½ in., an inner diameter of 3/8 in., and a width of 1/16 in.. Through holes were machined in components G and E in order to allow for gas flow into and out of the lamp chamber. The purpose of components D and E are only to be tightened down on to components F and G, respectively, in order to compress the size 001 o-rings around the electrodes to form a seal. These o-rings have an outer diameter of 3/32 in., an inner diameter of 1/32 in., and a width of 1/32 in. Components D and E were tightened down each with four 2-56 1 in. long bolts.

For the pulse repetition rate and ground plane experiments a 1.9-cm long, 1-cm inner diameter borosilicate glass tube was used. For the argon/xenon experiments with the use of the mercury lamp, quartz tubing was used instead to allow for the transmission of UV light through the tube for photoionization to occur as borosilicate does not transmit UV light.

The pen-lamp is an Oriel 6035 pencil style spectral calibration source with a mercury and argon fill, powered by an Oriel 6047 AC supply with an 18-mA current. The mercury lamp was used in order to supply a source of seed electrons to reduce the statistical lag time of the breakdown without causing substantial gas heating by having high frequency pulsing.

Components D, E, F, and G were machined out of Macor, an ultra-high temperature glass-mica ceramic. The components exposed to vacuum must exhibit good "vacuum characteristics" and be a nonconducting dielectric. Plastics would have too much adsorption and permeation resulting in large amounts of outgassing and requiring long periods to pump down. The other components not exposed to vacuum, components A, B, and C, were machined of less expensive Delrin, a homopolymer acetal (crystalline thermoplastic), a general purpose mechanical plastic. Good overall mechanical properties such as dimensional stability and low moisture absorption make it ideal for machining, and it holds threads well.

2.4 Vacuum and Gas Handling System

The system was able to obtain a base pressure of 10^{-7} Torr. This was achieved using a Pfeiffer TPU 050 turbomolecular pump with a pumping speed of 50 l/s. The

turbomolecular pump was controlled by a TCP 040 controller and had an Alcatel 2002BB dual stage rotary vane vacuum pump with a pumping speed of 1.4 cmh (cubic meters per hour) as the backing pump. The original backing pump failed and was replaced, requiring the controller to be rewired to account for the new pump's lack of a centrifugal switch for shutting down the turbomolecular pump. An additional 2002BB was also used as the roughing pump.

The base pressure was measured using a Huntington IK-150 Bayard-Alpert ionization gauge with an MKS type 290 controller. This gauge could only be turned on when the pressure was sufficiently low to prevent damage and could only measure pressures below 10^{-4} Torr. To measure the pressures for operating conditions, from 1 to 100 Torr, an MKS Baratron Type 626 capacitance manometer with a range to 100 Torr was used. It was controlled by a MKS PDR-C-1B power supply/readout. Unfortunately, the pressure gauge was not temperature controlled and was subject to slight variations with drift in the ambient temperature. It was more convenient to have a direct pressure measurement, such as from a capacitance manometer, especially with a gas mixture, instead of indirect measurements, such as with a convectron gauge. The use of these gauges with different gases requires different calibration curves that would make accurate measurements of gas mixtures difficult.

For the first pulse repetition rate and ground plane experiments only argon was used, and, to control the pressure, a needle valve and bellows valve were used. The needle valve was slowly cracked until the desired pressure was met and then turned off. However, since needle valves never completely close, small amounts of argon were being

leaked in and the pressure was controlled by cracking the angle valve to the turbomolecular pump until the desired steady state pressure was achieved.

For the argon/xenon composition experiments, flow through could not be achieved while controlling composition with the just described apparatus. Therefore, new bellows valves were installed. In order to allow for good mixing, the lowest percentage gas was filled first. For example, a 10% xenon in argon mixture at 100 Torr would be achieved by filling the chamber first with 10 Torr of xenon and then filling the rest of the way with argon.

2.5 Experimental Procedures

For all experiments, the pressure, composition, voltage, and pulse repetition frequency were all first set and allowed to run until steady state conditions were met. Time lengths varied depending on conditions, but were, in general, no longer than 5 min. However, when the mercury lamp was being used, the lamp was turned on at least a half an hour before the experiments started in order to reach a steady state. The heat generated from the lamp required a "settling time." Based on manufacturer's recommendations, 2 min. are required for the mercury vapor to dominate the discharge and 30 min. for complete stabilization of the UV output. The system was judged to be in the steady state by monitoring drift in the average values or standard deviations.

Tungsten was used to reduce damage to the electrodes caused by sputtering and vaporization. Since the lower electrode was electrically connected to the experimental apparatus it could not be powered without compromising safety, possibly causing damage, and upsetting normal operation of the gauges. In order to make the top

electrode the anode, it was positively biased since the cathode was grounded. For the argon experiments a ballast resistance of 10 kΩ was used, and for the argon/xenon experiments the ballast resistance was 11.5 kΩ.

All data were taken on a TDS 5104 digital phosphor oscilloscope with a Tektronix P5100 probe. The P5100 is a low-input capacitance, high-voltage (2.5 kV) probe designed for higher frequency applications, up to 250 MHz. The TDS 5104 has an analog bandwidth of 1 GHz with a typical rise time of 400 ps. The trigger jitter (RMS) is typically 8 ps and the time base ranges down to 200 ps per division. The digital scope also has an open Microsoft Windows ME architecture, allowing screen and waveform capturing. Data can be directly downloaded or copied to disk. The oscilloscope also allows for real-time statistics on the incoming data.

The mean breakdown time measurements were only possible with an apparatus similar to the TDS 5104 because of the need to perform real-time statistics and data capturing. The breakdown time was defined as the time between 10% of the rise and 10% of the fall as referenced to the maximum voltage of the pulse as shown in Figure 2.13. The fall is due to a voltage drop across the ballast resistor when the plasma starts drawing larger currents. This definition can be set on the scope and values can be obtained in real time. At least 300 measurements of the breakdowns were taken after steady state conditions were met. These were then averaged in real time, and the mean breakdown time, as well as the corresponding standard deviation, were recorded. The actual pulse was captured and saved to disk.

2.6 Recommendations

If further experiments are to be performed several issues should be addressed. First, to avoid gas heating and contamination from sputtering of the electrodes and other sources, the design needs to allow for gas to flow through the lamp chamber. Since the gas is now stagnant, leaks into the chamber also become critical. A flow-through design would carry away most of the impurities and provide a more pure gas on the average.

Future designs should also eliminate the use of o-rings to allow for a lower base pressure, leaving a cleaner system with less contamination with very low leak rates. This could be done with UHV (ultra high vacuum) components. Lower base pressures can also be achieved by increasing the conductance by increasing the cross-sectional flow areas and by shortening lengths of piping and tubing. The largest gains could be made by redesigning the lamp to allow for larger inflow areas than provided by the eight through holes now. Also, since the discharges exhibit quite different behaviors with different pressures, having temperature-controlled pressure gauges would eliminate errors due to ambient temperature drifts.

Finally, the system needs to be redesigned to allow for either electrode to be powered. Most systems generally have negative biases applied to the cathode, and the anode is grounded instead of having positive bias on the anode while the cathode is grounded. Lamp manufacturers even recommend that metal halide HID lamps be operated at negative voltage potential in order to lengthen lamp life.[2] This can be accomplished by electrically insulating the electrodes and by not having direct electrical connections to the system housing.

2.7 Figures

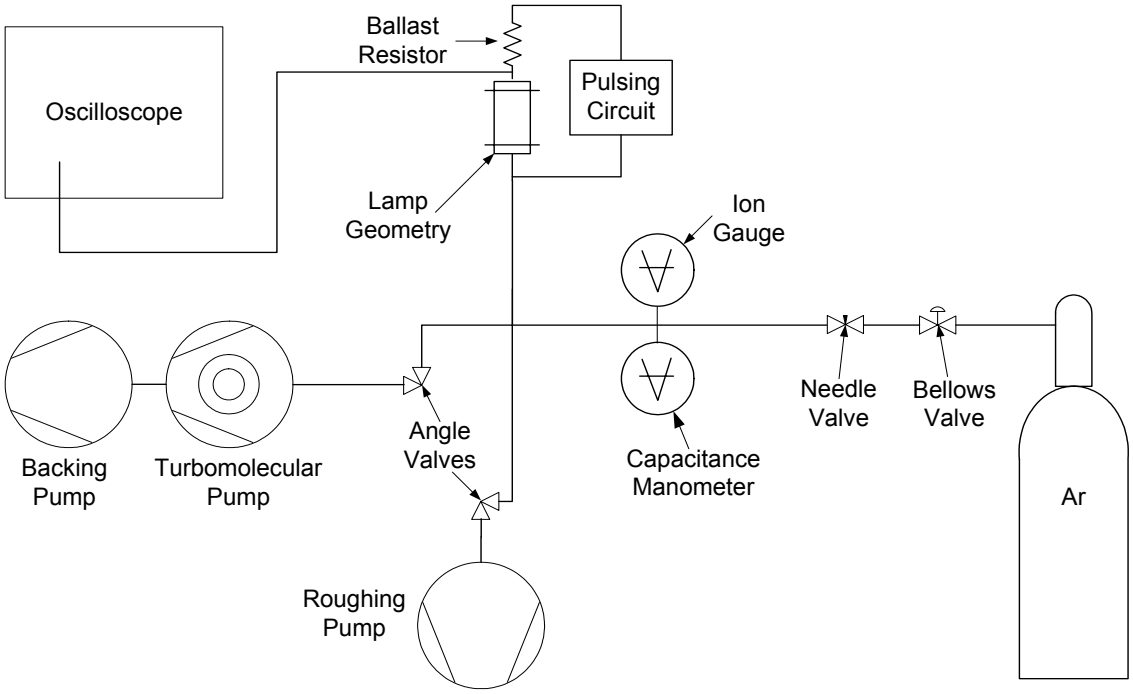

Figure 2.1 Experimental setup for argon breakdown measurements.

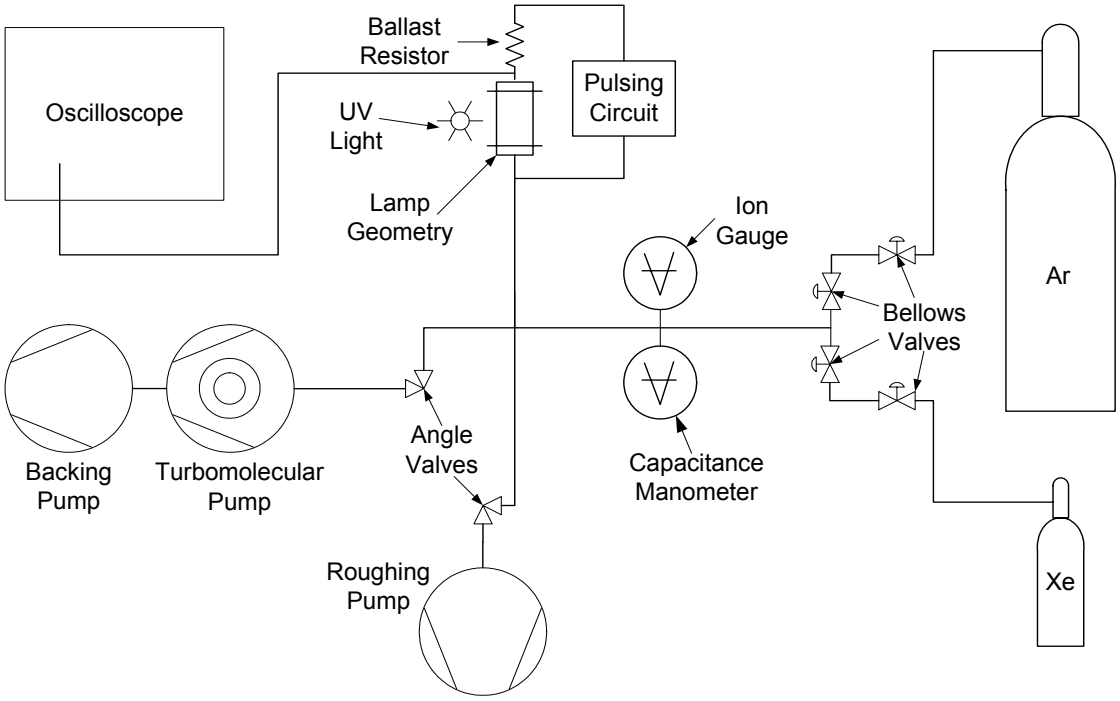

Figure 2.2 Experimental setup for argon/xenon breakdown measurements.

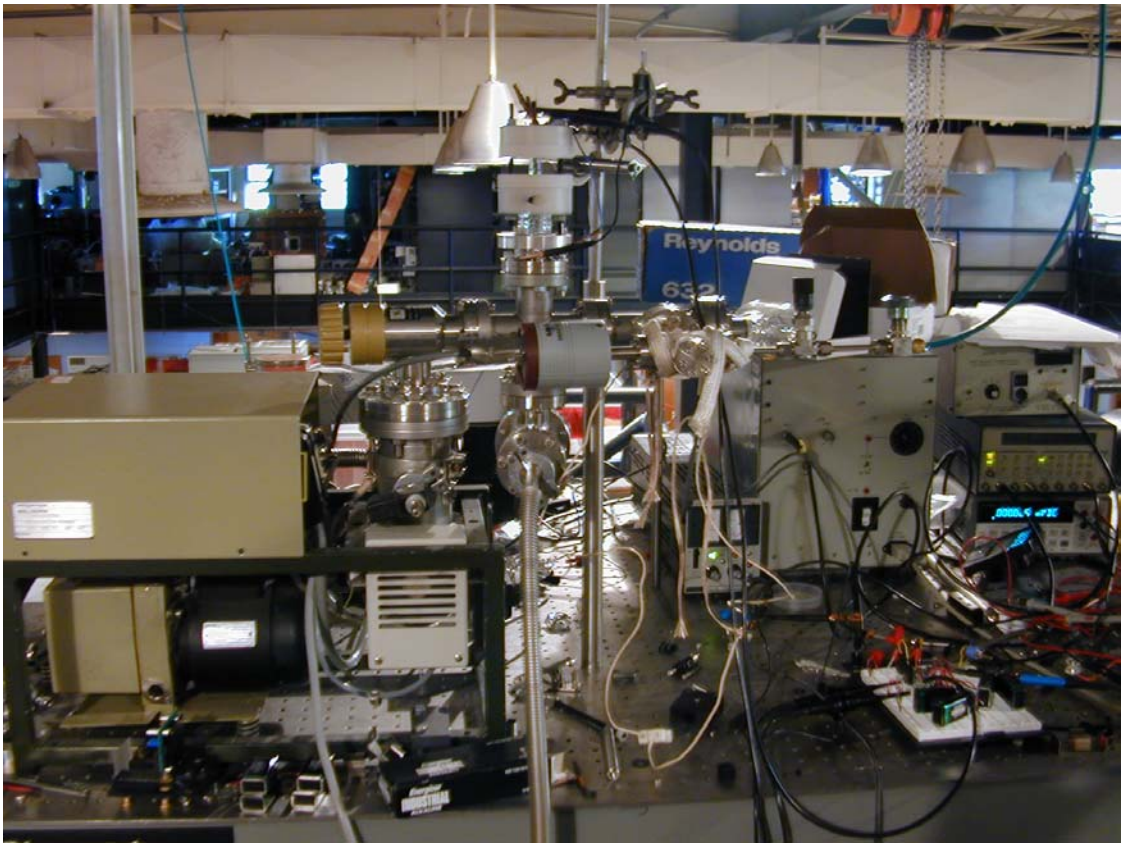

Figure 2.3 Setup for argon ground plane and pulse repetition experiments.

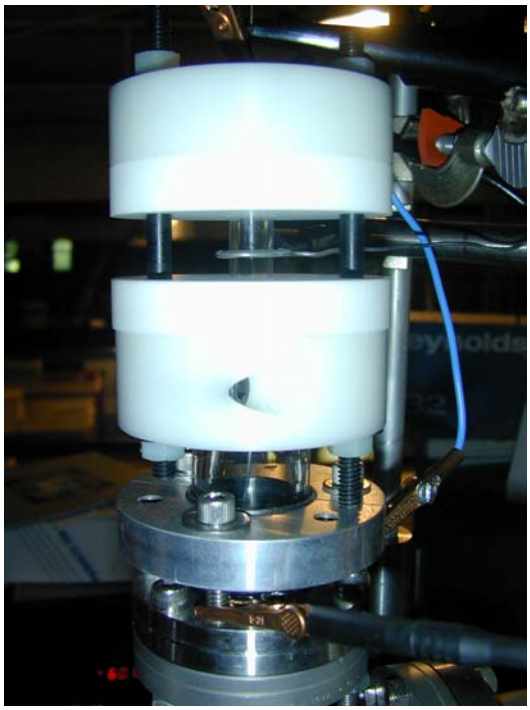

Figure 2.4 A close-up of the lamp geometry with the adjustable ground plane.

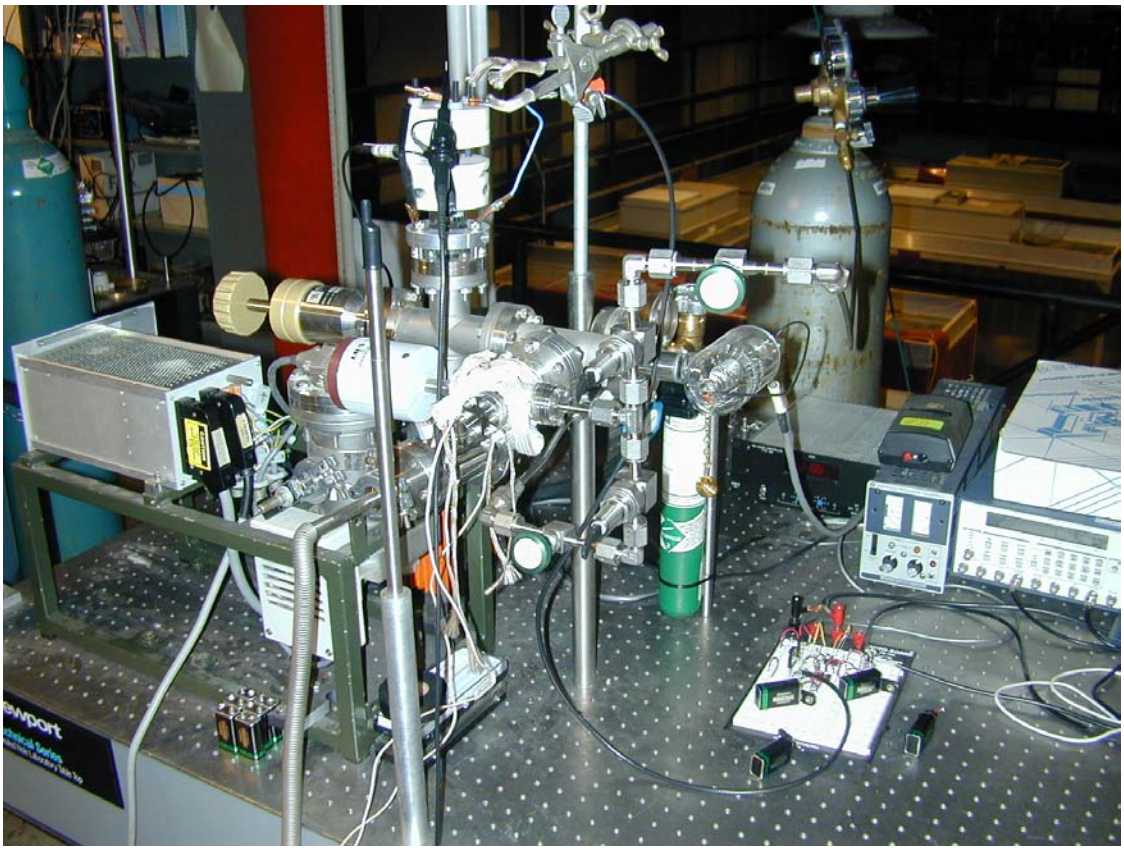

Figure 2.5 Setup for argon/xenon composition experiments.

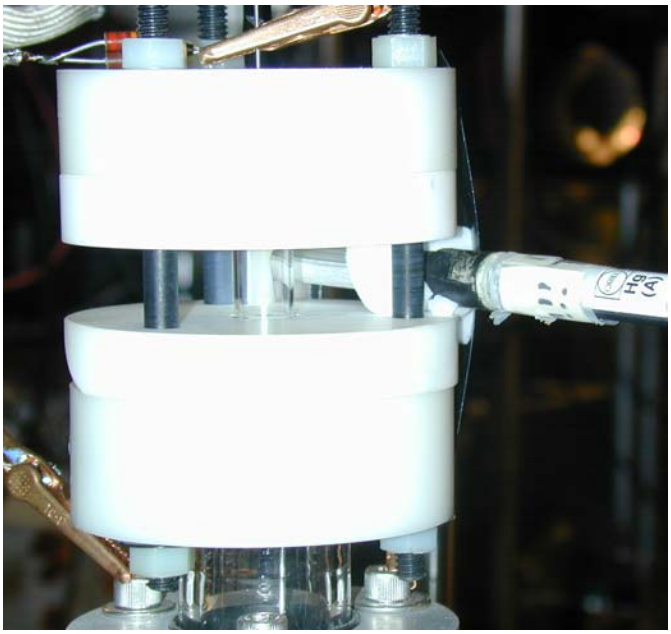

Figure 2.6 Close-up of lamp geometry with the mercury lamp supported by high-temperature foam.

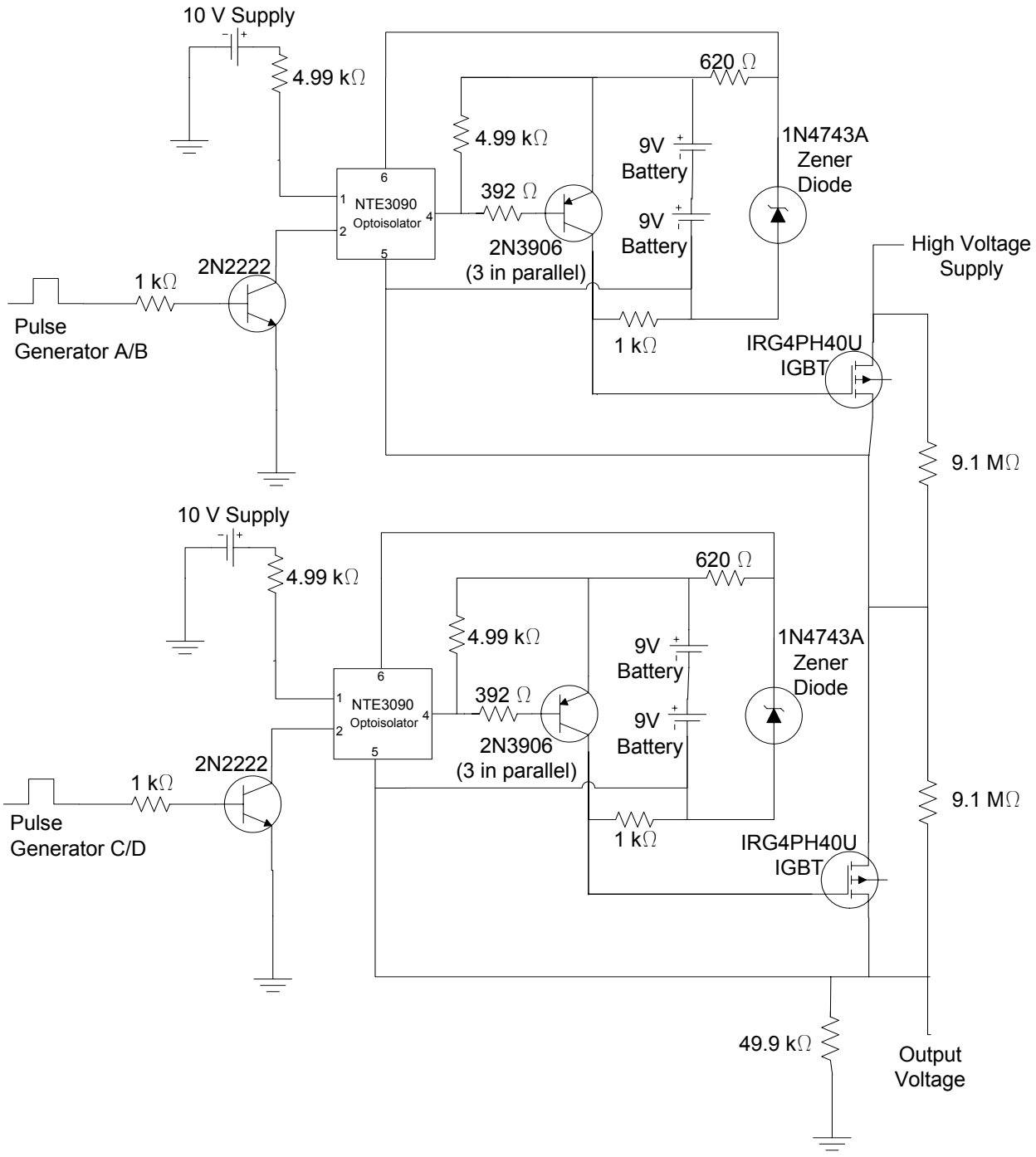

Figure 2.7 Circuit diagram of the pulsing circuit.

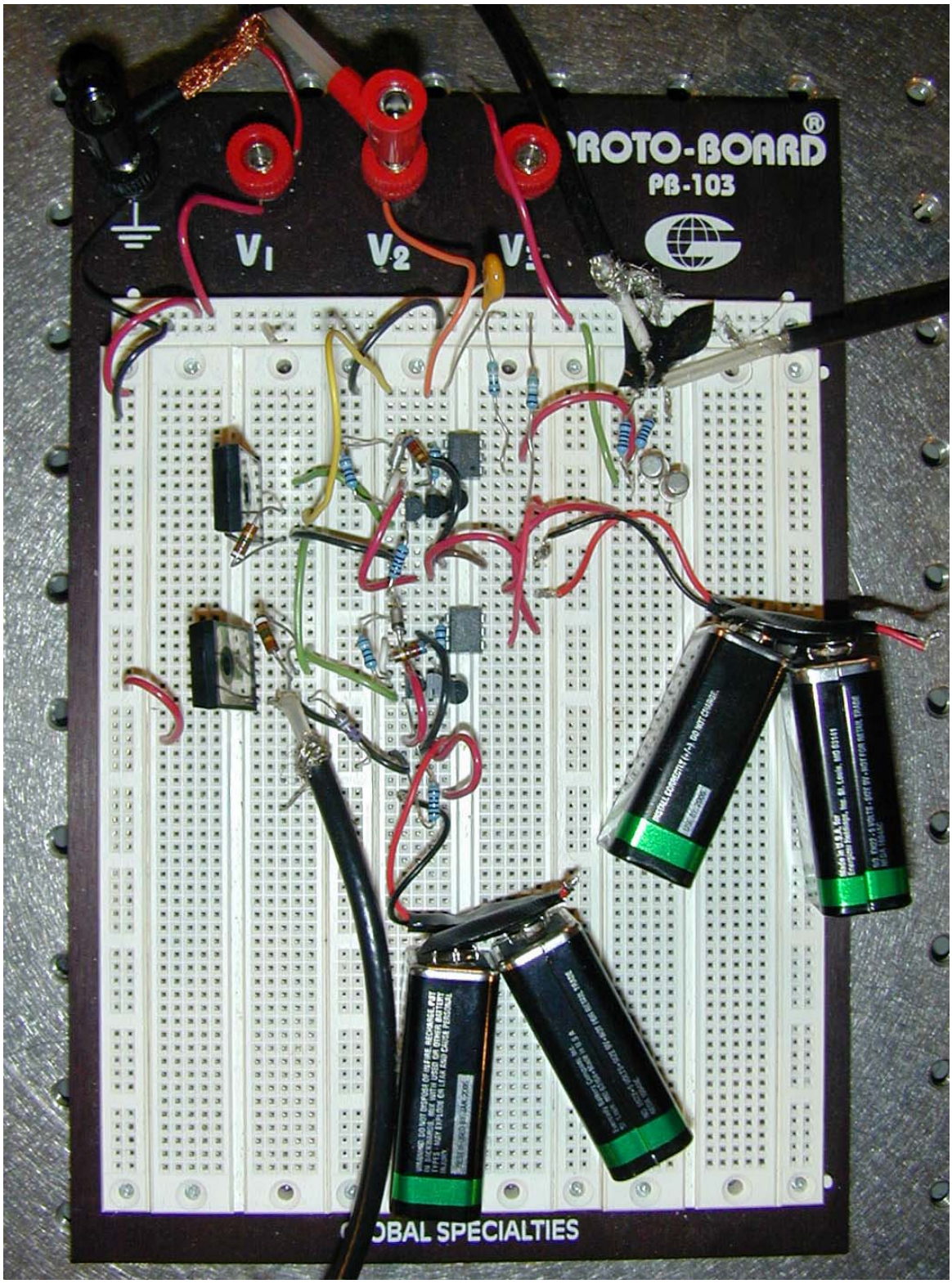

Figure 2.8 Final circuit on breadboard.

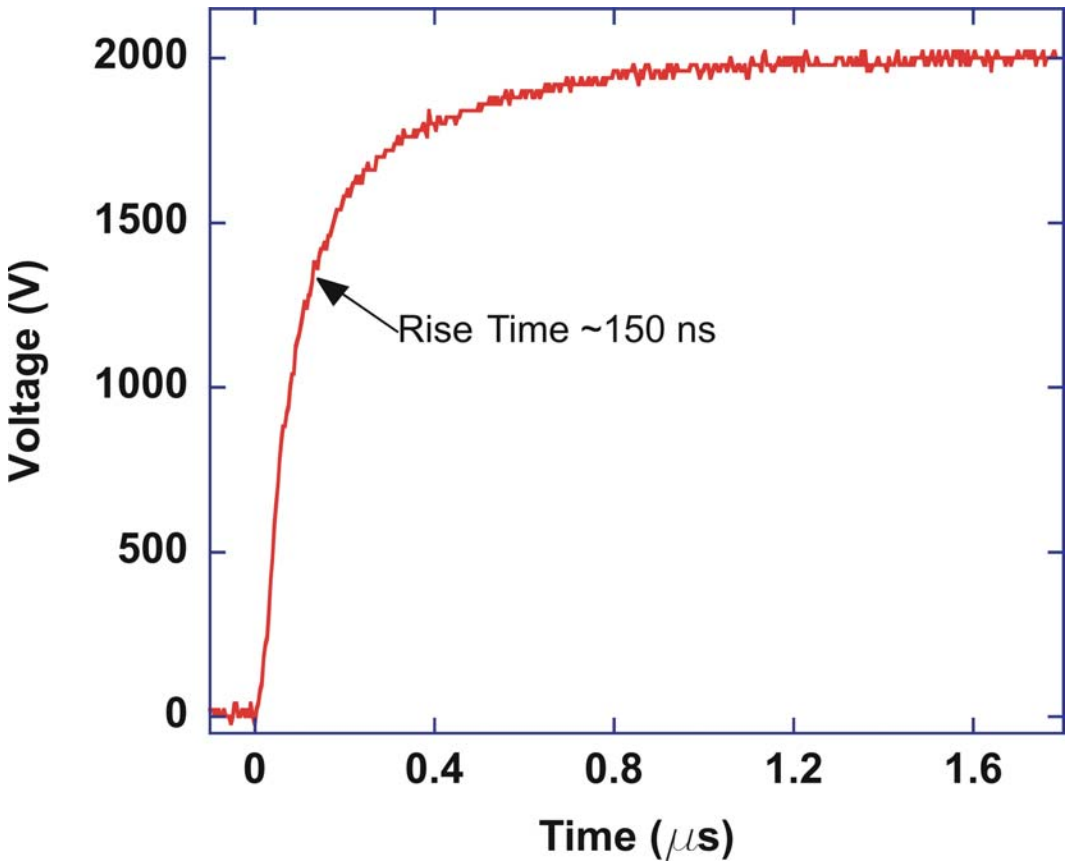

Figure 2.9 Typical voltage pulse from the circuit. A 2000-V pulse is shown.

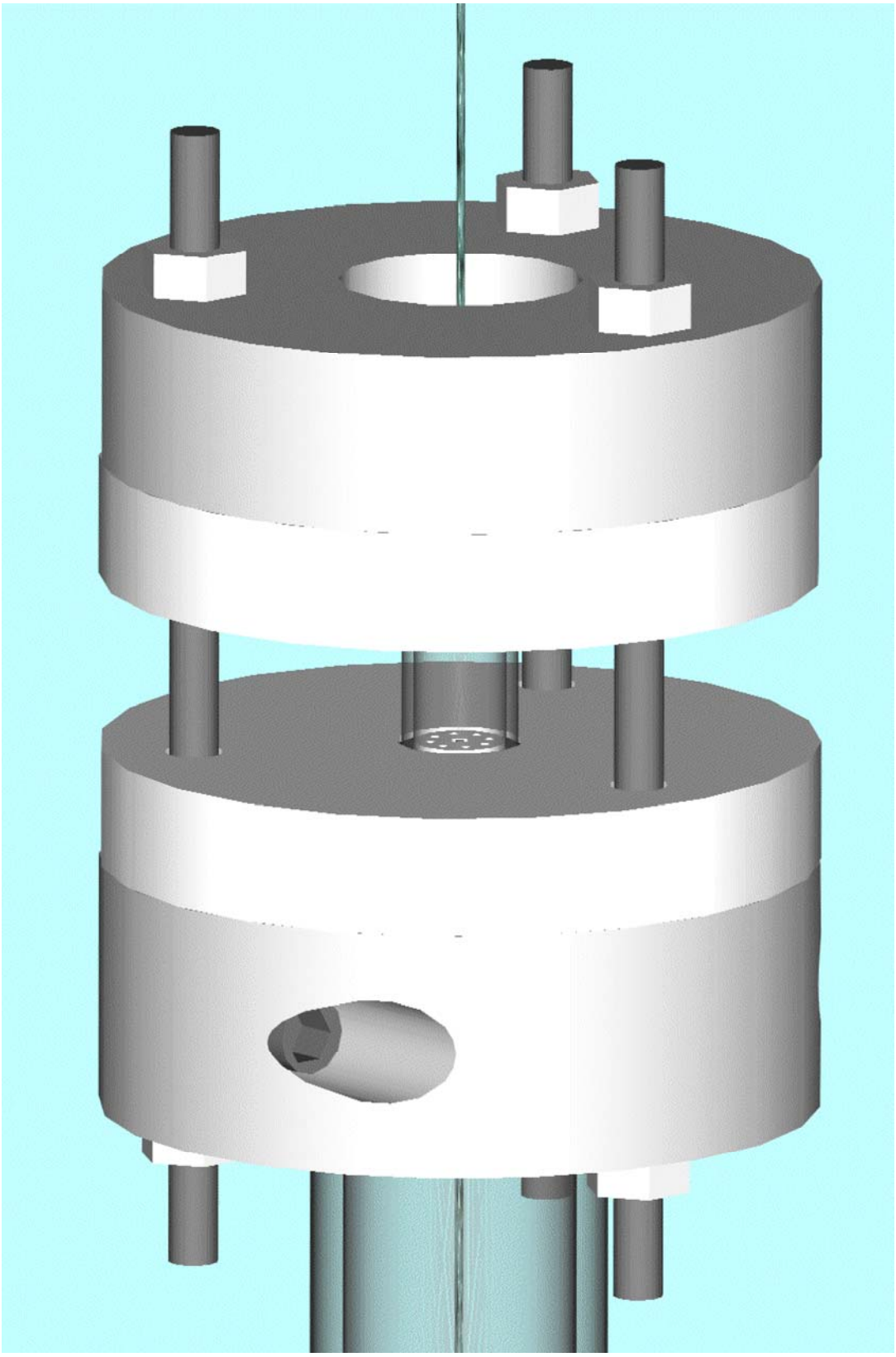

Figure 2.10 Final assembly of the lamp geometry.

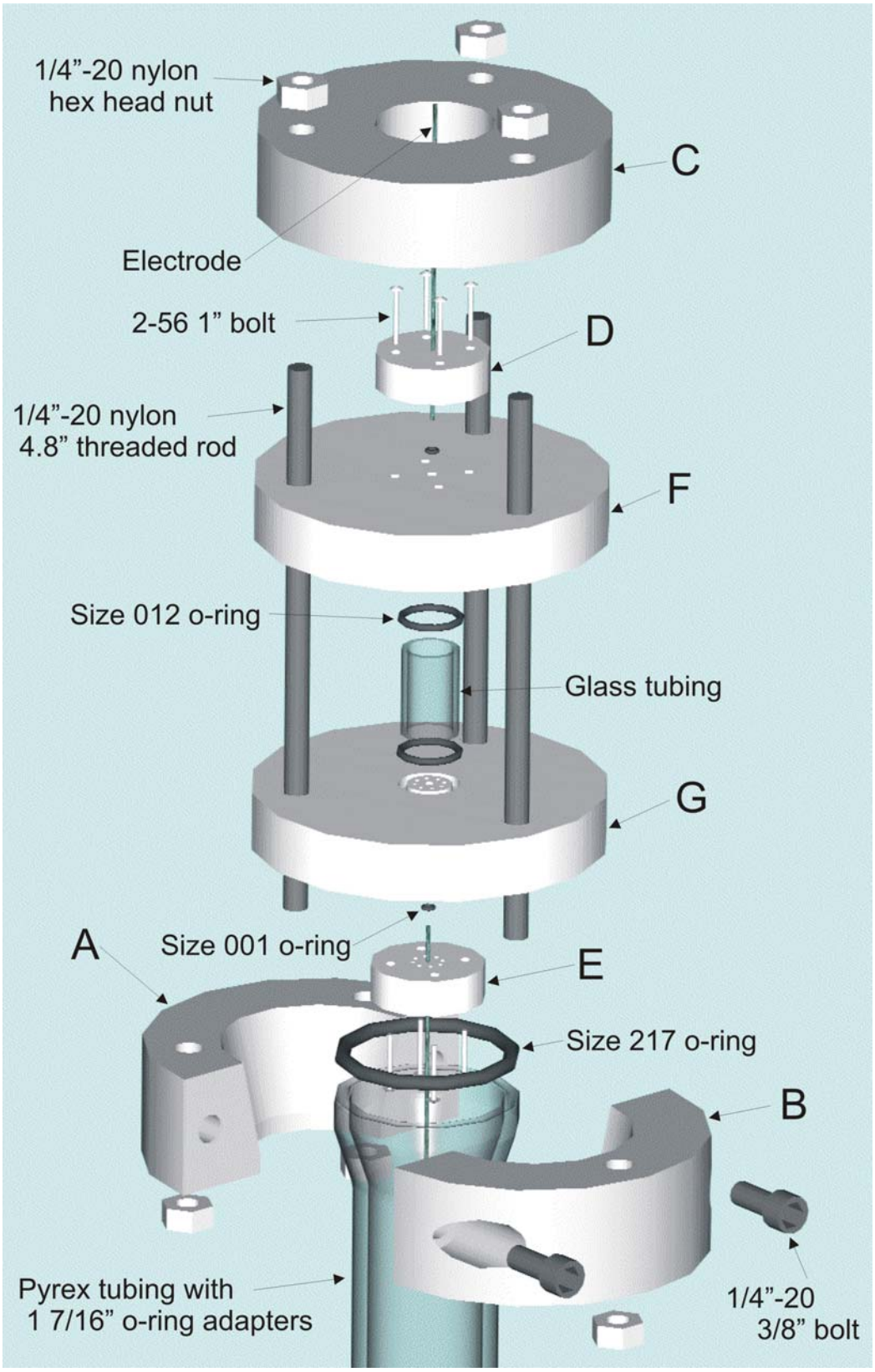

Figure 2.11 Exploded assembly view of the lamp geometry.

Figures 2.12 Machine drawings of individual components of the lamp geometry as shown in the exploded assembly view of Figure 2.11 and labeled as components A through G.

(a) Component A
(b) Component B
(c) Component C
(d) Component D
(e) Component E
(f) Component F
(g) Component G

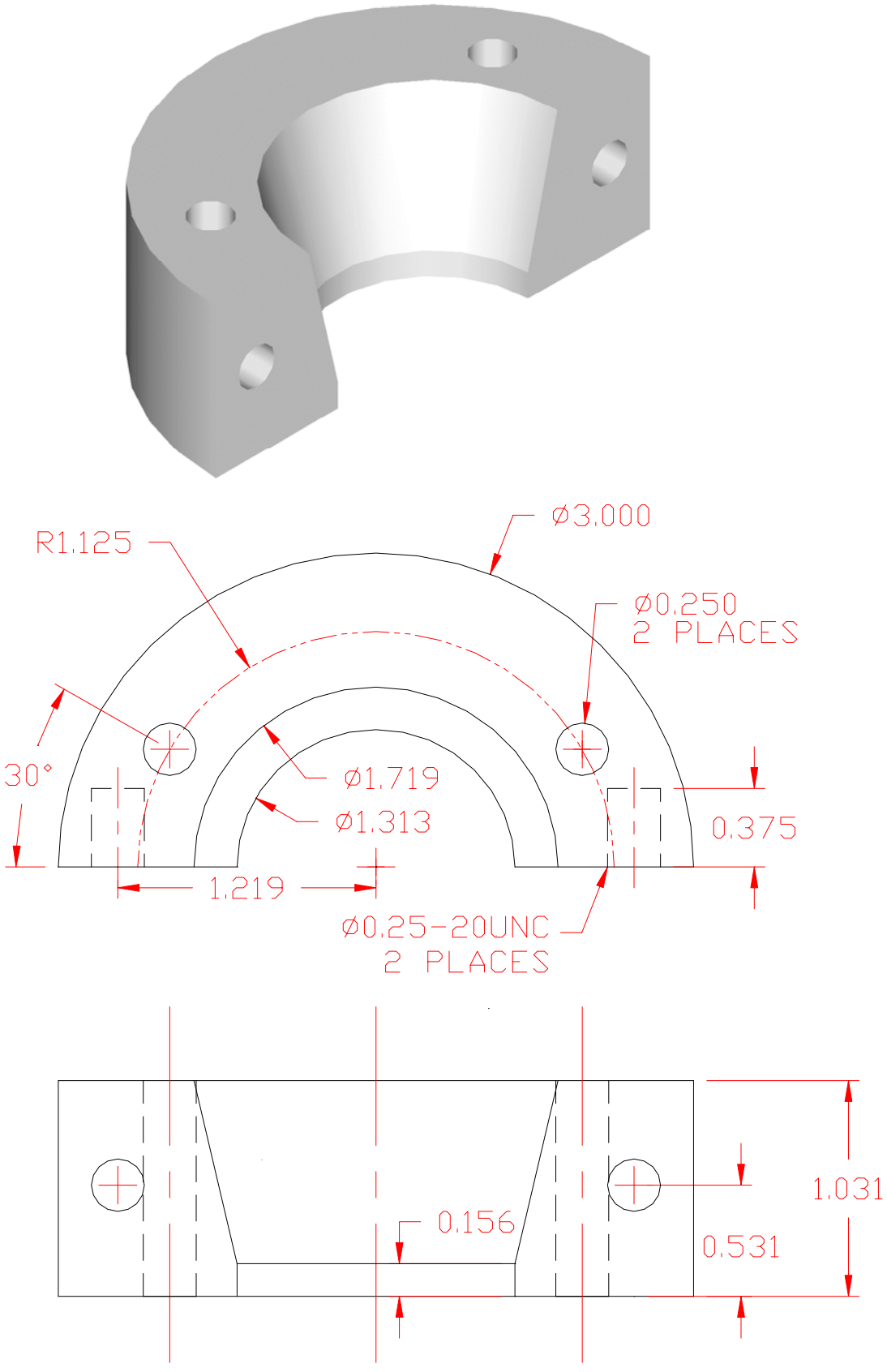

Figure 2.12(a) Component A machined of Delrin.

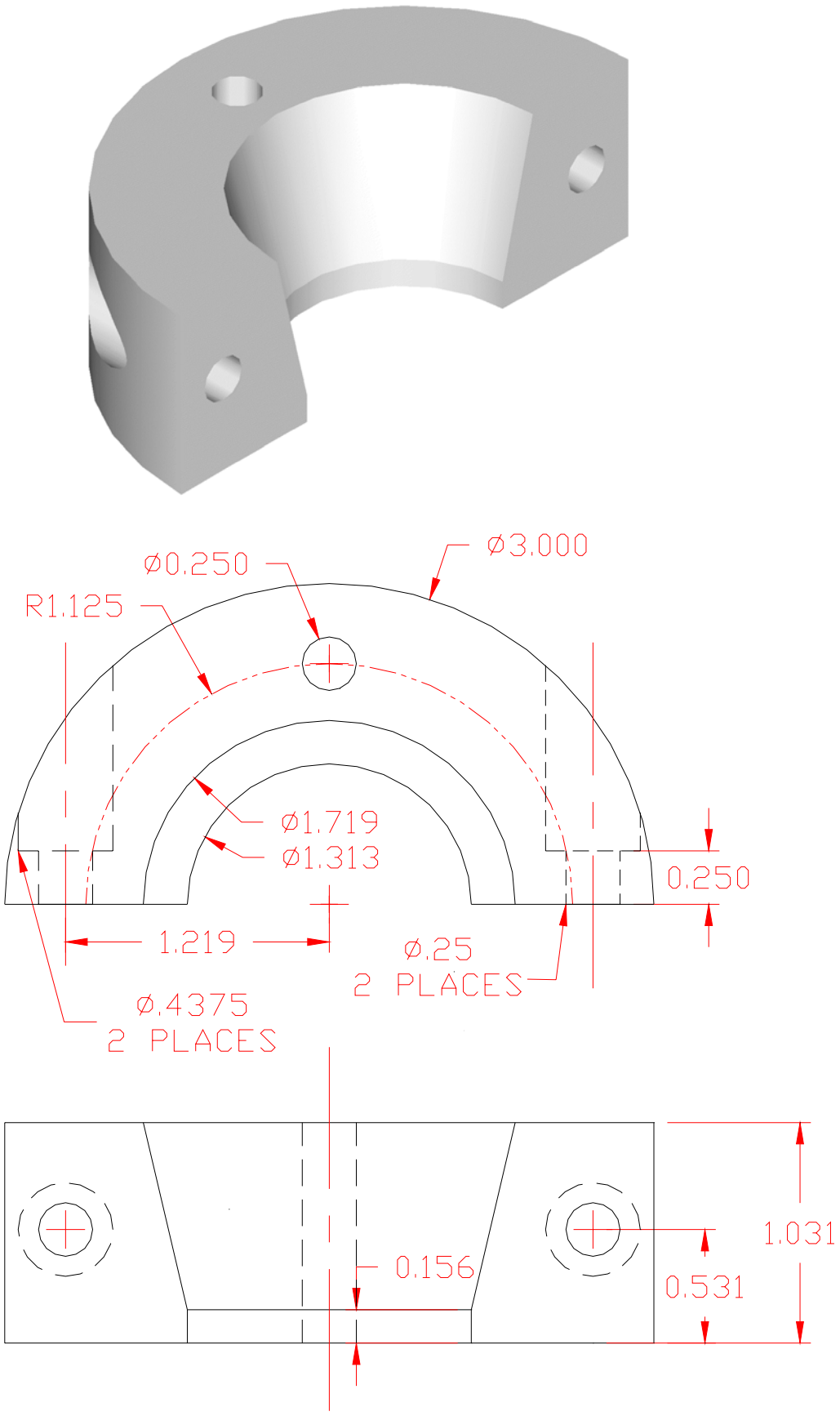

Figure 2.12(b) Component B machined of Delrin.

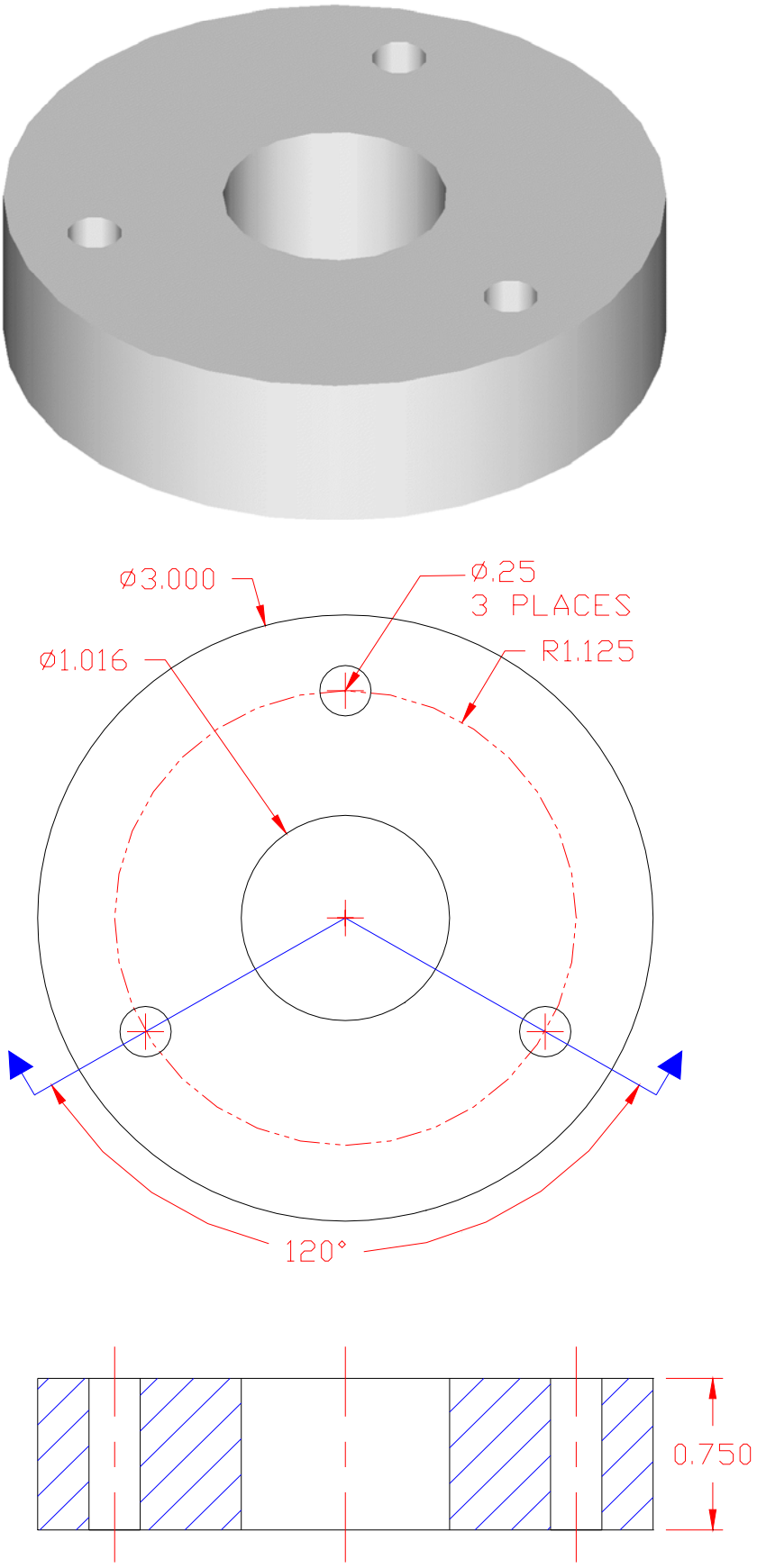

Figure 2.12(c) Component C machined of Delrin.

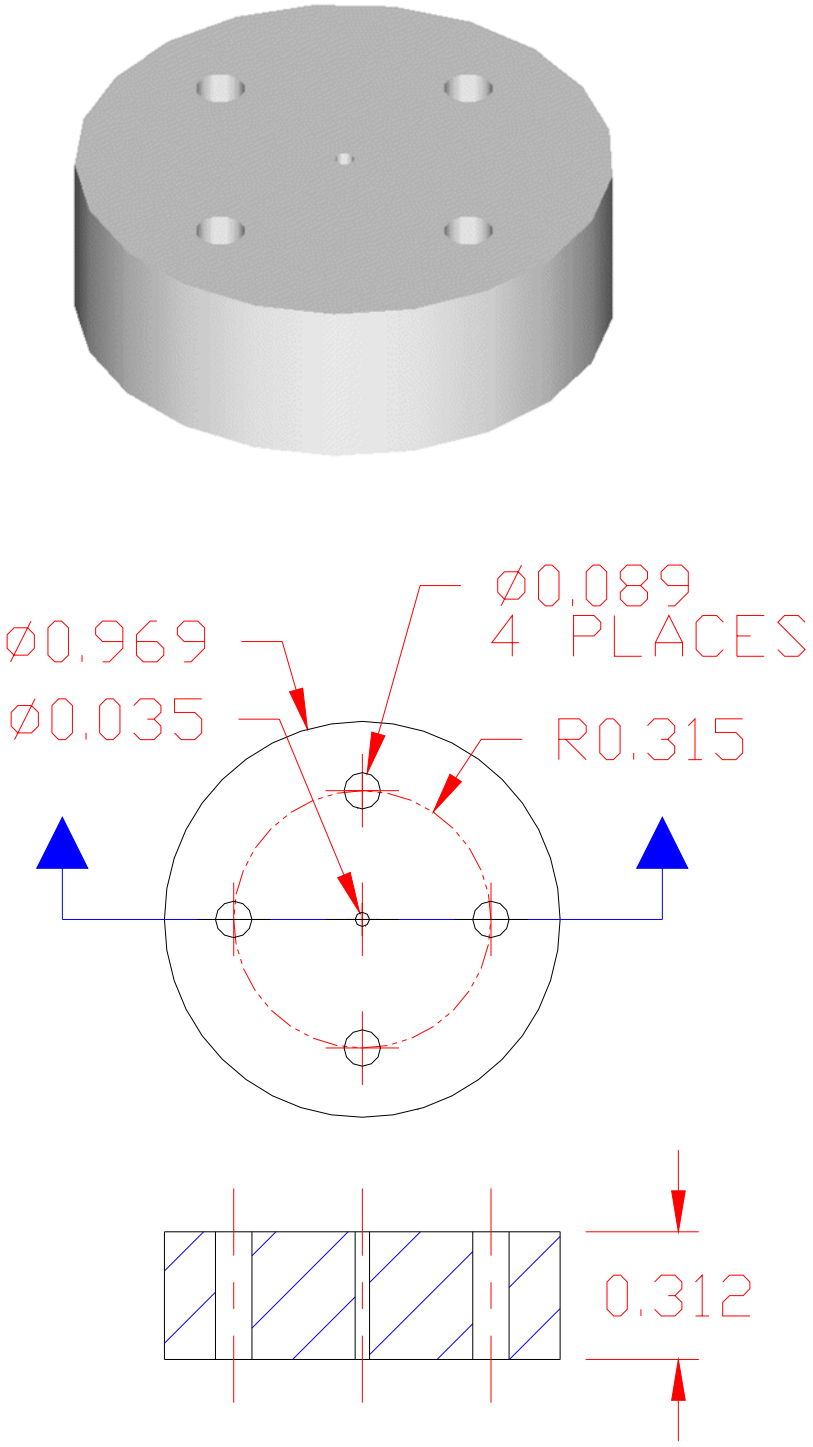

Figure 2.12(d) Component D machined of Macor.

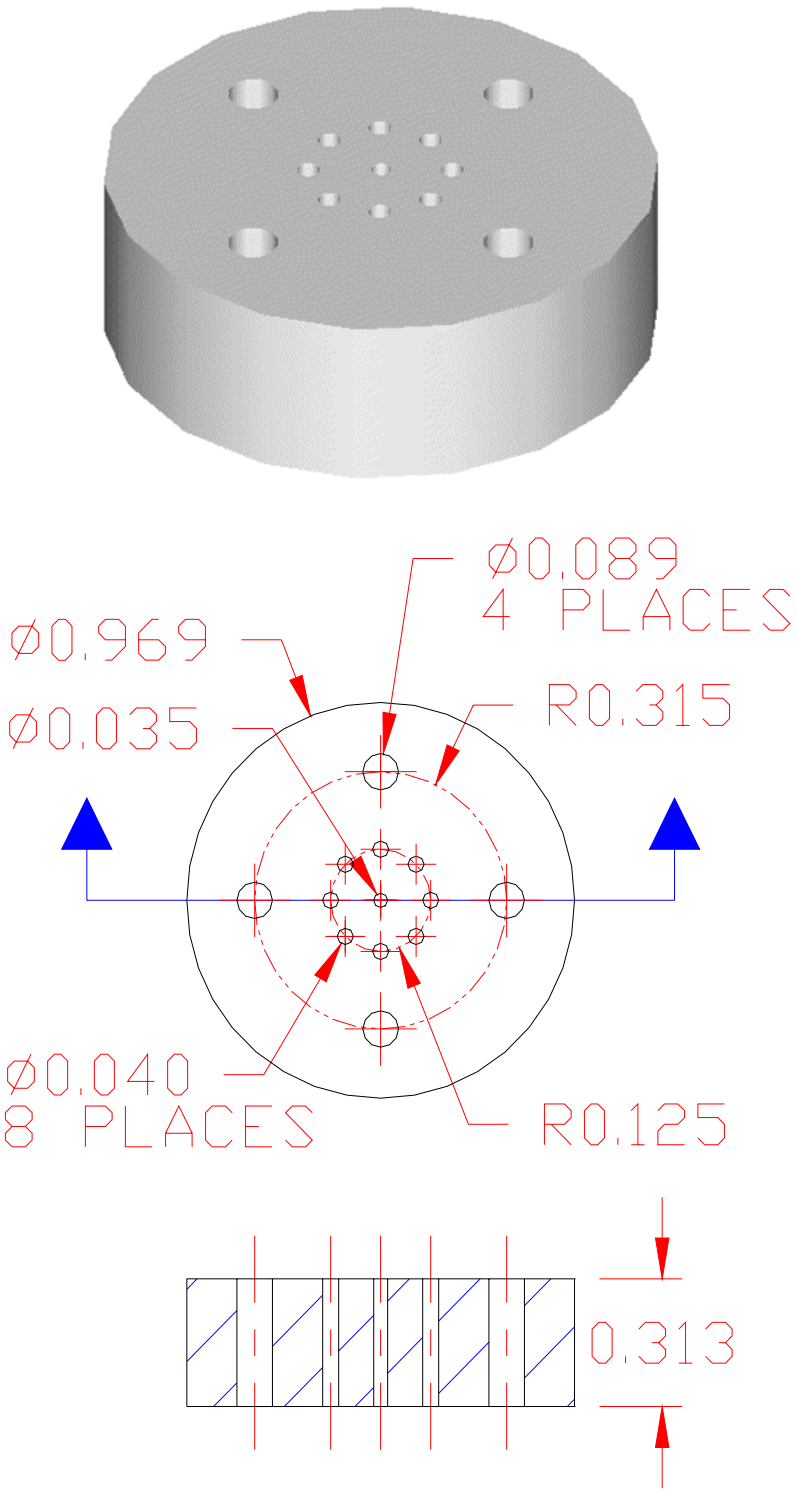

Figure 2.12(e) Component E machined of Macor.

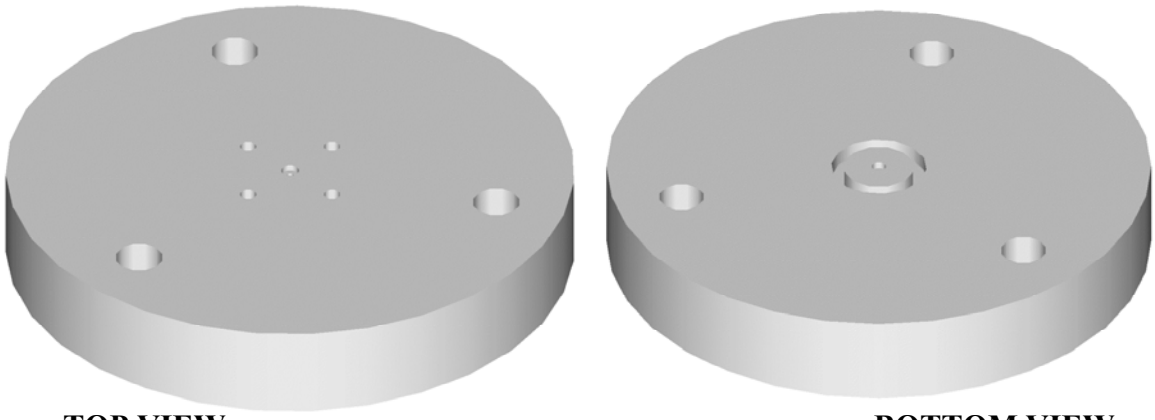

TOP VIEW **BOTTOM VIEW**

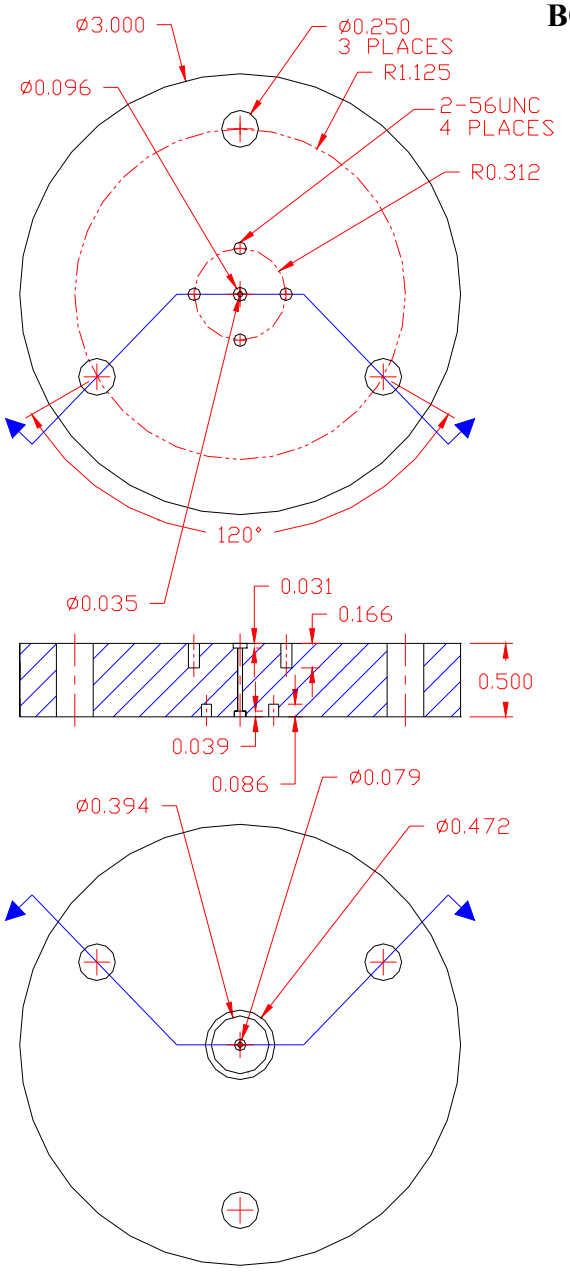

Figure 2.12(f) Component F machined of Macor.

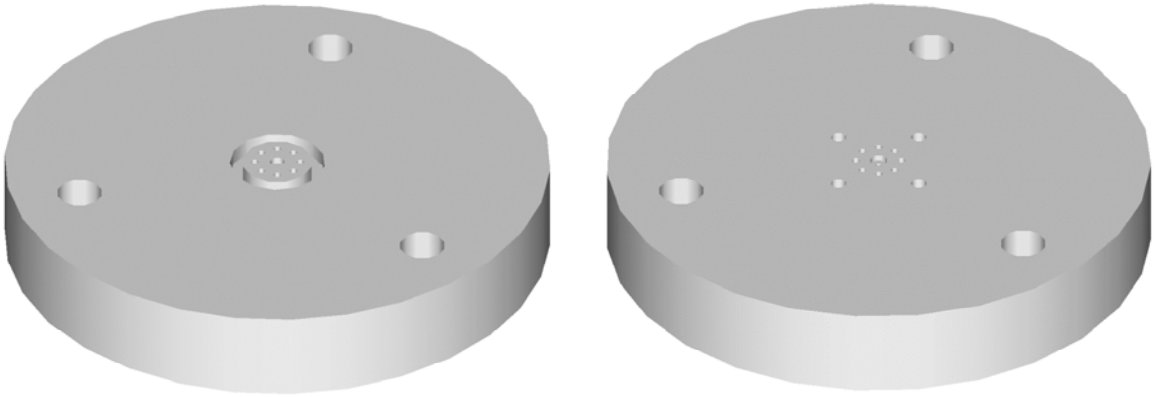

TOP VIEW **BOTTOM VIEW**

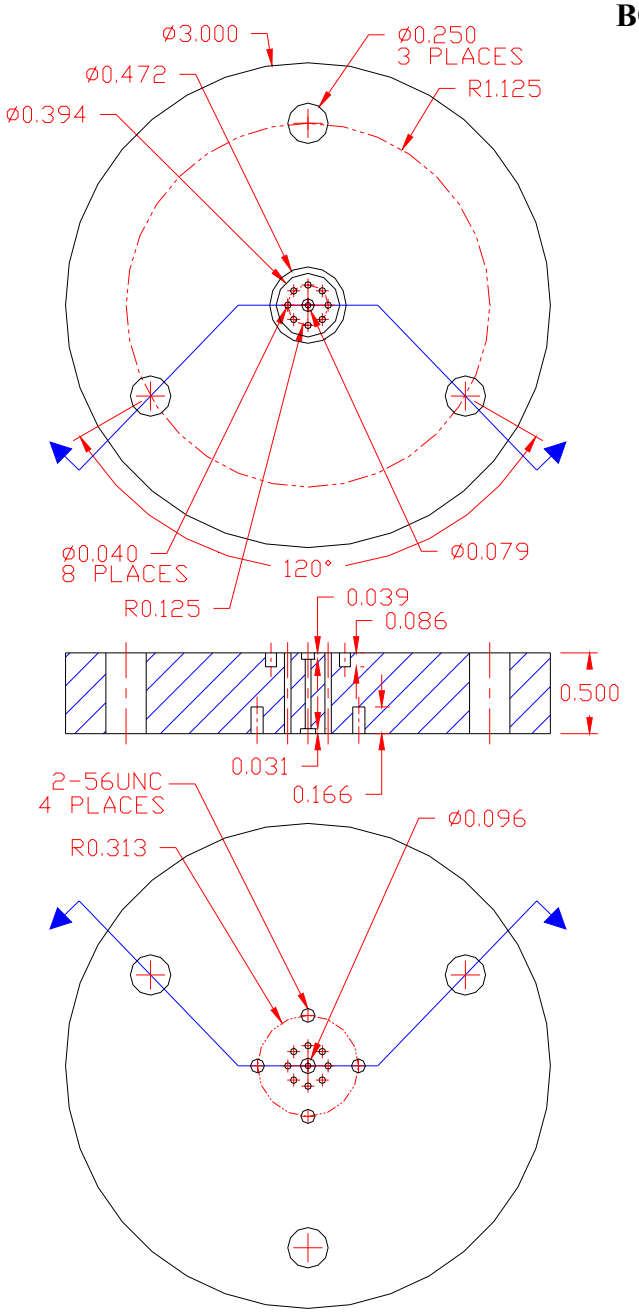

Figure 2.12(g) Component G machined of Macor.

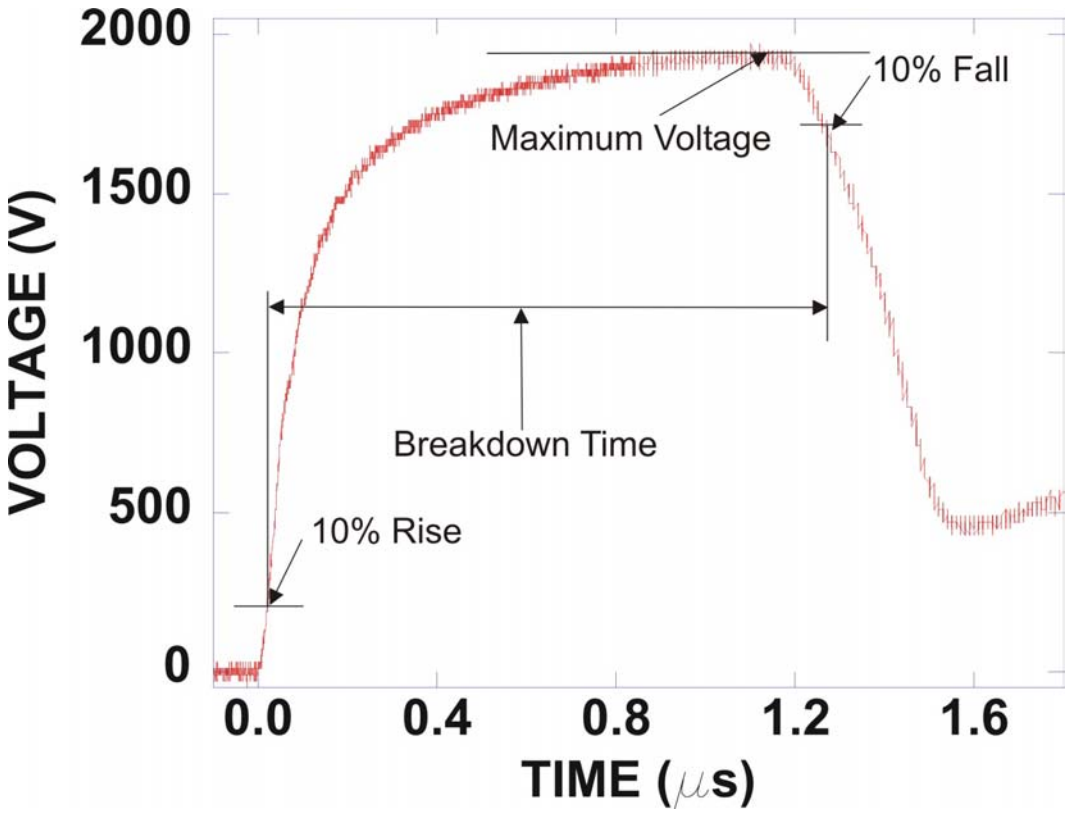

Figure 2.13 The definition of the mean breakdown time as used in the experiments.

2.8 References

1. C. Wagner and S. McCain (private communication, 2002).

2. N. Aoike, M. Hoshino, and A. Iwabuchi, "Automotive HID headlamps, producing compact electronic ballasts using power ICs," Industry Applications Magazine **8** (1), 37 (2002).

3. BREAKDOWN IN PURE ARGON

3.1 Theory of Breakdown

The mean breakdown time reflects the rate at which electrons are created. A simplified reaction mechanism will be presented for pure argon to demonstrate this scaling. A more complete reaction mechanism for argon is in Appendix C.1. The following reactions produce free electrons:

$$e + Ar \rightarrow Ar^+ + e + e \quad \text{(ionization)} \tag{3.1}$$

$$e + Ar^* \rightarrow Ar^+ + e + e \quad \text{(excited state ionization)} \tag{3.2}$$

$$Ar^* + Ar^* \rightarrow Ar^+ + Ar + e \quad \text{(Penning ionization)} \tag{3.3}$$

In addition to diffusion and recombination on the walls, the following reactions result in the removal of free electrons:

$$e + Ar^+ \rightarrow Ar^* \quad \text{(recombination)} \tag{3.4}$$

$$e + e + Ar^+ \rightarrow Ar^* + e \quad \text{(recombination)} \tag{3.5}$$

From these reactions, the rate equation for the electron density is:

$$\begin{aligned}\frac{\partial n_e}{\partial t} = {} & n_e k_{3.1}\left[Ar\right] + n_e k_{3.2}\left[Ar^*\right] + \left[Ar^*\right] k_{3.3}\left[Ar^*\right] \\ & - n_e k_{3.4}\left[Ar^+\right] - n_e{}^2 k_{3.5}\left[Ar^+\right]\end{aligned} \tag{3.6}$$

Neglecting the Penning ionization process because of low excited state densities during breakdown and neglecting the three-body recombination because of the low electron density, the electron density can be directly factored out, and the rate of electron production will be directly linear with the electron density:

$$\frac{\partial n_e}{\partial t} \approx n_e\left[k_{3.1}\left[Ar\right] + k_{3.2}\left[Ar^*\right] - k_{3.4}\left[Ar^+\right]\right] \tag{3.7}$$

It is therefore expected that an increase in initial electron density will result in a linear decrease in the breakdown times.

One other method of increasing the production of electrons is to increase the rate coefficients of the ionization reactions which is accomplished by raising the electron temperature. For example, a general form for such rate coefficients, where *a*, *b*, and *c* are constants, is:

$$k = aT_e^{\,b} e^{\left(\frac{-c}{T_e}\right)} \tag{3.8}$$

The electron temperature can be obtained from a power balance, is elevated above the gas temperature due to heating by the electric field, and is reduced by inelastic collisions. By rearranging the following power balance

$$\begin{array}{ccccc} \dfrac{d}{dt}\left(\dfrac{3}{2}k_b T_e n_e\right) & = & \dfrac{n_e q^2 E^2}{m k_m N} & - & n_e\left(\dfrac{2m_e}{M}\right)k_m N \dfrac{3}{2}k_b\left(T_e - T_g\right) \\ \begin{pmatrix} Total\ energy \\ density \end{pmatrix} & & \begin{pmatrix} j\cdot E \\ power\ deposition \end{pmatrix} & & \begin{pmatrix} power\ loss\ due\ to \\ elastic\ collisions \end{pmatrix} \end{array}$$
$$- n_e N \sum_i k_i \Delta\varepsilon_i$$
$$\begin{pmatrix} power\ loss\ due\ to \\ inelastic\ collisions \end{pmatrix} \tag{3.9}$$

an expression for the electron temperature can be obtained:

$$T_e = T_g + \frac{2}{3k_{boltz}} \frac{1}{\left(\dfrac{2m_e}{M}\right)} \left[\frac{q^2}{m_e k_m^{\,2}} \left(\frac{E}{N}\right)^2 - \frac{\sum_i k_i \Delta\varepsilon_i}{k_m} \right] \tag{3.10}$$

In Equations (3.9) and (3.10), T_g is the gas temperature, k_{boltz} is the Boltzman constant, m_e is the mass of the electron, q is the charge of an electron, M is the mass of the neutral species, N is the density of the neutral species, E is the electric field, k_m is the

rate coefficient for momentum transfer, k_i are the rate coefficients for each specific inelastic reaction, and $\Delta\varepsilon_i$ is the threshold energy for each specific inelastic reaction.

For a given gas composition, T_e is controlled by (electric field)/(gas number density), or E/N. In order to increase the electron temperature, which increases the ionization rate coefficients and hence creates faster breakdown times, the E/N must be increased. Exponential changes are expected when this value is changed. E/N can be changed in three basic ways: increasing the voltage, decreasing the gap across which the voltage is applied, and decreasing the gas pressure. Therefore, exponential decreases in breakdown times are expected by decreasing pressure, increasing voltage, or by decreasing the voltage gap, which can be accomplished with the strategic placement of ground planes.

3.2 Pulse Repetition Frequency (PRF) Effects

Breakdown is subject to statistical and formative time lags. Statistical lag is the time it takes for the "first" electron to become available after the application of voltage and the formative time lag is the time required for the discharge to become established after the first electron is available.[1] The formative lag time is controlled by the gas dielectric property and, for a given gas mixture, depends on the applied reduced field E/N. The statistical lag time depends on the presence of free electrons inside the arc tube volume.[2] In general, without a means of supplying initial electrons, statistical time lag can be on the order of minutes.

Breakdown times as a function of the pulse repetition frequency are in Figure 3.1 for a 2000-V pulse. There is a linear dependence of the mean breakdown time on the

pulse repetition frequency in the pressure range shown from 30 to 70 Torr. Higher frequencies result in shorter breakdown times. The shorter time between pulses reduces the amount of recombination of the electrons, leaving higher initial electron densities for each successive pulse. Lower pressures result in shorter breakdown times due to the larger E/N. Longer breakdown times result in larger standard deviations, indicating impending instability of the discharge. Increasing pressure results in larger deviations until the discharge cannot be sustained, and lowering the PRF has the same result.

3.3 Ground Plane Effects

The importance of the proximity of the ground plane has been realized in commercial lamps and in the patent literature.[3] Commercially, control of the ground plane is achieved by the use of the return ground wire or additional trigger wires. From the previous discussion in Section 3.1, it is apparent that proper placement of the ground plane should increase the E/N and reduce breakdown times. There is another important effect of ground plane placement: the increase of the sidewall capacitance, or the increase in the ability of the sidewall to store electrical charge. For a pulsed system, this increased capacitance should increase the initial electron density, also resulting in faster breakdown times. Numerical simulations of the effects of ground planes, albeit on a different geometry than used in this experiment, demonstrate this trend.[4]

Ground planes can significantly change the characteristics of the discharge as shown in Figure 3.2. In the case where there is no external wire (the ground plane), the discharge is unchanged. When one wire is placed in proximity to the discharge tube, the discharge tends to move toward it, and a more distinct glow is visible. When two wires

were placed on the side of the discharge tube the arc moved to the walls and closely followed the path from the ground plane to ground plane because of the increased capacitance on the walls.

The locations of the actual ground planes used for this experiment are shown in Figure 3.3. Solder wire, which is malleable, was used for these structures. The pulse was maintained at 150 Hz and 2000 V. Voltage waveforms without a ground plane are shown in Figure 3.4. Extended breakdown times occur with increasing pressure. The effects of the ground plane being placed directly on the glass on breakdown characteristics are shown in Figure 3.5. Breakdown is more rapid and the waveforms have a "double peak." This could be due to having two breakdown sequences. Since the anode is powered, it could initially break down between the anode and the ground plane, causing capacitive charging of the walls, and then breaking down to the cathode.

Mean time to breakdown time as a function of pressure is shown in Figure 3.6: when having no ground plane, a ground plane directly placed on the glass, and a ground plane placed ≈2 mm from the glass. The closer proximity of the ground plane decreases the breakdown time. As the ground plane is moved away from the discharge, the breakdown time will increase until the ground plane is further away than the distance between the anode and the cathode.

3.4 Figures

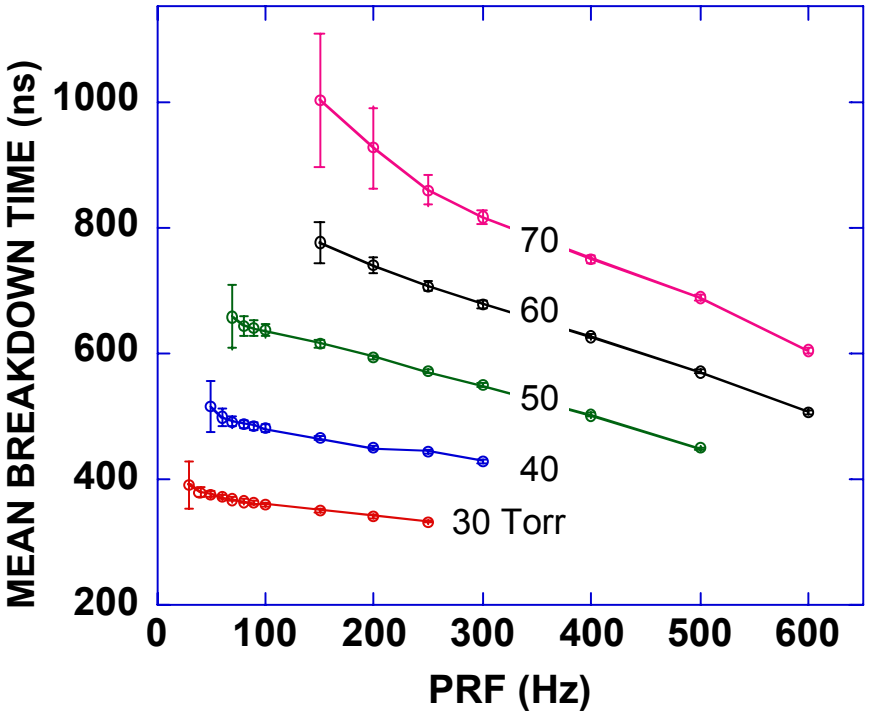

Figure 3.1 Mean breakdown time vs. PRF at various pressures for a 2000-V pulse.

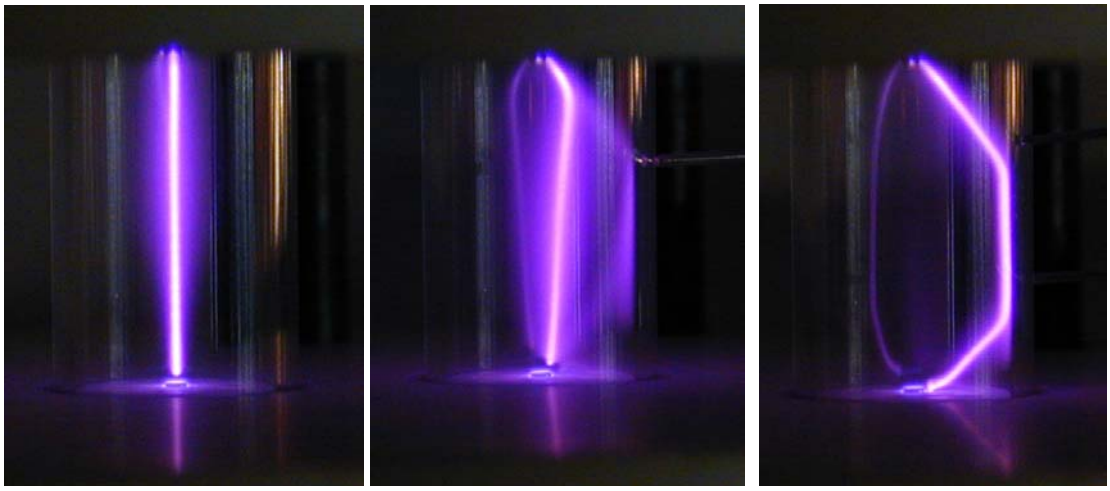

(a) (b) (c)

Figure 3.2 Discharge with (a) no ground plane, (b) one wire, and (c) two wires.

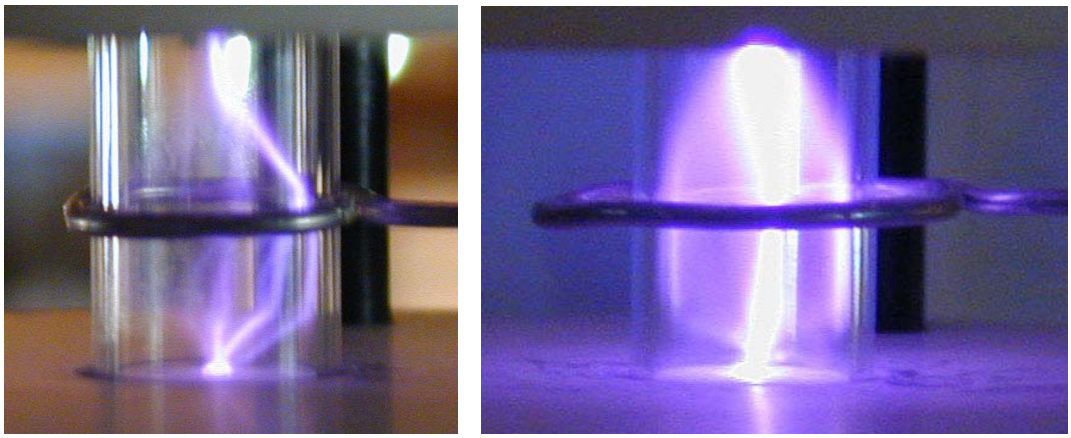

(a) (b)

Figure 3.3 Locations of the ground planes (a) directly on the glass, and (b) ≈2 mm off the glass.

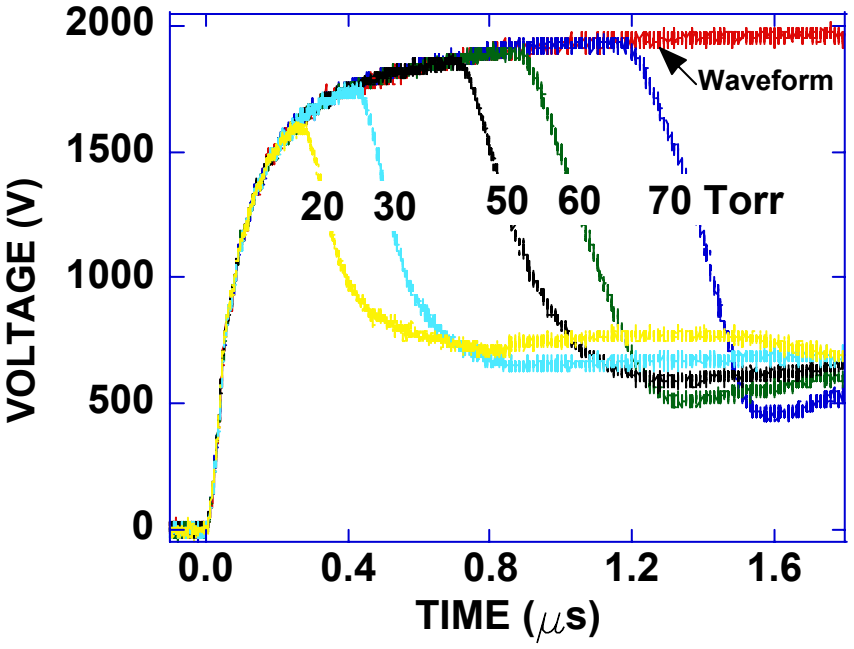

Figure 3.4 Waveform for a 150-Hz, 2000-V pulse with no ground plane.

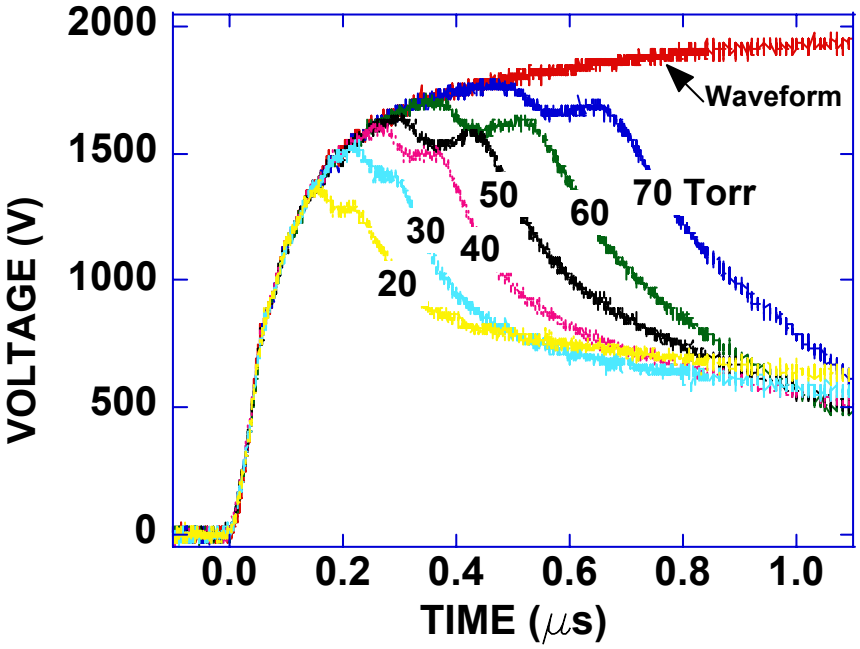

Figure 3.5 Waveform for a 150-Hz, 2000-V pulse with the ground plane directly on the glass.

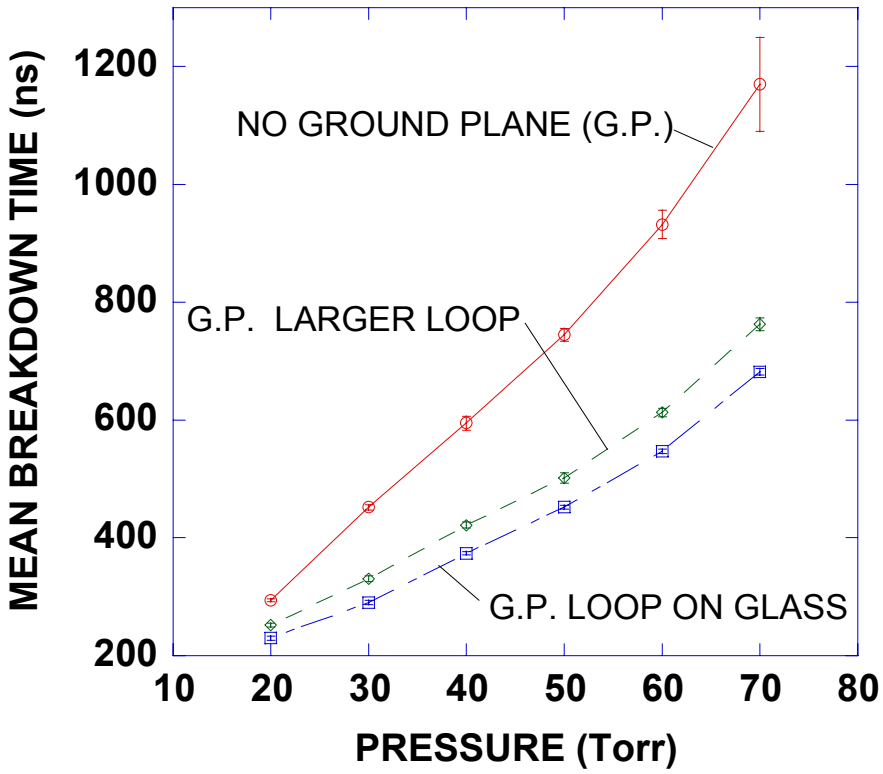

Figure 3.6 Mean breakdown time vs. pressure for a 150-Hz, 2000-V waveform for various ground plane locations.

3.5 References

1. W. B. Maier, A. Kadish, C. J. Buchenauer, and R. T. Robiscoe, "Electrical discharge initiation and a macroscopic model for formative time lags," IEEE Transactions on Plasma Science **21** (6), 676 (1993).

2. W. W. Byszewski, Y. M. Li, A. B. Budinger, and P. D. Gregor, "Advances in starting high intensity discharge lamps," Plasma Sources Science and Technology **5**, 720 (1996).

3. E. G. Fridrich and R. S. Bergman, "Short-arc discharge lamp with starting device," United States Patent 4,053,809. Filed June 18, 1976; granted October 11, 1977.

4. B. Lay, R. Moss, S. Rauf, and M. J. Kushner, "Breakdown processes in metal halide lamps," Plasma Sources Science and Technology **12** (1), 8 (2003).

4. BREAKDOWN IN ARGON/XENON MIXTURES

4.1 Overview

A few modifications to the experimental breakdown measurements in pure argon were made for the argon/xenon mixture. The most influential change was the addition of the UV source. Zaslavsky et al.,[1] and Byszewski and Budinger[2] investigated the time it takes for lamps to break down with and without a UV source and found that the addition of a source reduced the statistical time lag by providing a reliable external source of free electrons. Small UV sources[1,2] have been used commercially, and are positioned within the glass shroud that encloses the lamp. Free electrons are produced by either photoemission from the cathode or arc tube or by photoionization of metal vapor. From these findings and the need to avoid high frequency gas heating, a mercury pen-lamp was used as a photoionization source for this experiment.

To evaluate the effects the mercury lamp illumination had on this system, experiments were conducted with and without the mercury lamp at various frequencies at a constant pressure and voltage. The mean breakdown times as a function of PRF at 30 Torr for a 1500 V pulse are shown in Figure 4.1. Without the mercury lamp, the standard deviations became very large at around 80 Hz. The discharge did not occur below 70 Hz due to the lack of seed electrons. With the lamp turned on, the ignition of the discharge did not require high pulse repetition frequencies. The breakdown time decreased with higher PRF as expected; however, at lower frequencies the same was also true. This decrease in breakdown time may be attributed to larger initial electron densities resulting from longer times between breakdowns. More charging of the walls may occur as a

result of photoionization from the mercury lamp. The differences in breakdown times "early" and "later" are primarily caused by two reasons. The data from the "early" curve was taken when the experimental apparatus had not come into thermal equilibrium, possibly due to the mercury lamp being directly on the Macor surface. Second, based on manufacturer's specifications, stabilized UV output from the pen-lamp requires 30 min. warm up.

For the archival experiments, the mercury lamp was turned on at least a half hour before use, and the mercury lamp was rested on high-temperature foam to insulate it from the experimental apparatus, allowing the experiment to reach a steady state sooner. The PRF was chosen to be 1 Hz for further measurements because that is where the maximum breakdown time occurred. Performing experiments at this value would presumably allow larger fluctuations to be seen and allow easier recognition of trends.

Voltage waveforms at various pressures for pure argon and a 10% xenon in argon mixture are shown in Figures 4.2 and 4.3, respectively. The decrease in breakdown time with lower pressure is again observed, as was discussed in Chapter 3, and a decrease in the breakdown time is also observed with the addition of 10% xenon.

4.2 Xenon Compositional Effects

Electron impact rate coefficients are defined as the average of the product of the cross section and the velocity of the electron:

$$\begin{aligned} k &= \langle \sigma_0 \nu \rangle \\ &= \int_0^\infty f(\varepsilon)\sigma_0(\varepsilon)\nu d\varepsilon \end{aligned} \tag{4.1}$$

where ε is the energy, σ_0 is the cross section as a function of energy, ν is the speed of the electron, and f(ε) is the energy distribution function normalized as

$$\int_0^\infty f(\varepsilon)\, d\varepsilon = 1 . \tag{4.2}$$

Note that the ionization and momentum transfer cross sections are larger for xenon compared to argon (see Appendix C.) Xenon also has a lower threshold energy for ionization. The electron temperature is inversely dependent upon the momentum transfer coefficient. As xenon has larger rates of momentum transfer, one expects lower T_e and longer breakdown times at large xenon concentrations.

The mean breakdown times as a function of voltage at fixed argon/xenon compositions and various pressures are shown in Figures 4.4(a)-(g). The fixed compositions were at 0, 5, 10, 20, 40, 60, and 100% xenon in argon. The breakdown time decreases with pressure and with an increase in voltage, and both trends change exponentially as discussed in Chapter 3. These characteristics are the same regardless of the change in composition, owing to the fact that these trends depend on E/N. For each composition, the discharge becomes unstable at approximately the same breakdown time regardless of the pressure, but these times do depend on composition.

The mean breakdown time as a function of the xenon fraction in argon for a fixed voltage pulse at various pressures is shown in Figures 4.5(a)-(n). The voltage pulses were reduced from the maximum value of 2000 V by 100 V until no discharge could be sustained. The mean breakdown time decreases with pressure. It is interesting to note that the minimum in the breakdown time occurs at xenon fractions of 5-20% depending on the value of E/N. At lower E/N the compositional affects are more pronounced. This

means that larger dips occur at higher pressures and lower voltages. Similar effects occur when the pressure is fixed and the voltage is varied, as shown in Figures 4.6(a)-(f). Due to scaling effects, it may appear that there is no variation at higher E/N. The same trend can indeed be seen, with an expanded scale, in Figure 4.6(f).

At many pressures only the low composition xenon mixtures resulted in stable discharges, as shown in Figure 4.5(h) for a 1300-V pulse. At this voltage, only a 5-20% xenon composition results in a discharge for 50 Torr and even smaller range of 5-10% for 70 and 90 Torr. Pure argon or pure xenon cannot be broken down at these pressures and voltage.

Several studies of argon/xenon mixtures have been performed.[3-6] The overall kinetics of argon/xenon is quite complicated and a diagram showing these processes is shown in Figure C.2. Reaction mechanisms for argon and xenon are in Appendix C. Even though the mechanisms are quite complex, the compositional dependence can be explained by the fact that xenon has a larger momentum transfer cross section than argon and has a lower ionization potential. Since the mean breakdown time reflects the rate at which electrons are created, the breakdown time is reduced with a few percent xenon due to the lower energy required to ionize xenon. The breakdown time starts to increase at higher concentrations of xenon because the plasma becomes more collisional and the electron temperature decreases. The effect is less dramatic at lower pressures due to the overall higher electron temperature.

Several benefits can be taken advantage of with the reduced mean breakdown time. Longer lamp lives can be expected because of the possibility of running at lower voltages for the same initial pressure. Warm restarting times should be decreased

because the discharge can be realized at higher pressures. The relationship between the maximum pressure at which the discharge can occur for a constant voltage, the maximum breakdown time before becoming unstable, and the mean breakdown time as a function of xenon composition in argon are shown in Figure 4.7. All have the same dependence on the xenon composition. The curve for breakdown at 1900 V and 70 Torr was offset to match the average maximum time before an unstable discharge occurred.

4.3 Figures

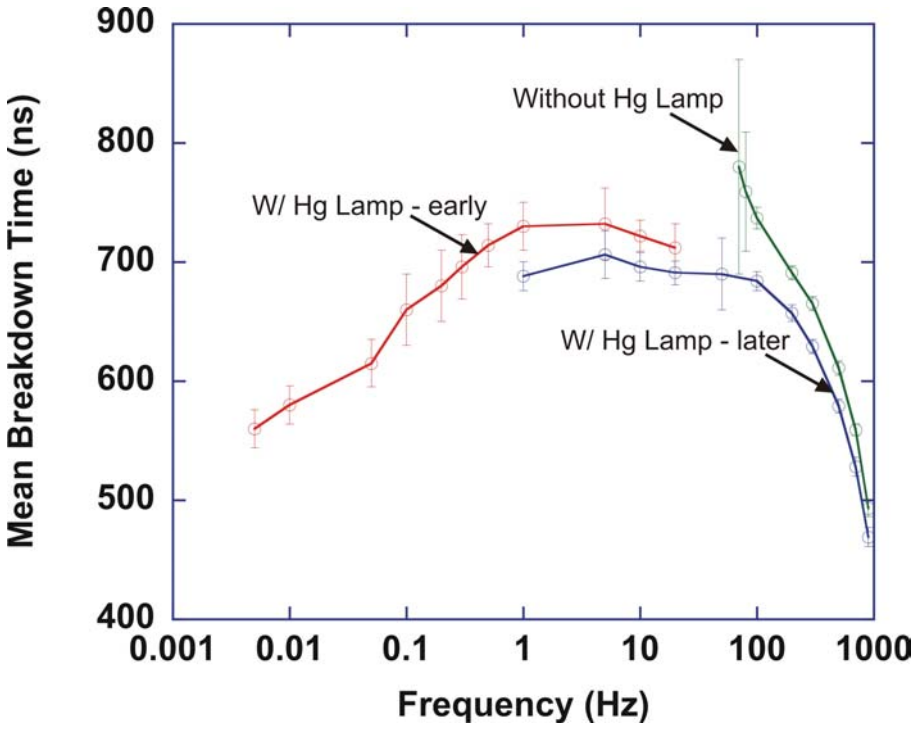

Figure 4.1 Mean breakdown time as a function of PRF with and without the mercury lamp at 30 Torr and a 1500-V pulse.

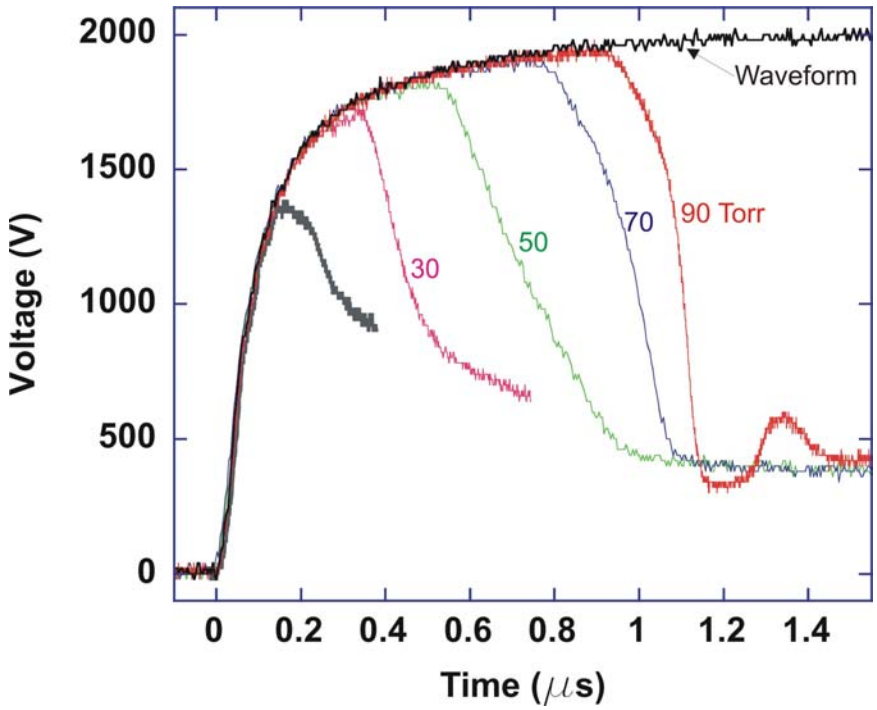

Figure 4.2 Pure argon discharge with a 1-Hz, 2000-V pulse and a UV light at various pressures.

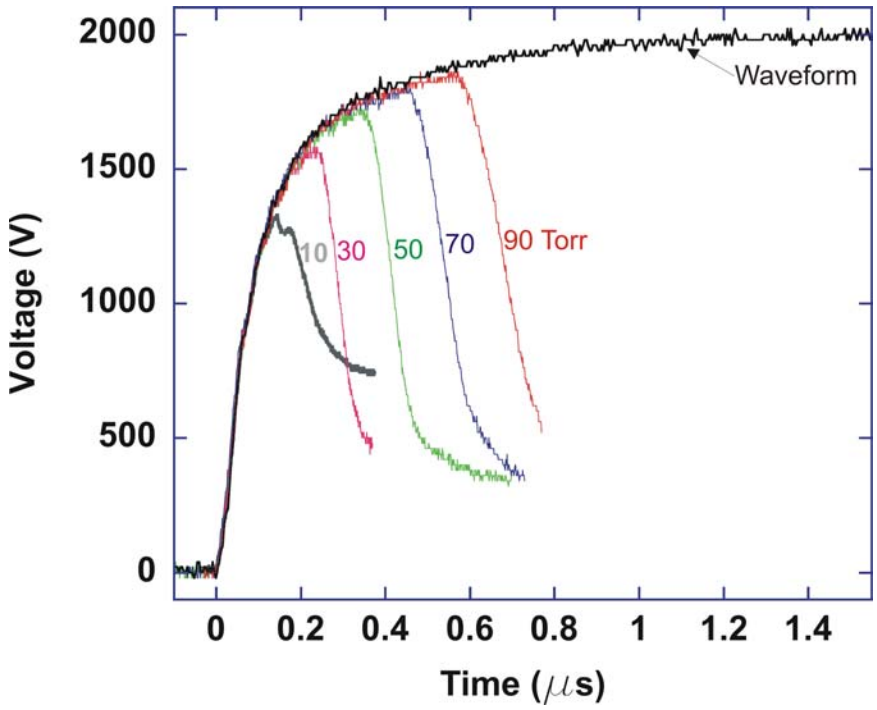

Figure 4.3 Argon/xenon discharge of 10% xenon with a 1-Hz, 2000-V pulse and a UV light at various pressures.

Figures 4.4 Mean breakdown time vs. voltage at various pressures at a constant xenon fraction in argon.

(a) 0% Xenon
(b) 5% Xenon
(c) 10% Xenon
(d) 20% Xenon
(e) 40% Xenon
(f) 60% Xenon
(g) 100% Xenon

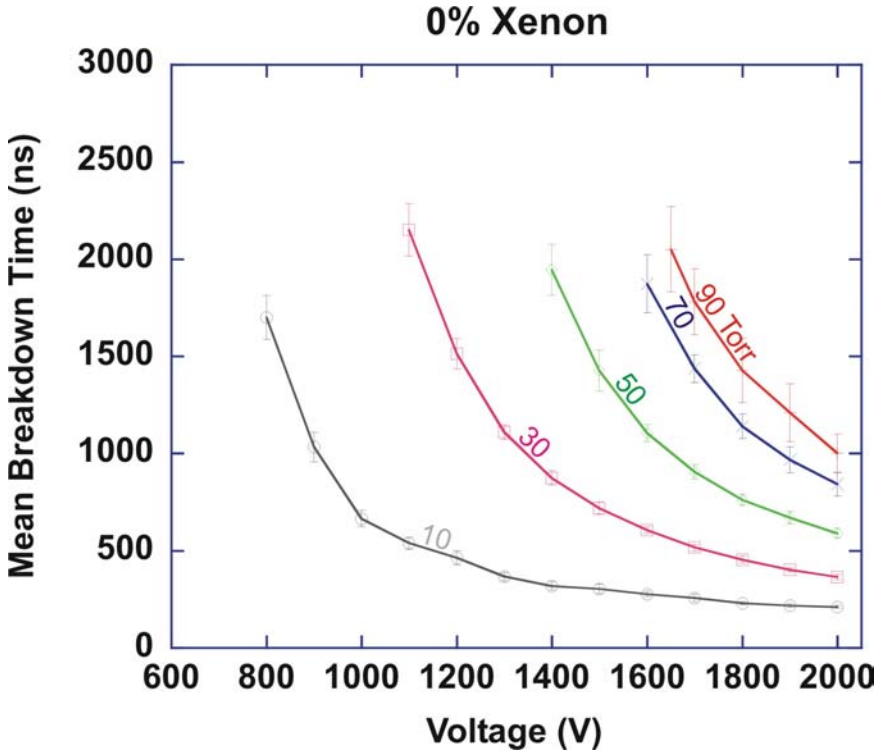

Figure 4.4(a) Xenon composition of 0%.

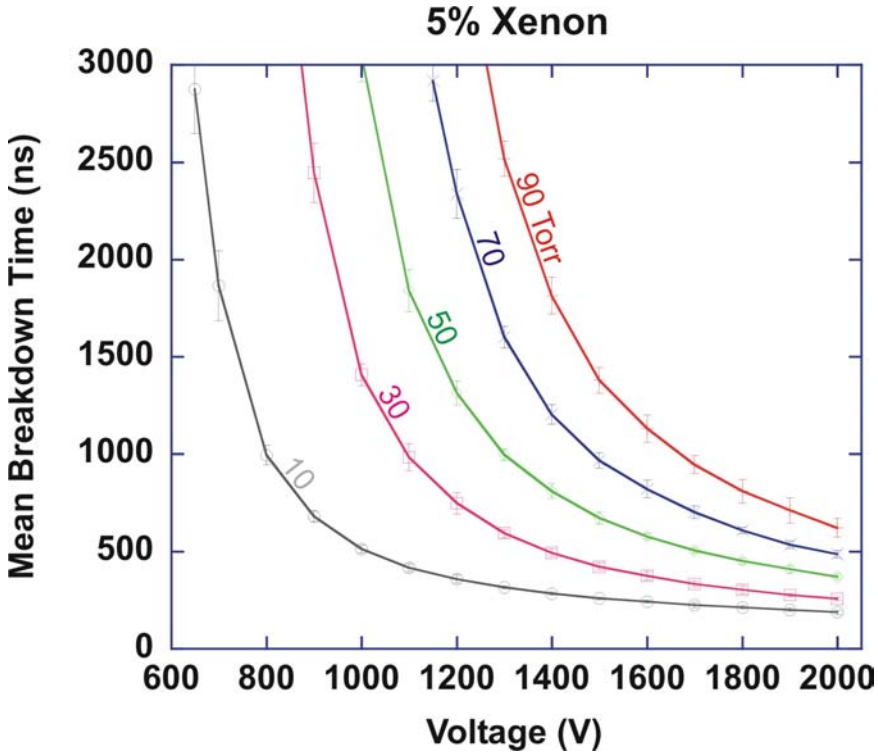

Figure 4.4(b) Xenon composition of 5%.

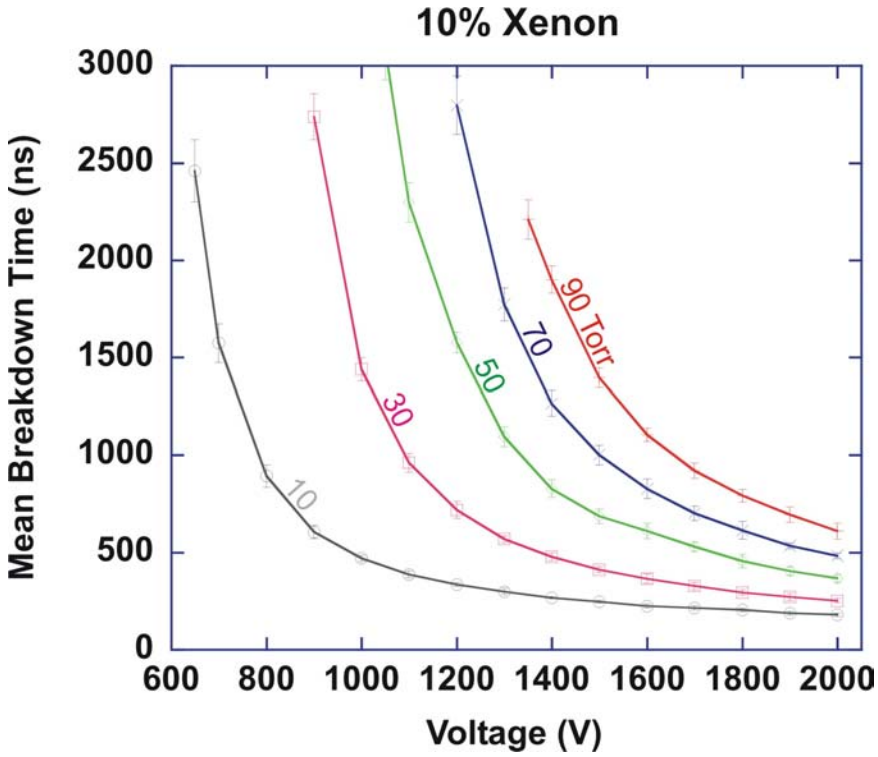

Figure 4.4(c) Xenon composition of 10%.

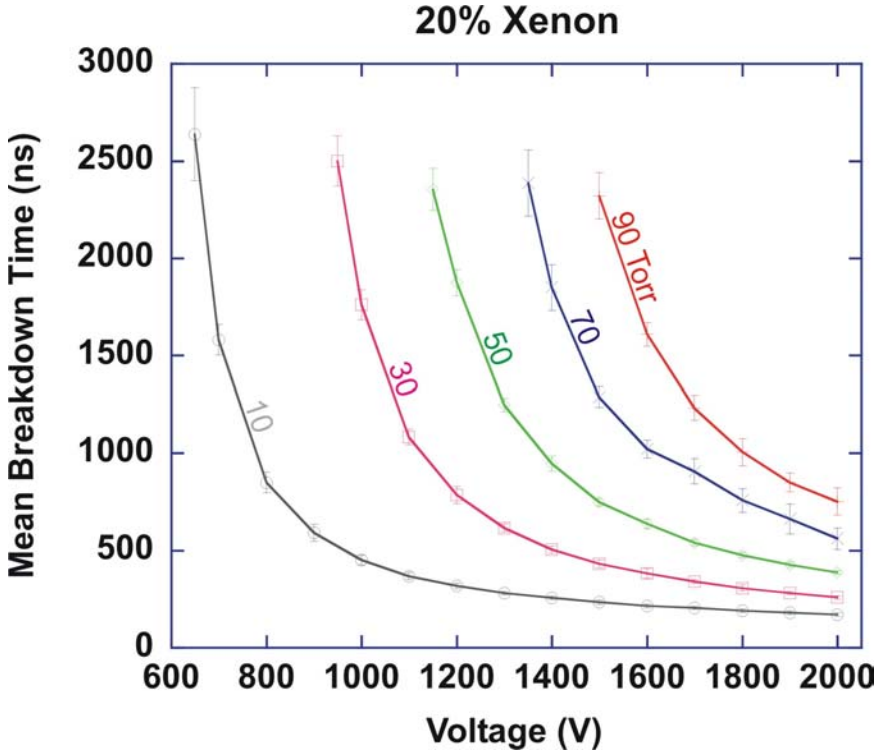

Figure 4.4(d) Xenon composition of 20%.

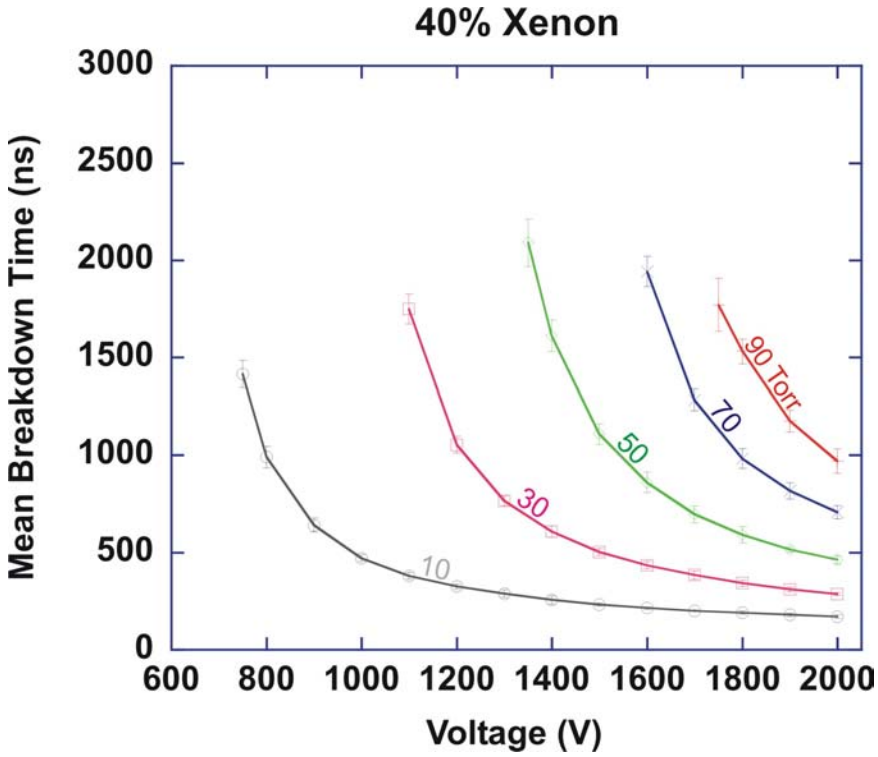

Figure 4.4(e) Xenon composition of 40%.

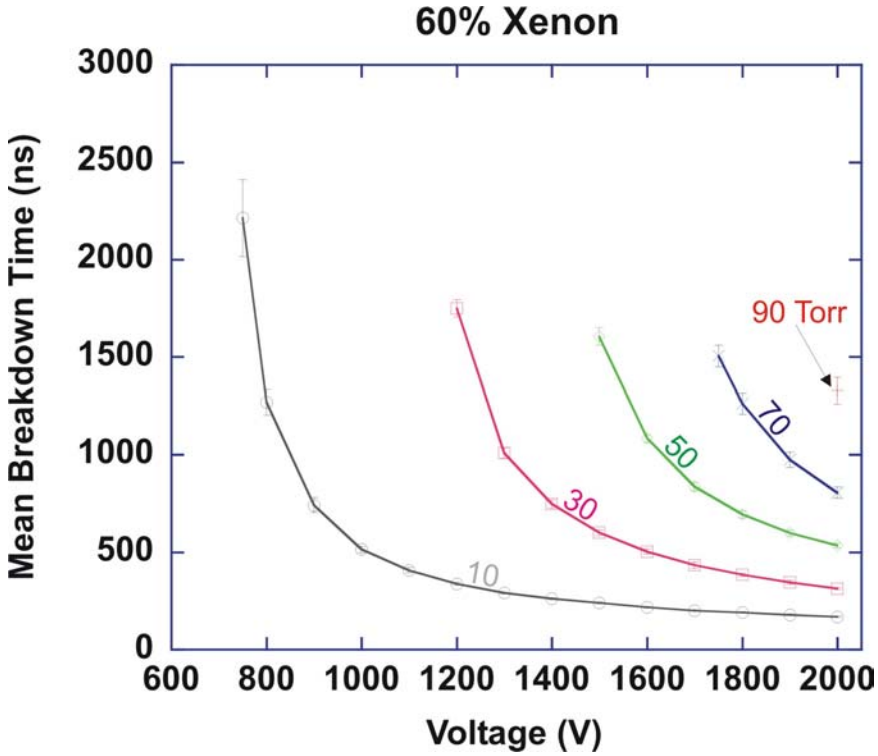

Figure 4.4(f) Xenon composition of 60%.

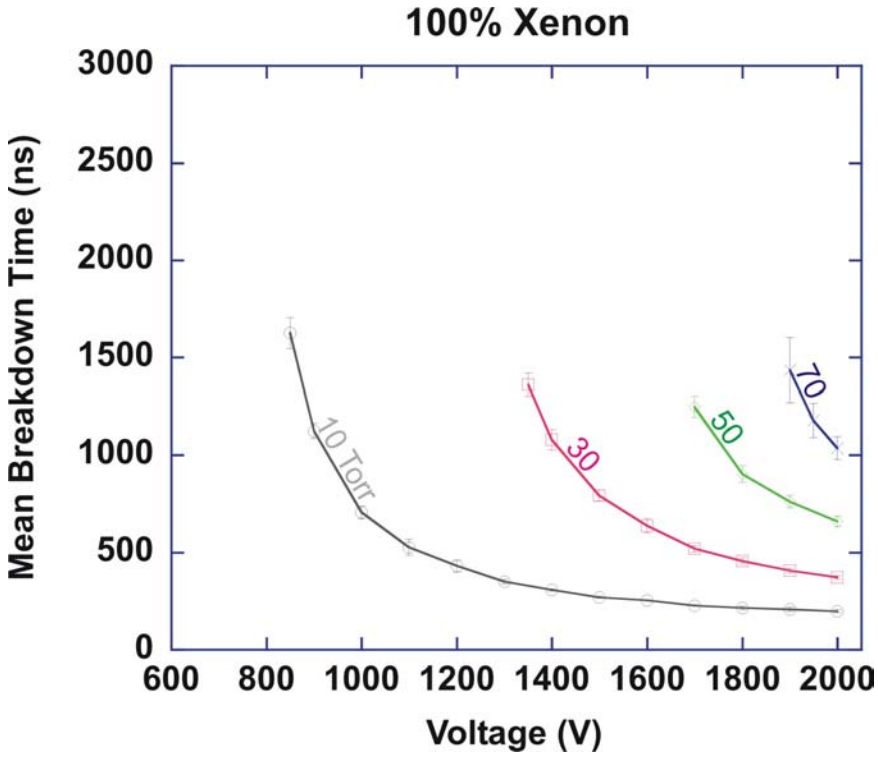

Figure 4.4(g) Xenon composition of 100%.

Figures 4.5 Mean breakdown time vs. xenon fraction in argon at various pressures with a constant 1-Hz voltage pulse.

(a) 2000 V
(b) 1900 V
(c) 1800 V
(d) 1700 V
(e) 1600 V
(f) 1500 V
(g) 1400 V
(h) 1300 V
(i) 1200 V
(j) 1100 V
(k) 1000 V
(l) 900 V
(m) 800 V
(n) 700 V

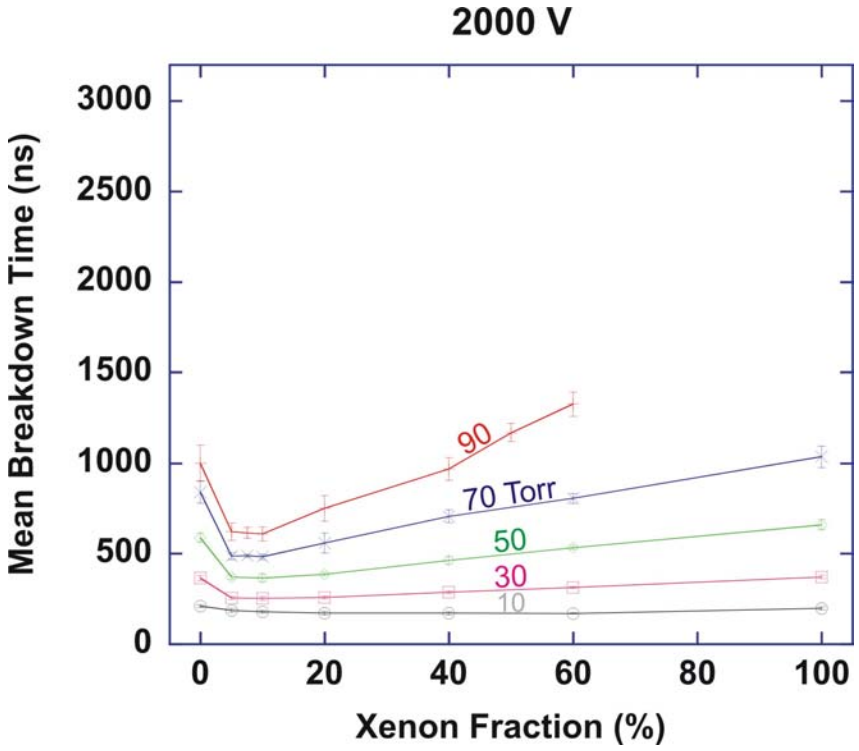

Figure 4.5(a) 2000-V pulse.

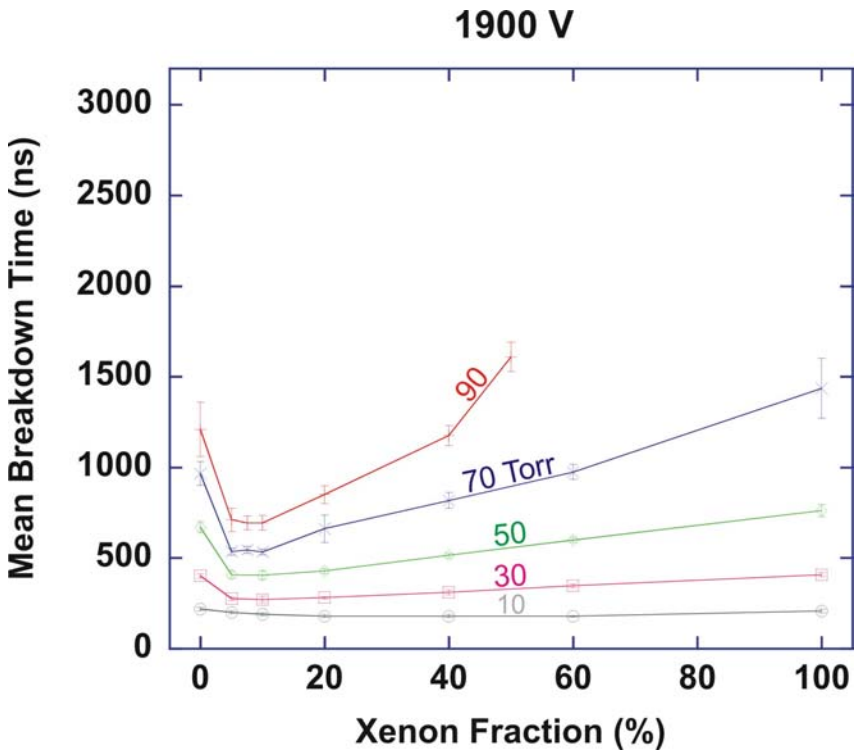

Figure 4.5(b) 1900-V pulse.

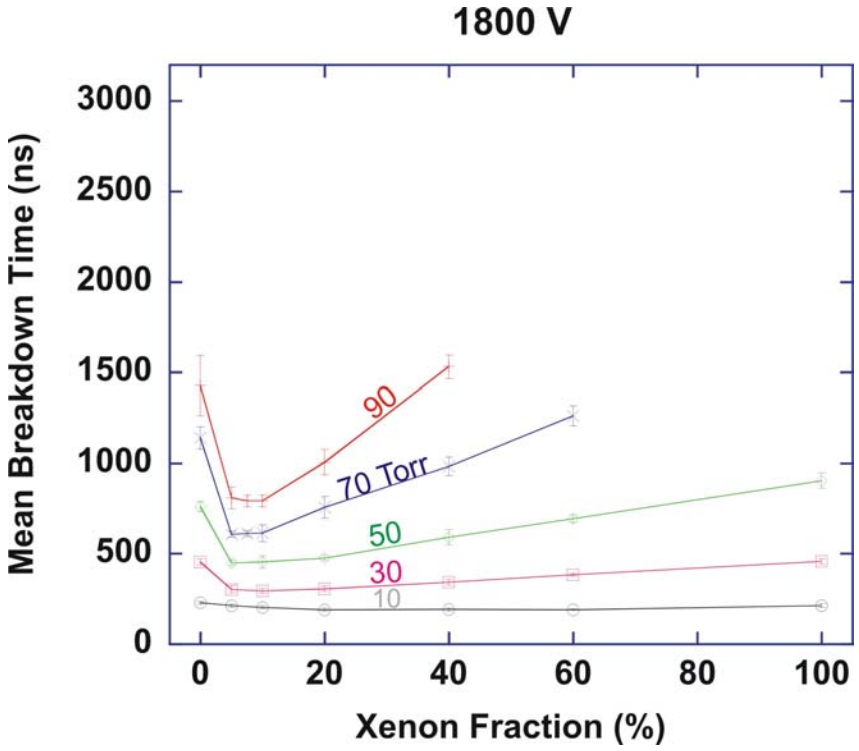

Figure 4.5(c) 1800-V pulse.

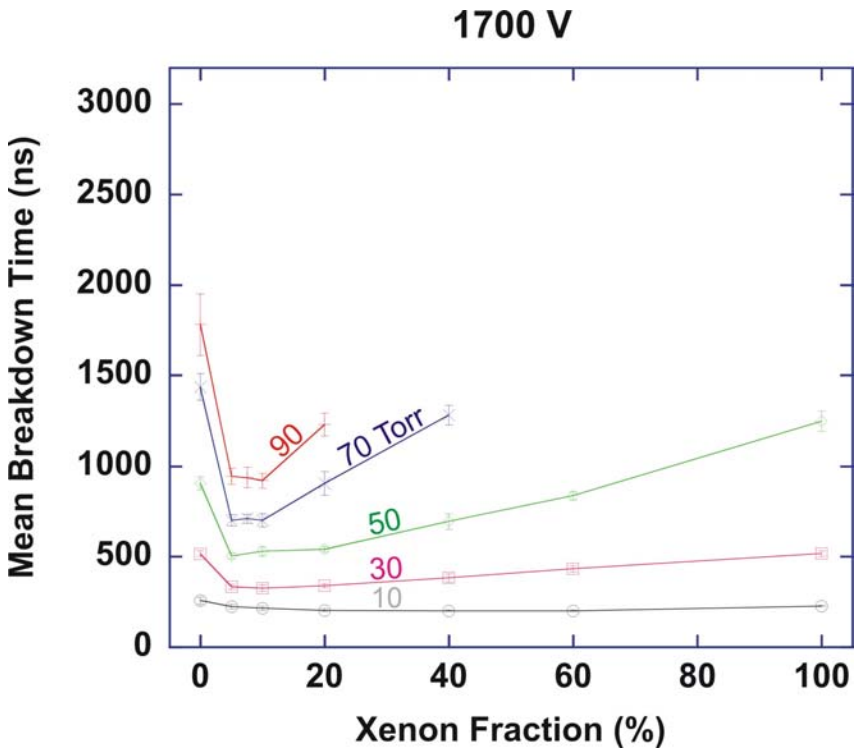

Figure 4.5(d) 1700-V pulse.

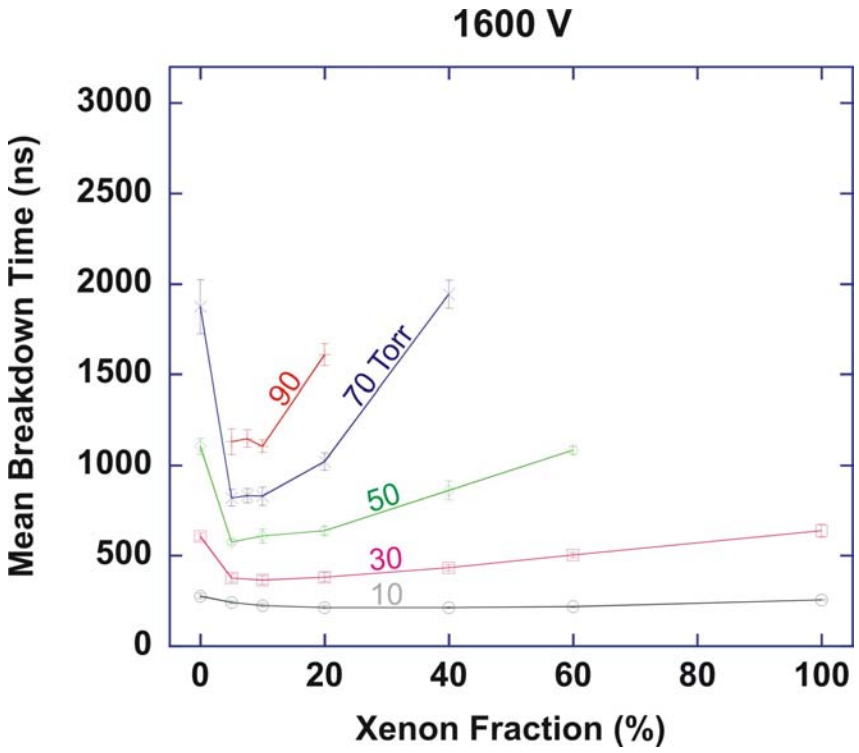

Figure 4.5(e) 1600-V pulse.

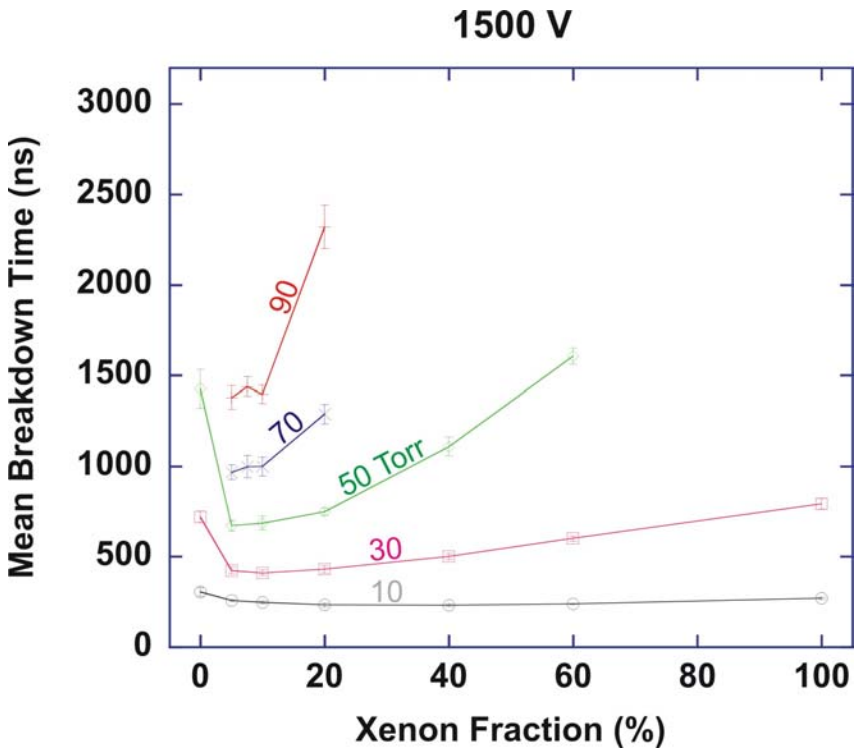

Figure 4.5(f) 1500-V pulse.

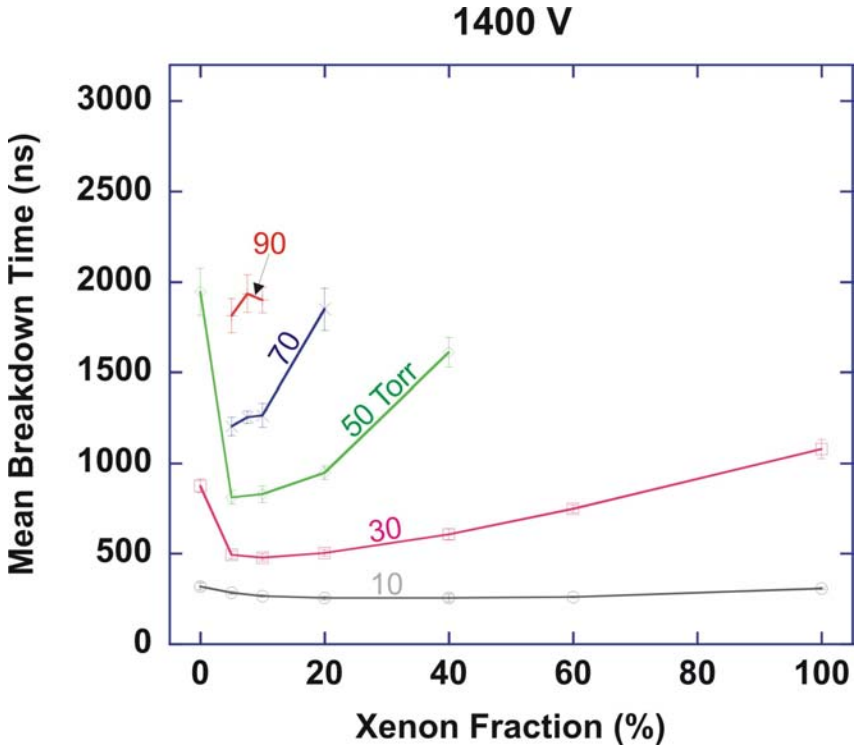

Figure 4.5(g) 1400-V pulse.

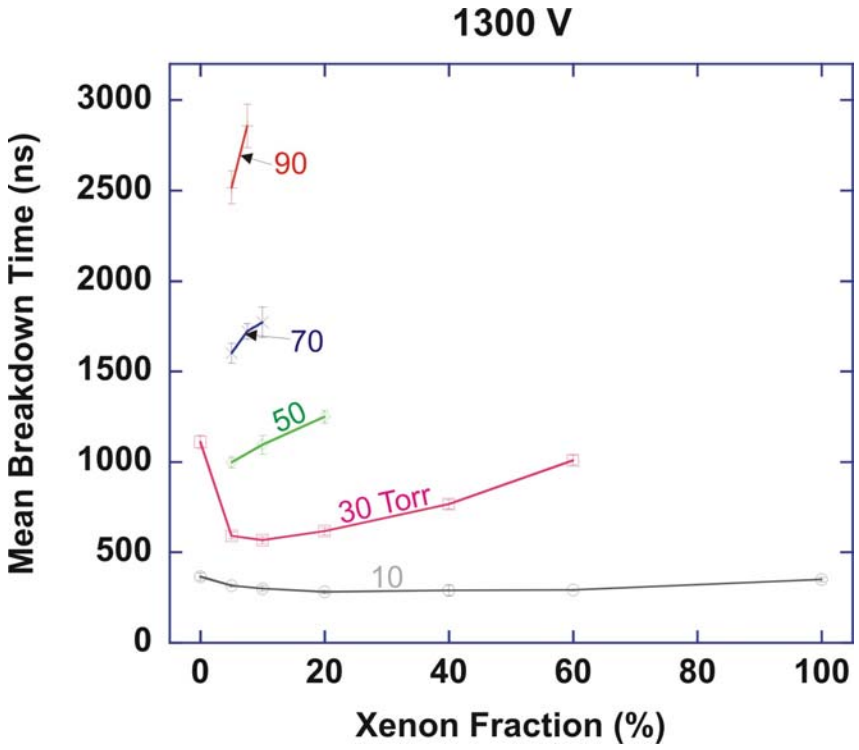

Figure 4.5(h) 1300-V pulse.

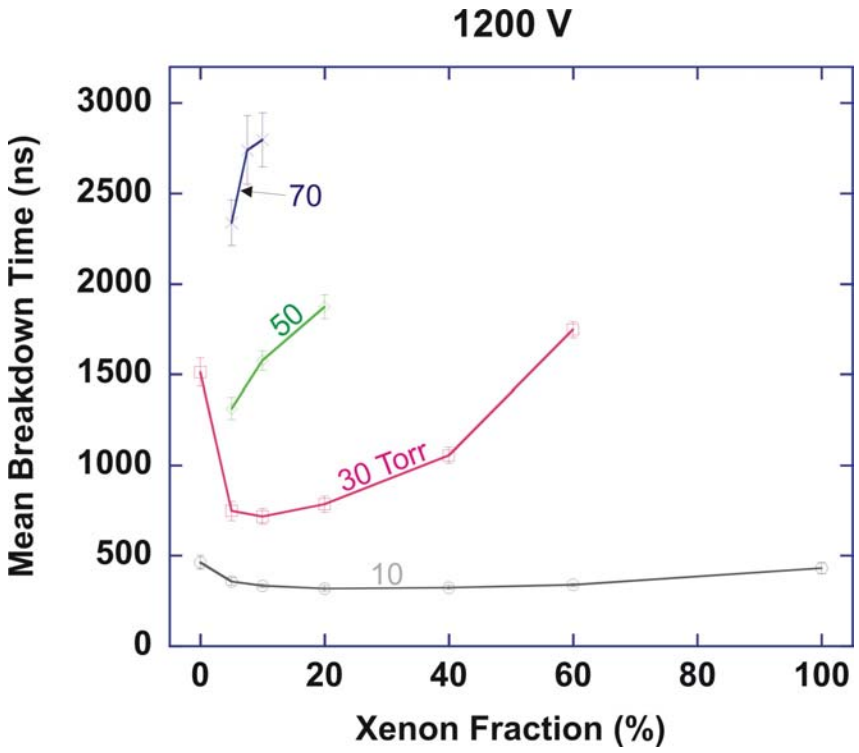

Figure 4.5(i) 1200-V pulse.

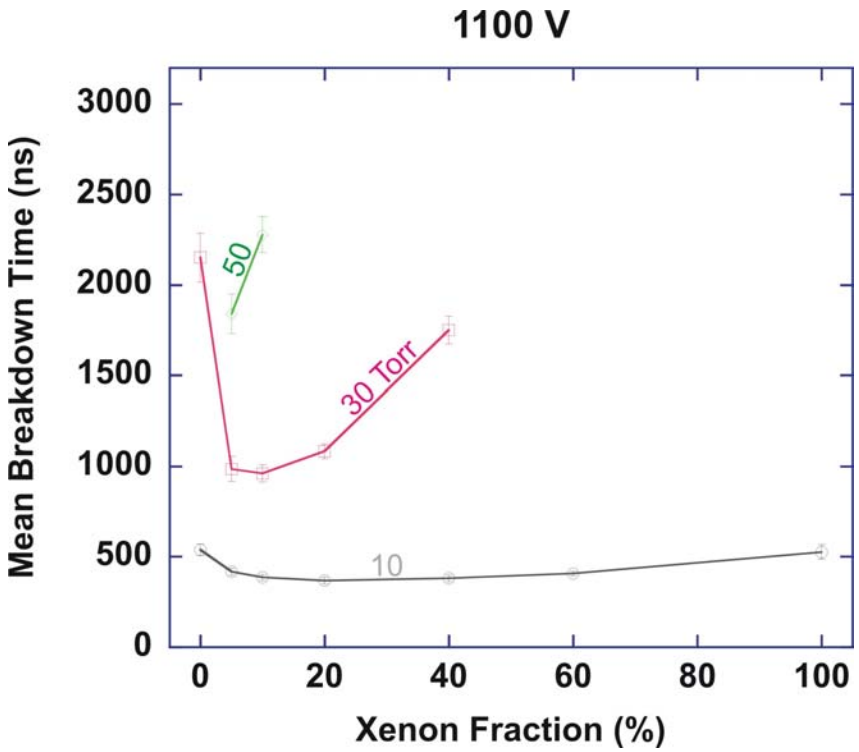

Figure 4.5(j) 1100-V pulse.

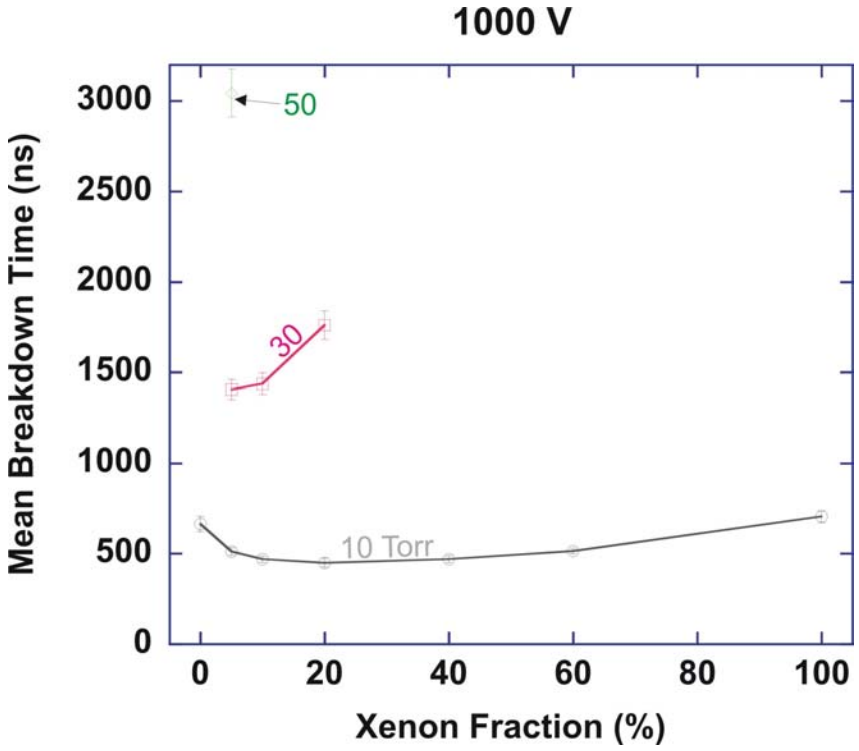

Figure 4.5(k) 1000-V pulse.

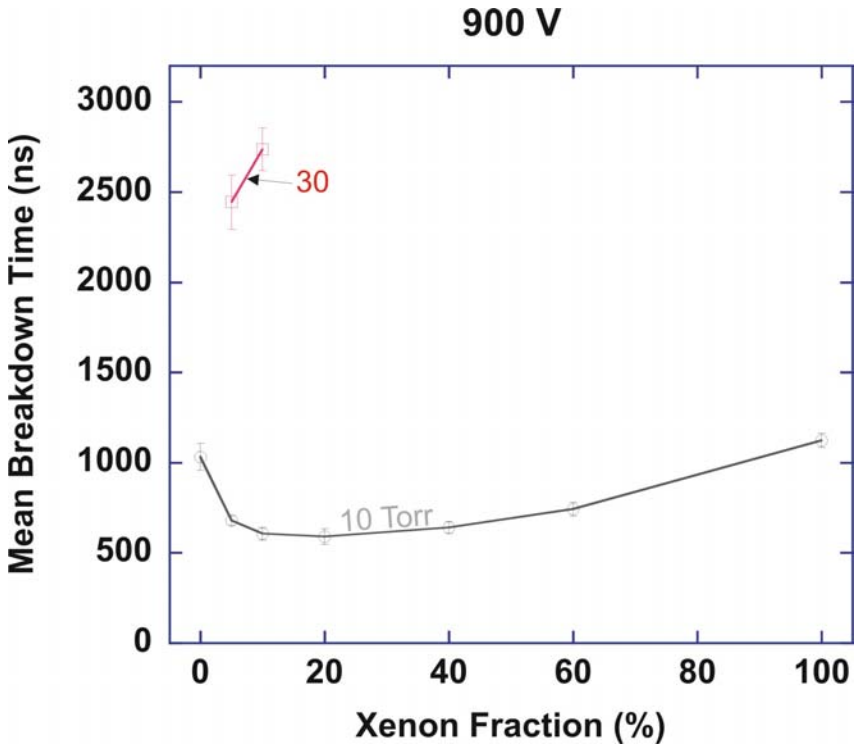

Figure 4.5(l) 900-V pulse.

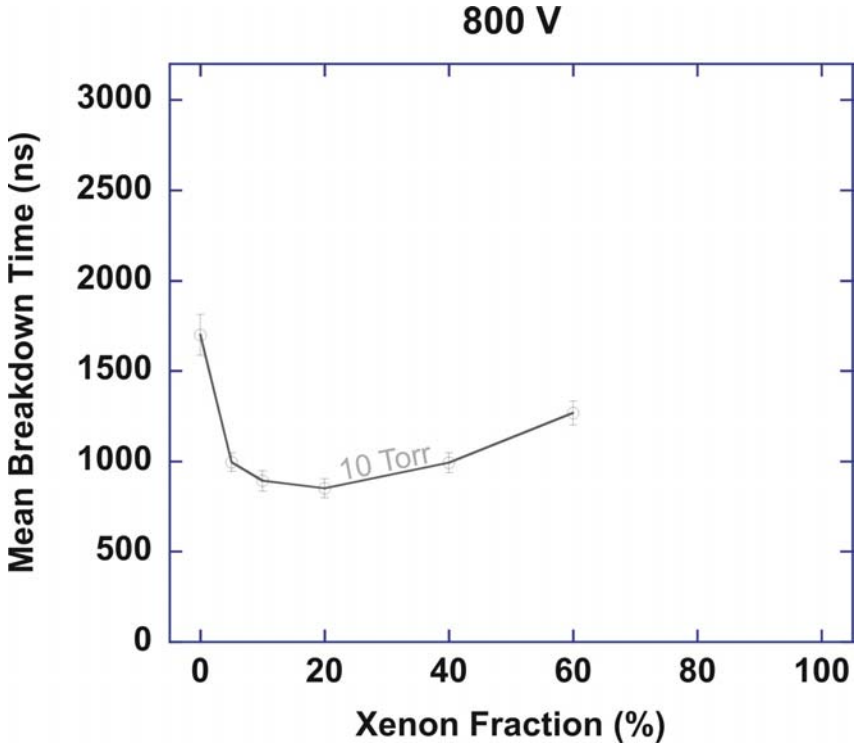

Figure 4.5(m) 800-V pulse.

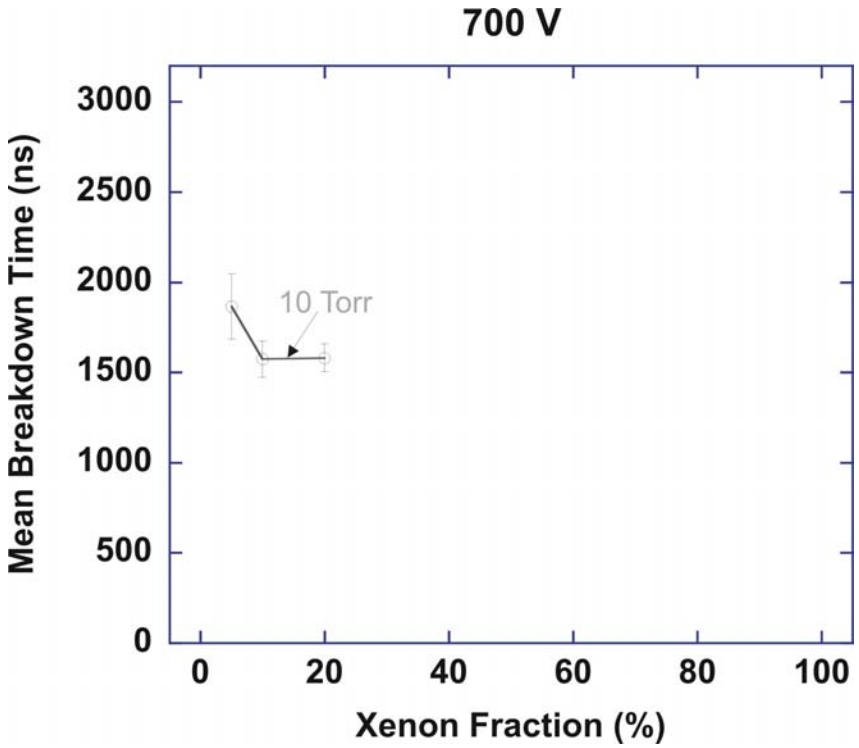

Figure 4.5(n) 700-V pulse.

Figures 4.6 Mean breakdown time vs. xenon fraction in argon at various voltages at a constant pressure.

(a) 90 Torr
(b) 70 Torr
(c) 50 Torr
(d) 30 Torr
(e) 10 Torr
(f) 10 Torr

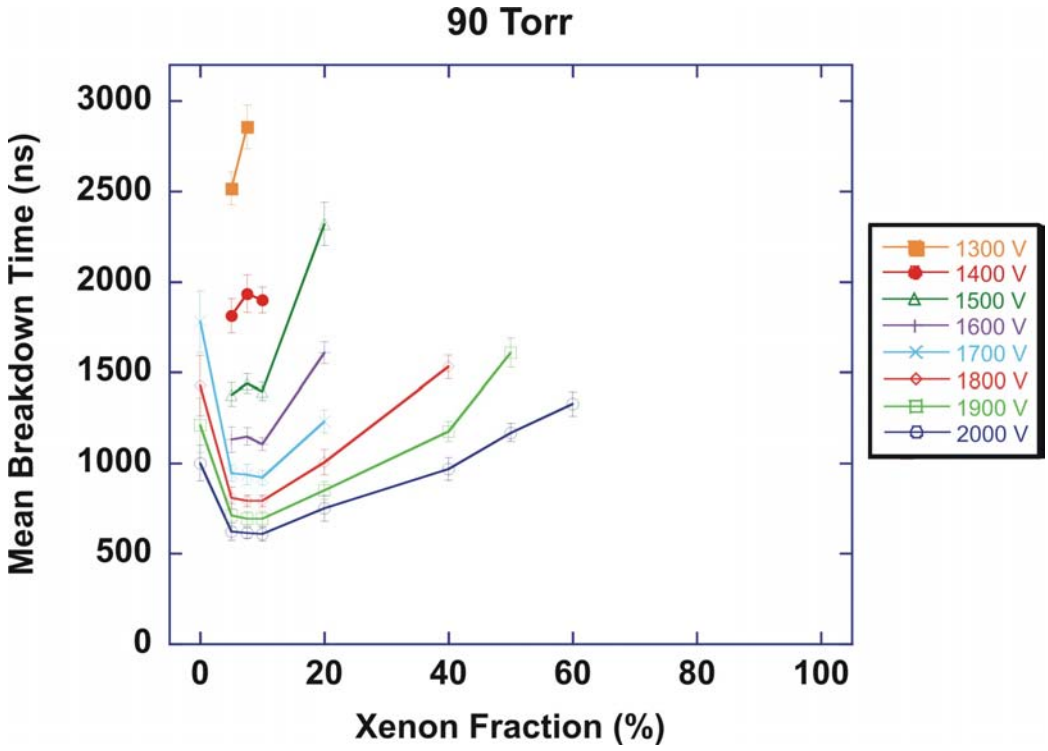

Figure 4.6(a) 90 Torr.

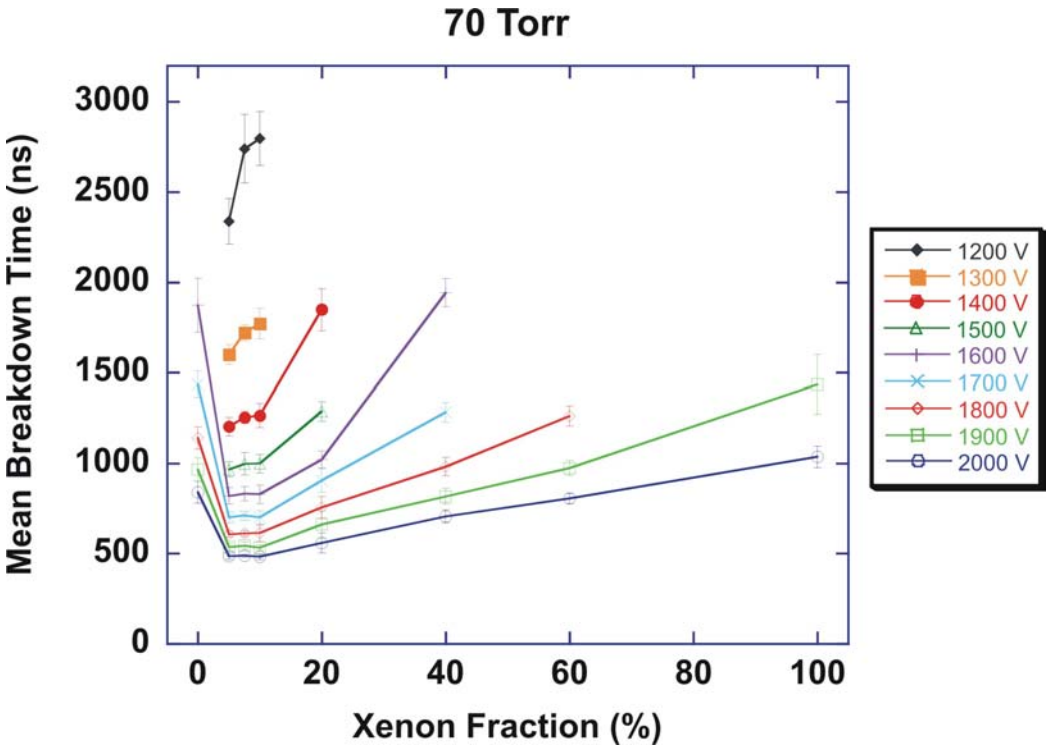

Figure 4.6(b) 70 Torr.

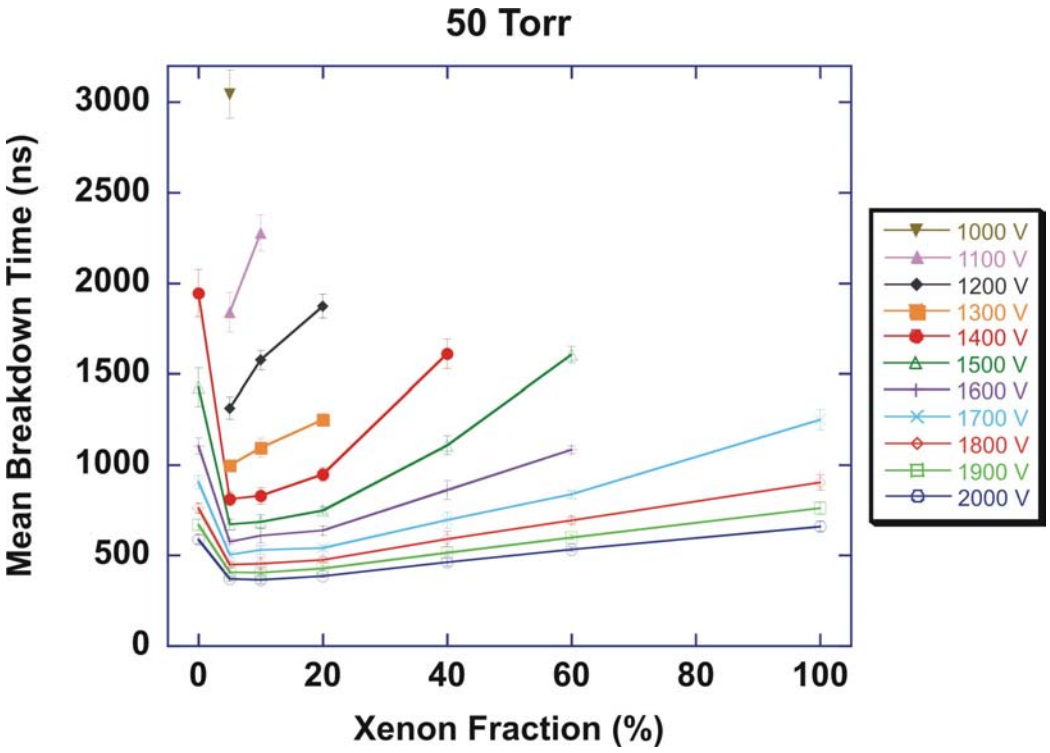

Figure 4.6(c) 50 Torr.

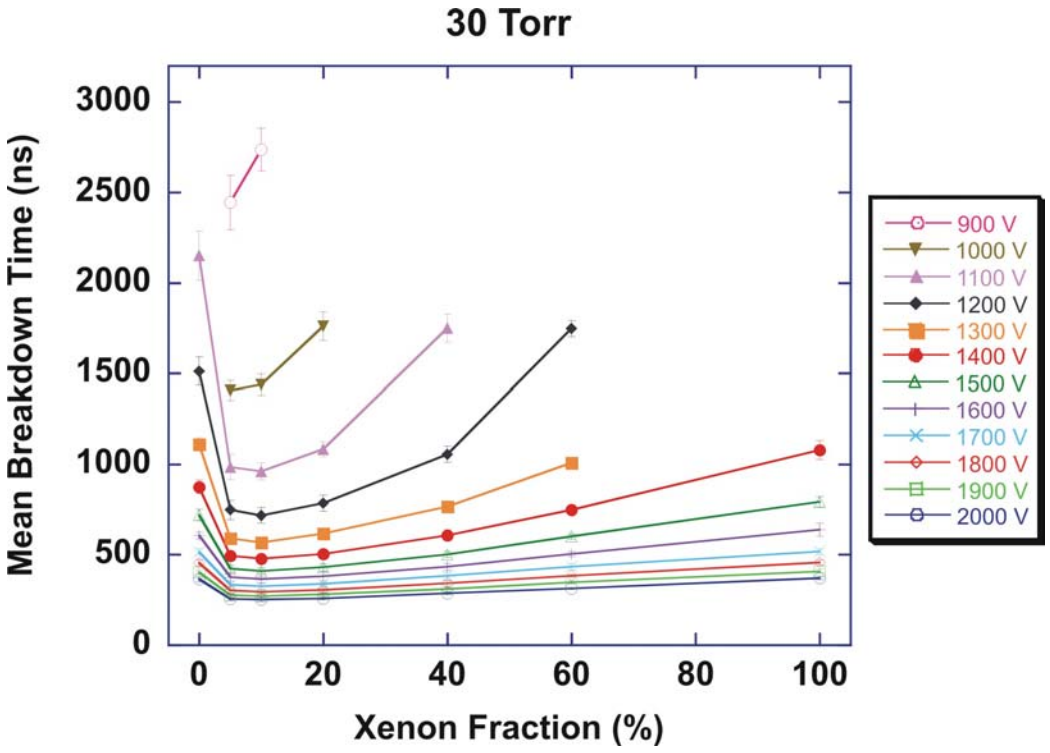

Figure 4.6(d) 30 Torr.

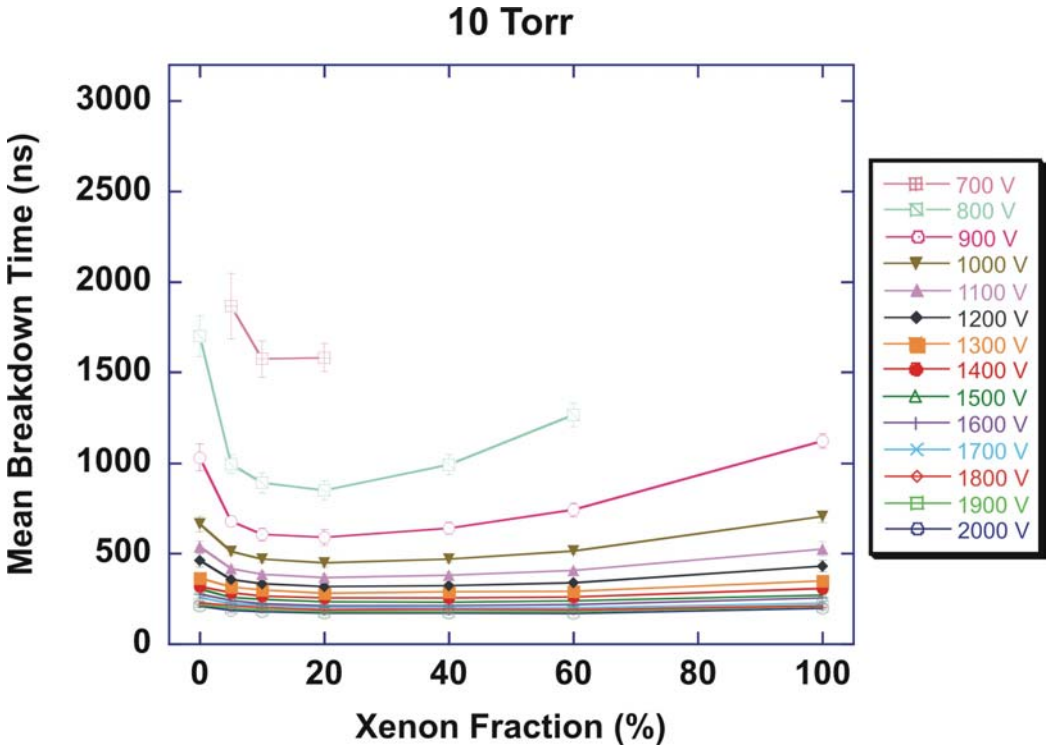

Figure 4.6(e) 10 Torr.

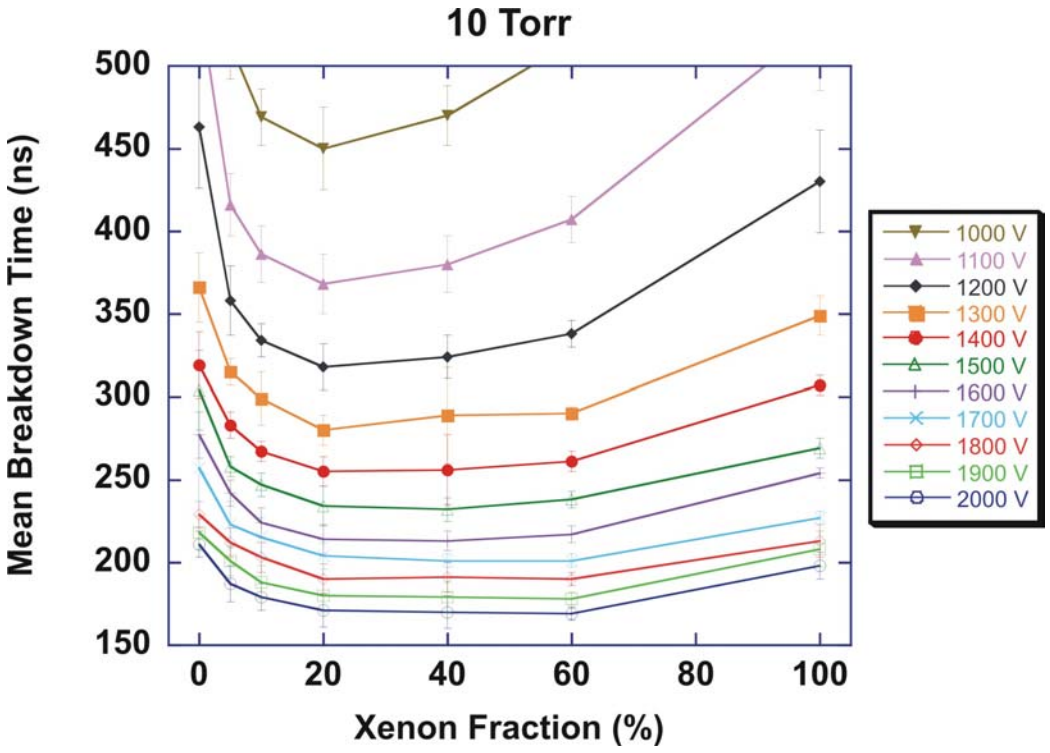

Figure 4.6(f) 10 Torr.

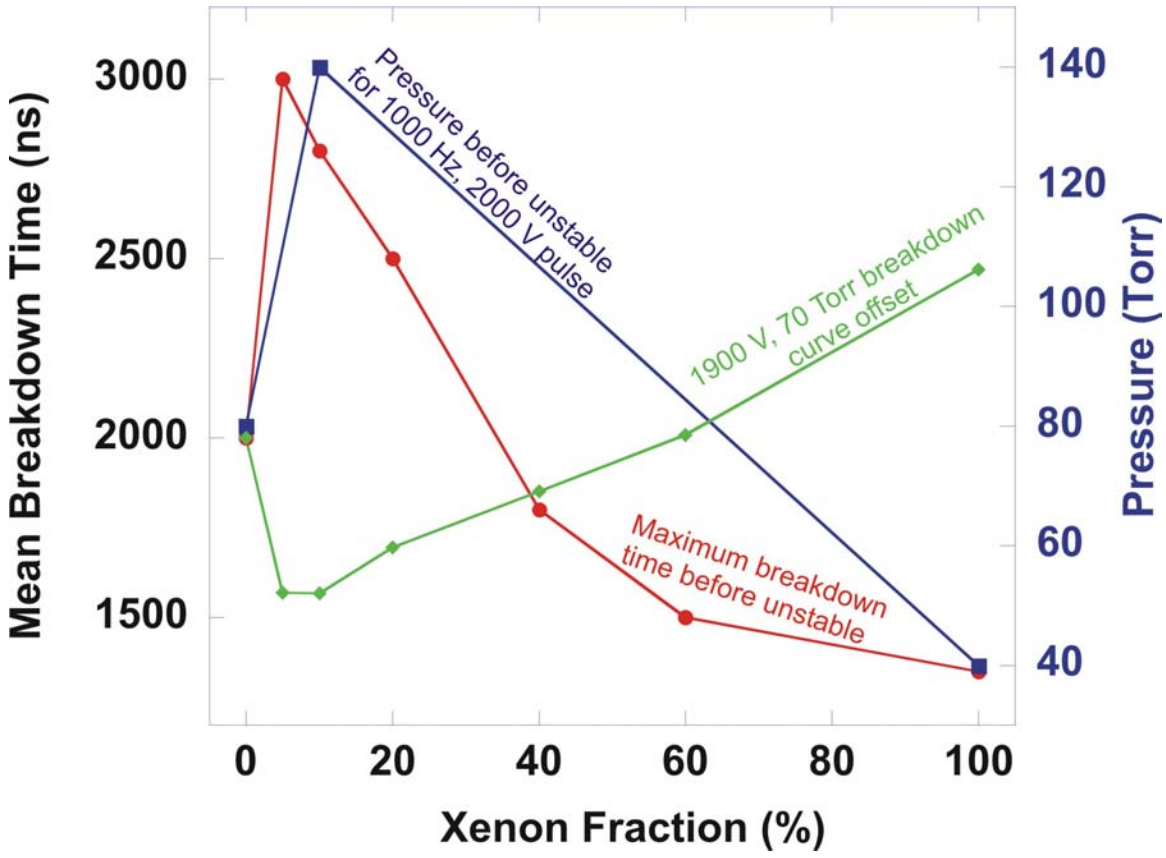

Figure 4.7 The maximum operating pressure, mean breakdown time, and the maximum breakdown time for a given xenon composition.

4.4 References

1. G. Zaslavsky, S. Cohen, and W. Keeffe, "Improved starting of the 100-W metal halide lamp," Journal of the Illuminating Engineering Society **19** (2), 76 (1990).

2. W. W. Byszewski and A. B. Budinger, "Enhanced starting of HID lamps," Journal of the Illuminating Engineering Society **19** (2), 70 (1990).

3. H. Brunet, A. Birot, H. Dijols, J. Galy, P. Millet, and Y. Salamero, "Spectroscopic and kinetic analysis of the VUV emissions of argon and argon-xenon mixtures: II. Energy transfer in Ar-Xe mixtures," Journal of Physics B : Atomics and Molecular Physics **15** (17), 2945 (1982).

4. R. E. Gleason, T. D. Bonifield, J. W. Keto, and G. K. Walters, "Electronic energy transfer in argon-xenon mixtures excited by electron bombardment," Journal of Chemical Physics **66** (4), 1589 (1977).

5. W. J. Alford, G. N. Hays, M. Ohwa, and M. J. Kushner, "The effects of He addition on the performance of the fission-fragment excited Ar/Xe atomic xenon laser," Journal of Applied Physics **69** (4), 1843 (1991).

6. A. F. Borghesani, G. Bressi, G. Carugno, E. Conti, and D. Iannuzzi, "Infrared fluorescence of Xe_2 molecules in electron/proton beam excited pure Xe gas and in an Ar/Xe gas mixture," Journal of Chemical Physics **115** (13), 6042 (2001).

5. ARGON/XENON DISCHARGE PHOTOGRAPHS

5.1 Overview

Photographs were taken of discharges sustained in three different gas compositions with varying pressures: pure argon, pure xenon, and a mixture of 10% xenon in argon. The range of pressures was 1 to 110 Torr. The experiment was performed without the mercury lamp because the light from the mercury lamp itself would overexpose the photos. The experiment was run at a pulse repetition frequency of 1000 Hz. This is about the highest frequency that is used in commercial lamps because of acoustical resonance effects.[1,2] Acoustical resonance can cause arc instability, light output fluctuation, color temperature variation, and may even crack arc tubes.[2]

The photos were taken with a Nikon Coolpix 950 2.11 megapixel digital camera. A timer was used for triggering the camera to allow for sufficient time for vibrations to damp out. Using the timer was critical since the exposure time was 1/8 second, thereby capturing approximately 125 discharge pulses.

5.2 Visual Characteristics of Discharge in Argon and Xenon

A thumbnail comparison of the argon, xenon, and Ar/Xe = 90/10 discharges is shown in Figures 5.1 and 5.2 at various pressures between 1 and 80 Torr. More comprehensive pressure ranges are shown for xenon, argon, and Ar/Xe = 90/10 in Figures 5.3-5.5. In all cases, no stable discharges occurred below pressures of 0.9 Torr. Argon discharges became unstable after 80 Torr, xenon after 40 Torr, and the mixture after approximately 140 Torr.

The most obvious differences between pure argon and pure xenon are the colors and behavior of the discharge. Argon emits a "purplish" glow and xenon emits more of a "bluish" glow.

At pressures for the 10% mixture below 3 Torr, the discharge is mostly purple resembling an argon discharge. This is due to the low collisionality and higher electron temperatures. With the higher electron temperature at low pressure, the majority of the emission will occur from the higher energy levels of argon. The electron temperature would also be higher at low pressure because the positive column is not present and the anode is in the negative glow. The transition in the color starts to appear at the pressure at which the positive column begins to form.

In all cases, the discharges exhibit a transition from a normal glow discharge to an abnormal glow discharge, with complex changes in the structure. The discharge is believed to be a glow for all of the experiments because line radiation is still being emitted. Accepted definitions of the discharge, based on voltage-current characteristics, are shown in Figure 5.6. A glow discharge is distinguished by the large voltage drop that occurs near the cathode. Glow discharges have been discussed extensively by several authors.[3-8] The basic structure of the glow discharge is shown in Figure 5.7. It can be subdivided into three regimes: the cathode fall, the negative glow, and the positive column.

The structures near the cathode are required, particularly the cathode fall, or the discharge cannot be sustained. These structures near the cathode are of fixed lengths at a given pressure. The anode glow and positive column do not necessarily exist when the tube length is short, especially at low pressures. These results demonstrate that only the

cathode fall and the negative glow exist in argon at 1 and 2 Torr. The positive column starts to appear at 3 Torr, and, at higher pressures, striations in the positive column are clearly visible. At 1 Torr, in argon, the cathode fall length is on the order of 1 cm. From Figure 5.4(a), knowing the electrode spacing is approximately 1.6 cm, the dark space follows theory closely. The length of the cathode fall in a normal glow discharge can be approximated by

$$d_{C.F.} = \frac{0.82}{P_{Torr}} \frac{\ln\left[1+(1/\gamma)\right]}{A} \tag{5.3}$$

where γ is the secondary electron emission coefficient and A is a gas specific constant. This length is inversely proportional to the pressure, a trend distinguishable from the photographs. Constricted discharges occur at lower pressures at which the electrode spacing is not sufficiently long for even the cathode fall to fully develop. This explains why no stable discharge was observed below about 0.9 Torr.

The negative glow also has a minimum spacing before the positive column can occur. This length can be approximated by

$$d_{N.G.} = \frac{1}{2} \frac{1}{N\sigma_0 \Delta\varepsilon^2} \left[V_c^{\,2} - \Delta\varepsilon^2\right] \tag{5.4}$$

where N is the neutral gas density, σ_0 is the total cross section, and $\Delta\varepsilon$ is the first ionization energy. V_c is the cathode fall voltage

$$V_c = \eta \ln\left(1+(1/\gamma)\right) \tag{5.5}$$

where η is the potential difference an electron has to fall to produce an ion pair, a quantity independent of the gas pressure, and, again, γ is the secondary electron coefficient. The length of the negative glow is also inversely proportional to the pressure.

The shrinking of the negative glow can be seen in the photographs. Because the ranges of the cathode fall and the negative glow are on the order of a few centimeters at 1 Torr of argon, there is insufficient electrode spacing (1.63 cm), for the positive column to form.

Argon tends to have a more chaotic behavior and breaks down in a bowed shape at random locations rather than having a centralized discharge. This can be explained by the expansion of the gas due to heat conduction. Thermal conductivity in gases is inversely proportional to the mass. Argon is three times lighter than xenon and so is more thermally conducting. The bowed shape is pushed upward due to the convective forces.

Convective forces have been known to change discharge behavior.[9,10] The random behavior in this lamp geometry occurs because of the vertical placement. If the lamp were to be positioned horizontally, convective forces push the discharge up, and only a single stable symmetric glow exists. This effect was experimentally observed in Ruzic's laboratory.[9] The upward discharge was also observed experimentally by Dempsey et al.[10] This experiment showed that in the absence of gravity, convection no longer exists, and the discharge becomes straight.

A 10% mixture of xenon eliminates the gas expansion and straight discharges occur. This is due to xenon being much more radiatively efficient than argon. This higher efficiency dissipates enough energy from the discharge to prevent the discharge from expanding to the walls.

At higher pressures, the discharge transitions from a diffuse mode to a "constricted" mode. A diffuse mode has a uniform attachment and the "constricted"

mode has a small region of current transfer. The constricted region can be seen on the anode in Figure 5.3(h) in xenon at 40 Torr before it becomes unstable. At lower pressures in xenon (Figures 5.3(e) and 5.3(f) at 10 at 20 Torr, respectively) a completely uniform attachment can be seen at the anode.

In the purely normal glow discharge regime, regardless of the gas composition, auxiliary plumes of plasma are emitted from the gas feed-through holes. This was also observed experimentally by Ruzic.[9] These additional plumes do not occur at higher pressures because the gas becomes more collisional and the mean free path is too small for this effect to be substantial.

5.3 Figures

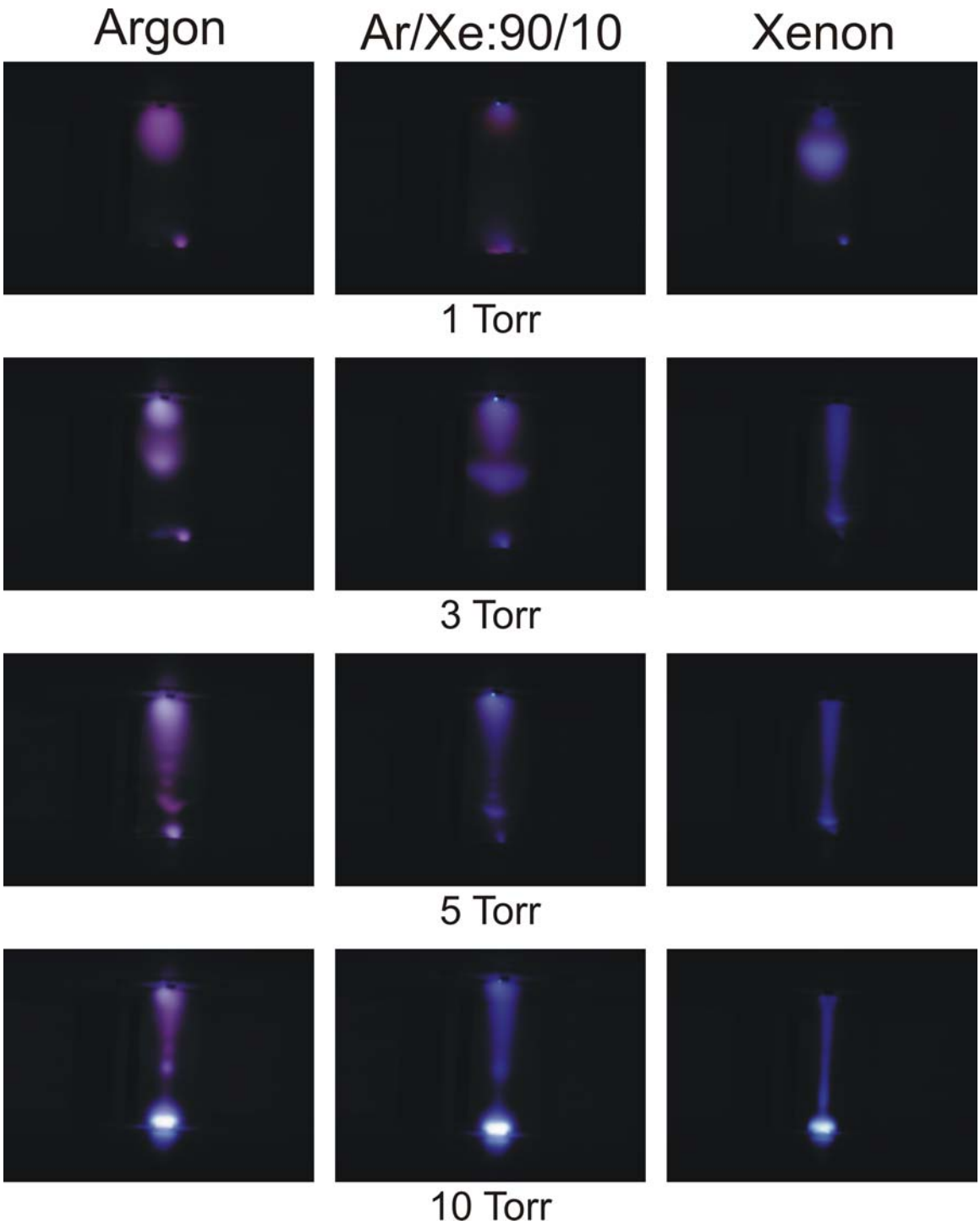

Figure 5.1 Comparison of discharges in argon, xenon, and a 90/10 mixture of argon/xenon at pressures of 1, 3, 5, and 10 Torr.

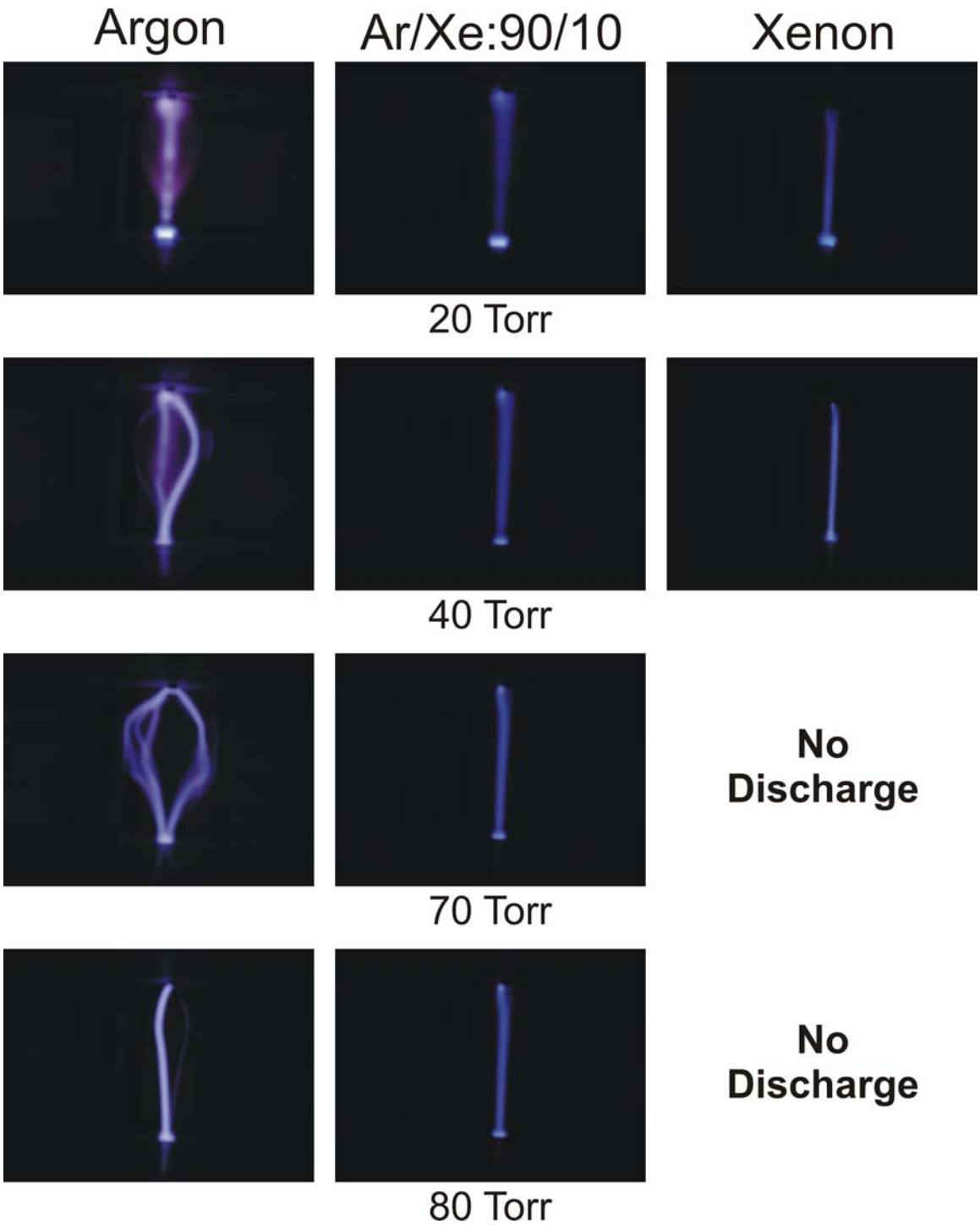

Figure 5.2 Comparison of discharges in argon, xenon, and a 90/10 mixture of argon/xenon at pressures of 20, 40, 70, and 80 Torr.

Figures 5.3 Pure xenon discharges for different pressures with a constant applied 2000-V pulse at 1000 Hz.

(a) 1 Torr
(b) 2 Torr
(c) 3 Torr
(d) 5 Torr
(e) 10 Torr
(f) 20 Torr
(g) 30 Torr
(h) 40 Torr

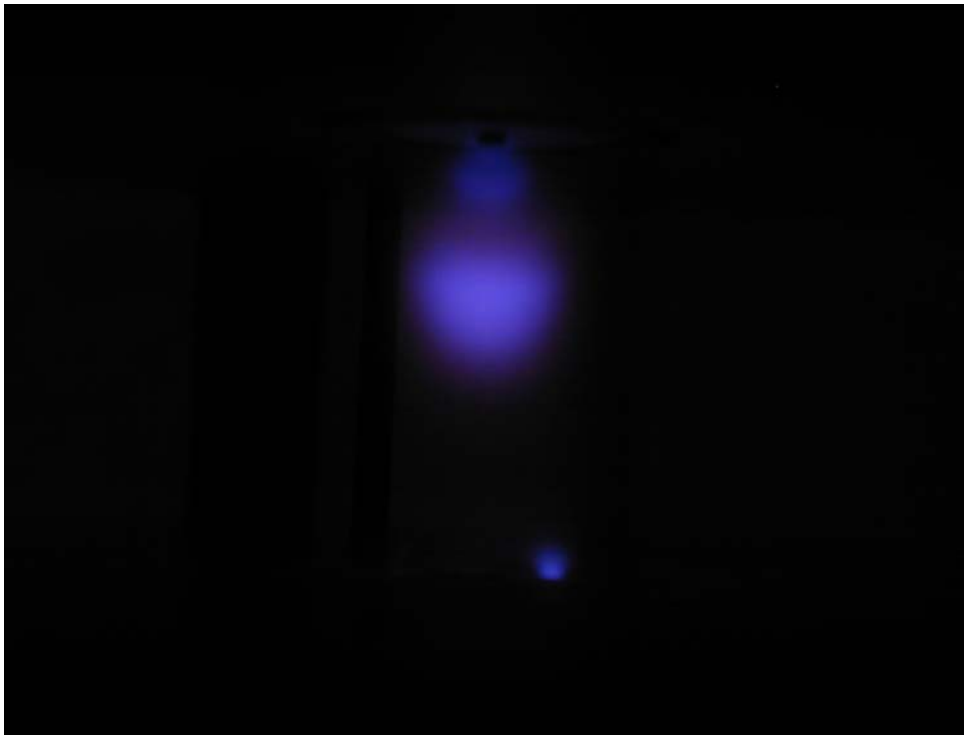

Figure 5.3(a) 1 Torr.

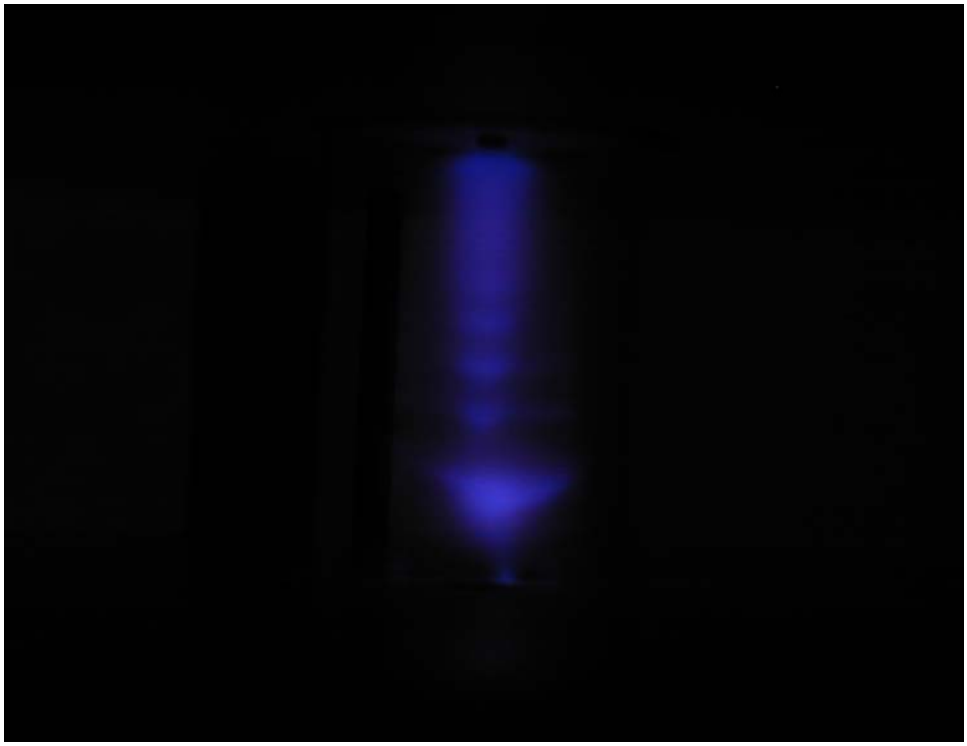

Figure 5.3(b) 2 Torr.

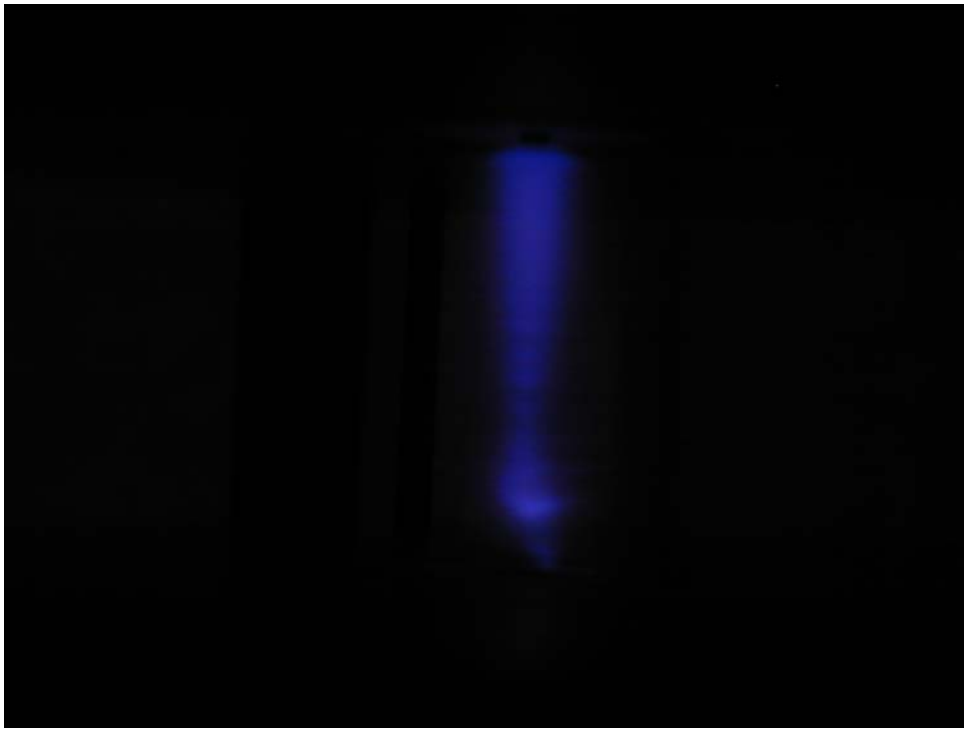

Figure 5.3(c) 3 Torr.

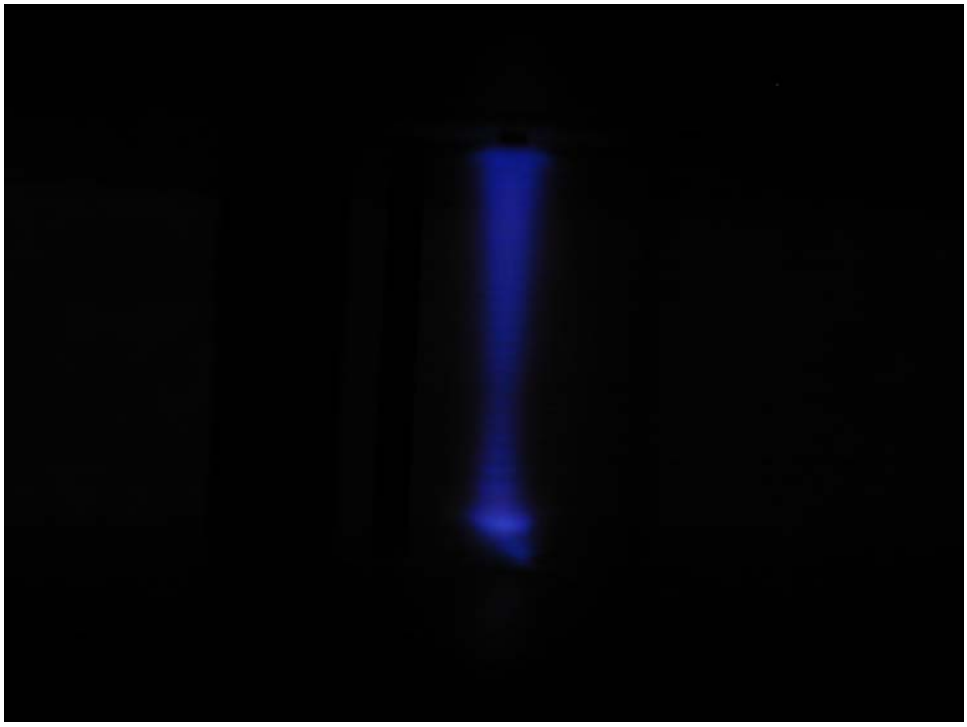

Figure 5.3(d) 5 Torr.

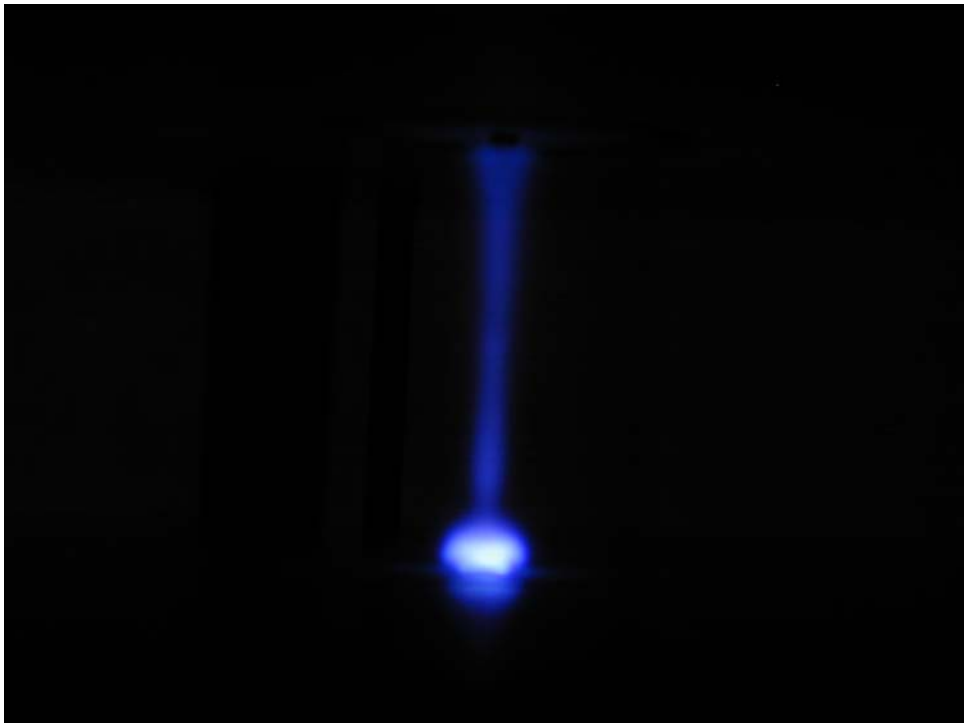

Figure 5.3(e) 10 Torr.

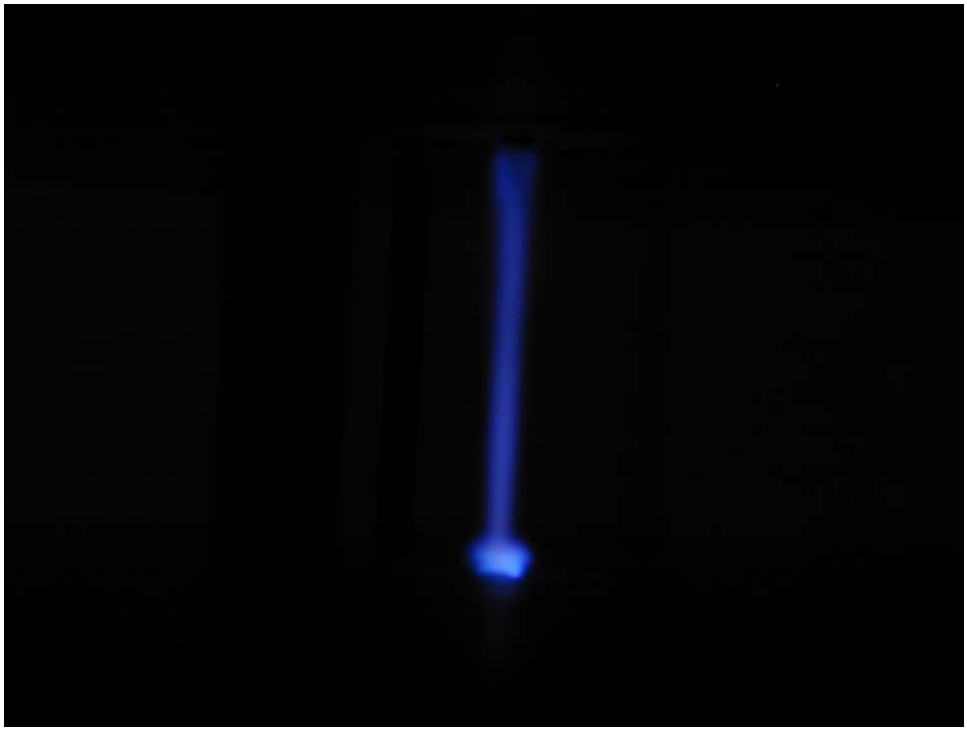

Figure 5.3(f) 20 Torr.

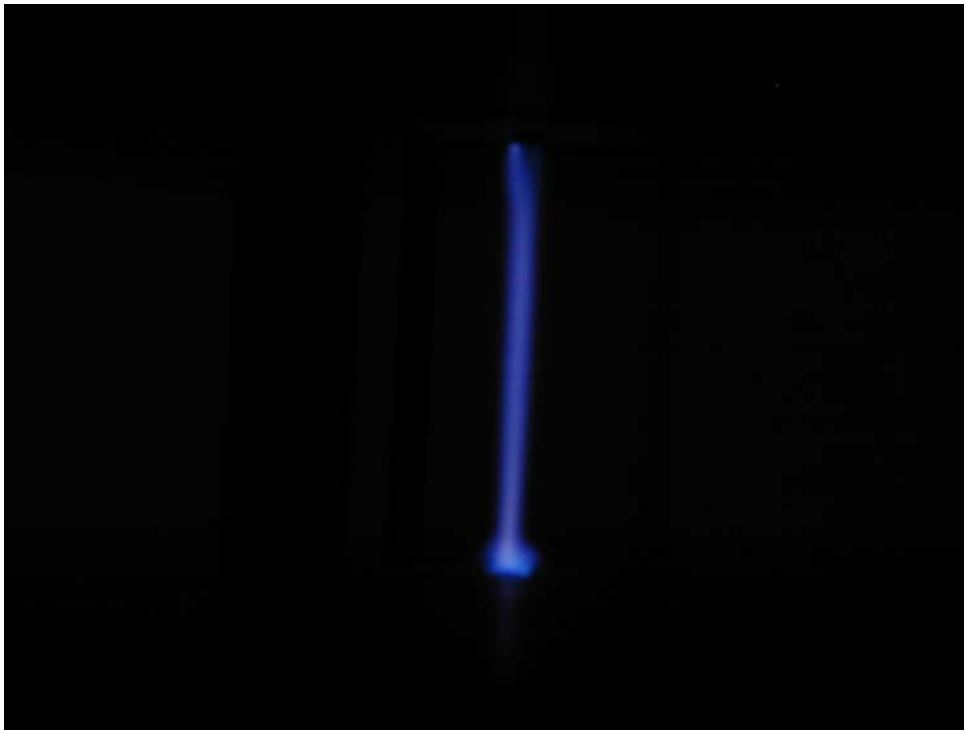

Figure 5.3(g) 30 Torr.

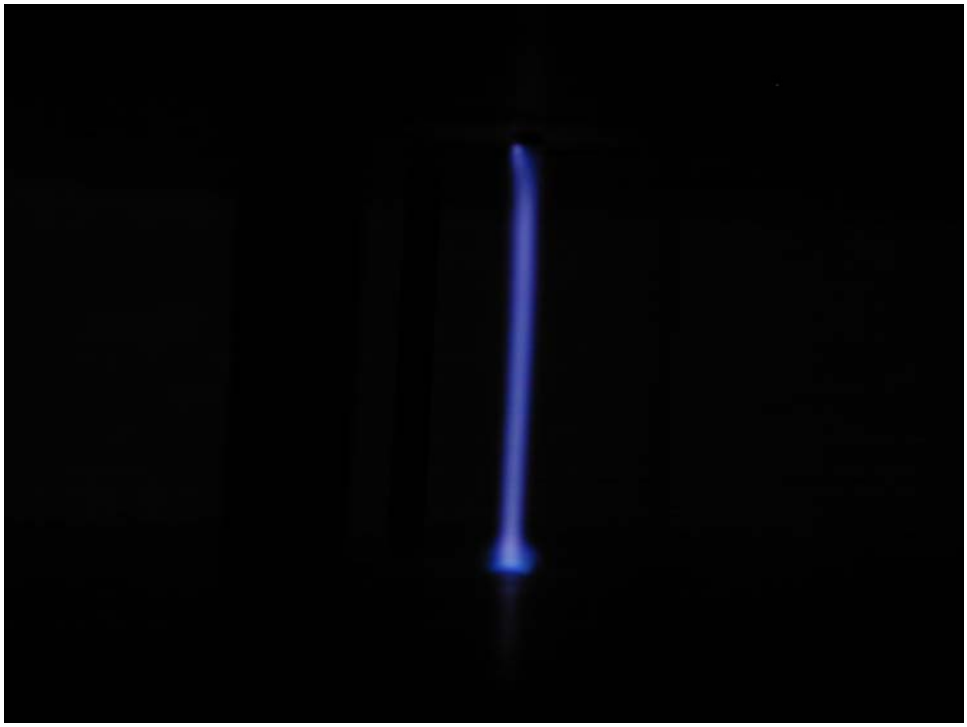

Figure 5.3(h) 40 Torr.

Figures 5.4 Pure argon discharges for different pressures with a constant applied 2000-V pulse at 1000 Hz.

(a) 1 Torr
(b) 2 Torr
(c) 3 Torr
(d) 4 Torr
(e) 5 Torr
(f) 6 Torr
(g) 7 Torr
(h) 8 Torr
(i) 9 Torr
(j) 10 Torr
(k) 15 Torr
(l) 20 Torr
(m) 25 Torr
(n) 30 Torr
(o) 35 Torr
(p) 40 Torr
(q) 45 Torr
(r) 50 Torr
(s) 55 Torr
(t) 60 Torr
(u) 65 Torr
(v) 70 Torr
(w) 75 Torr
(x) 80 Torr

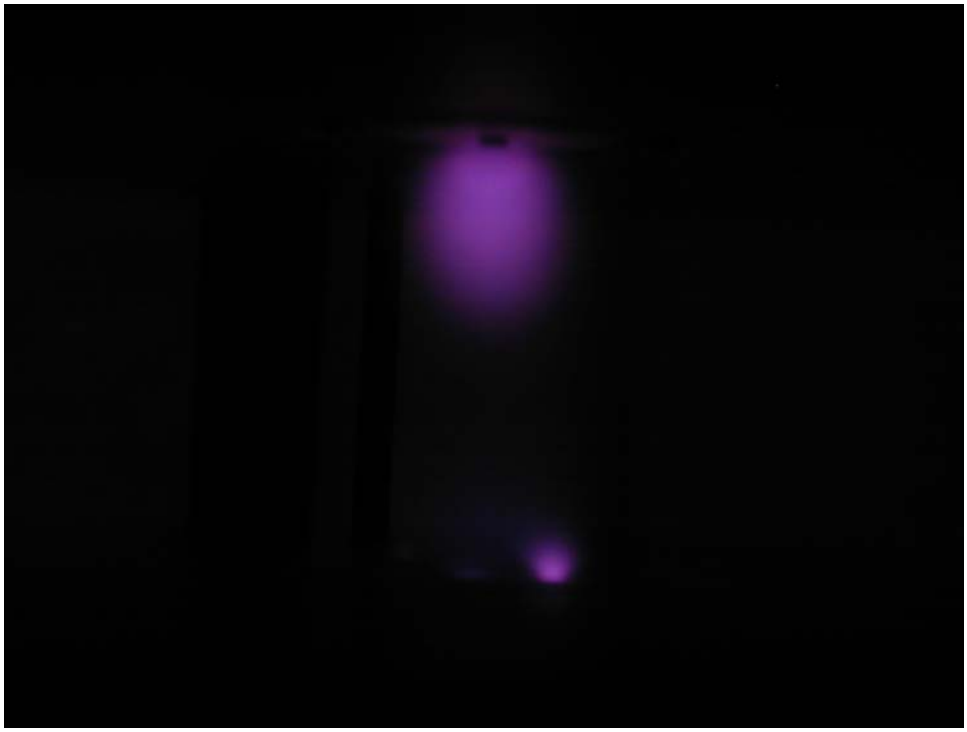

Figure 5.4(a) 1 Torr.

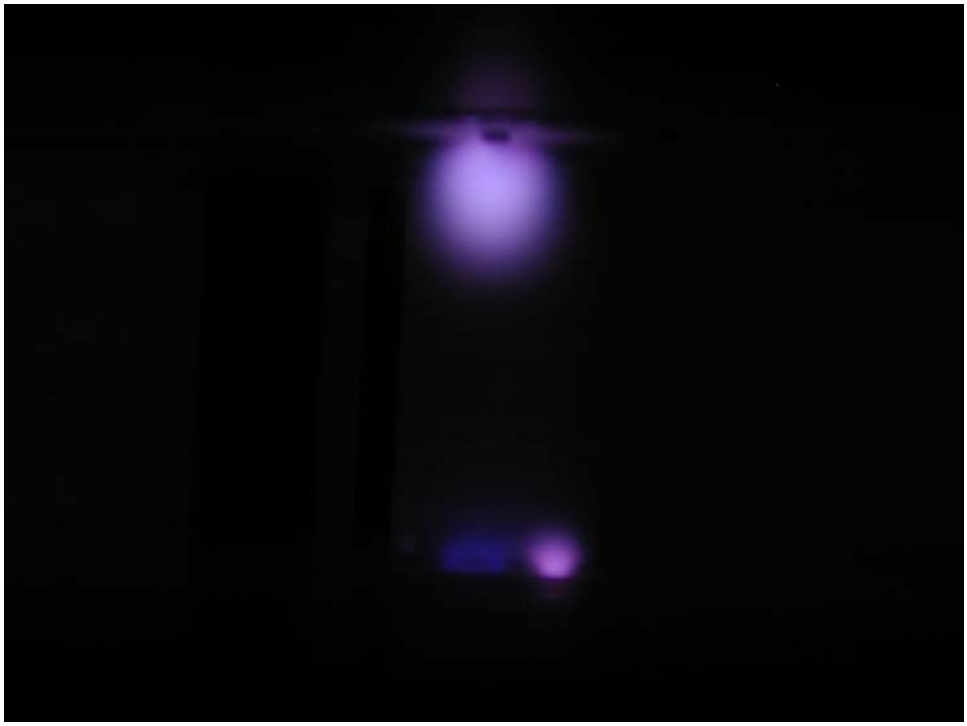

Figure 5.4(b) 2 Torr.

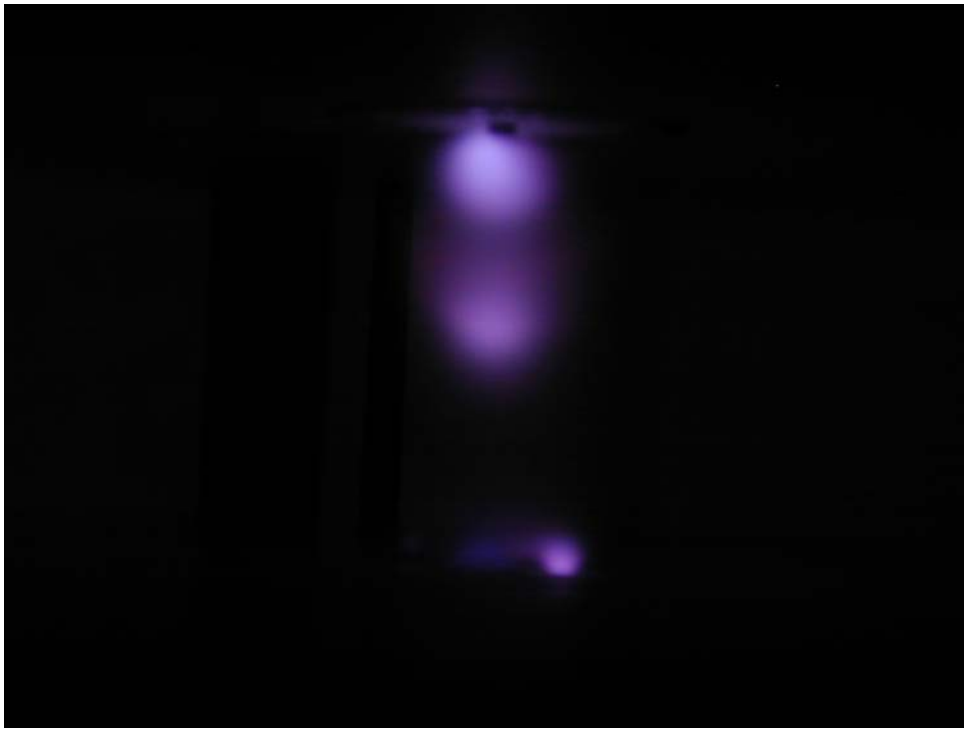

Figure 5.4(c) 3 Torr.

Figure 5.4(d) 4 Torr.

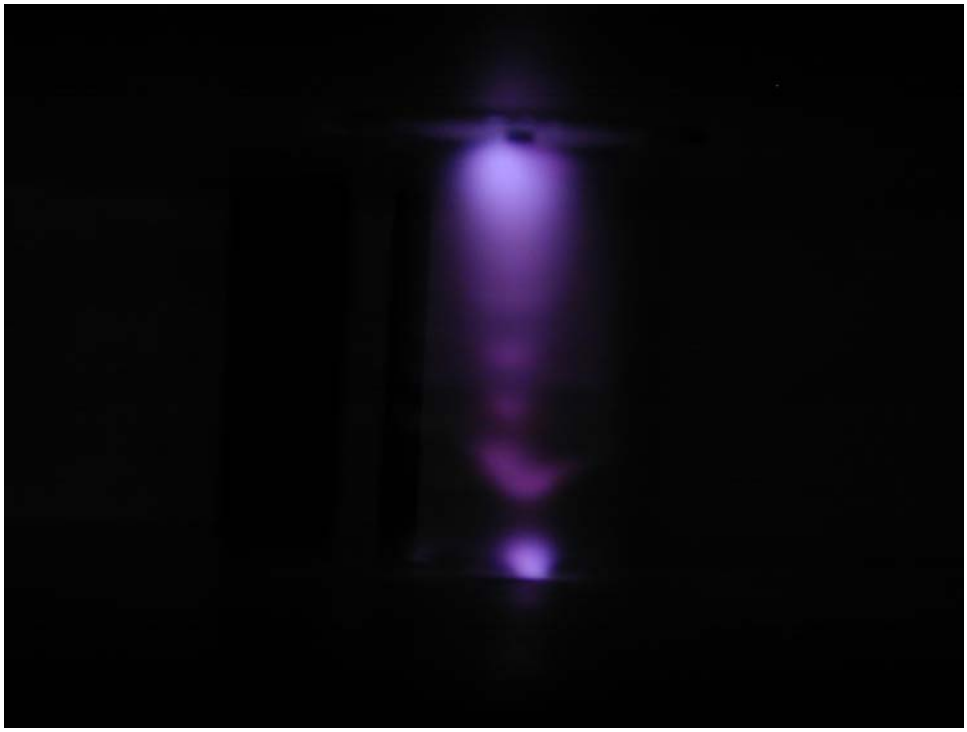

Figure 5.4(e) 5 Torr.

Figure 5.4(f) 6 Torr.

Figure 5.4(g) 7 Torr.

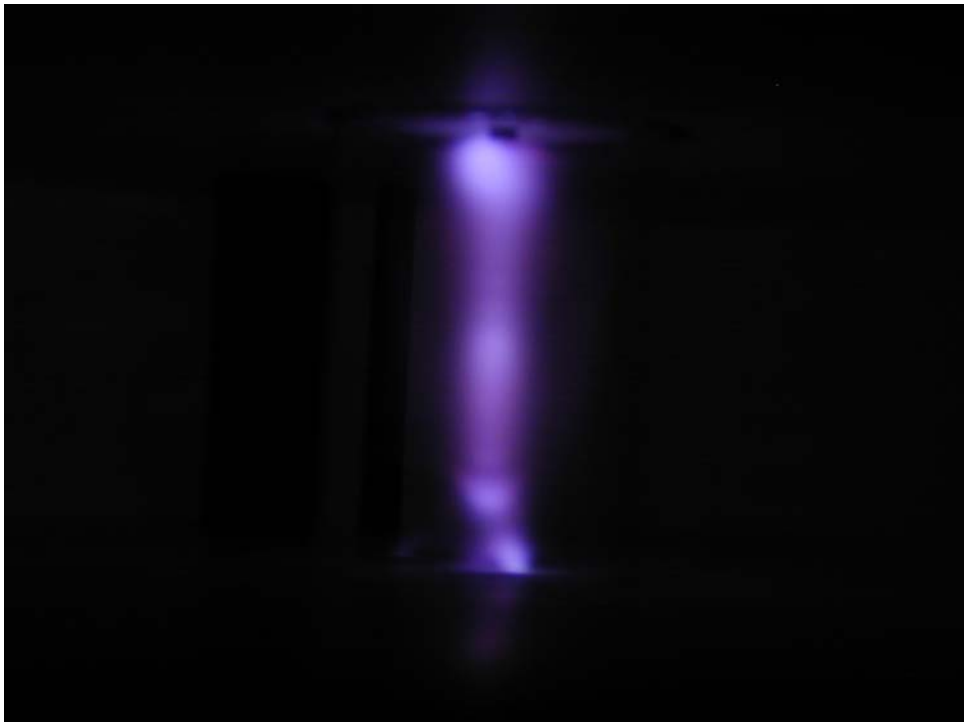

Figure 5.4(h) 8 Torr.

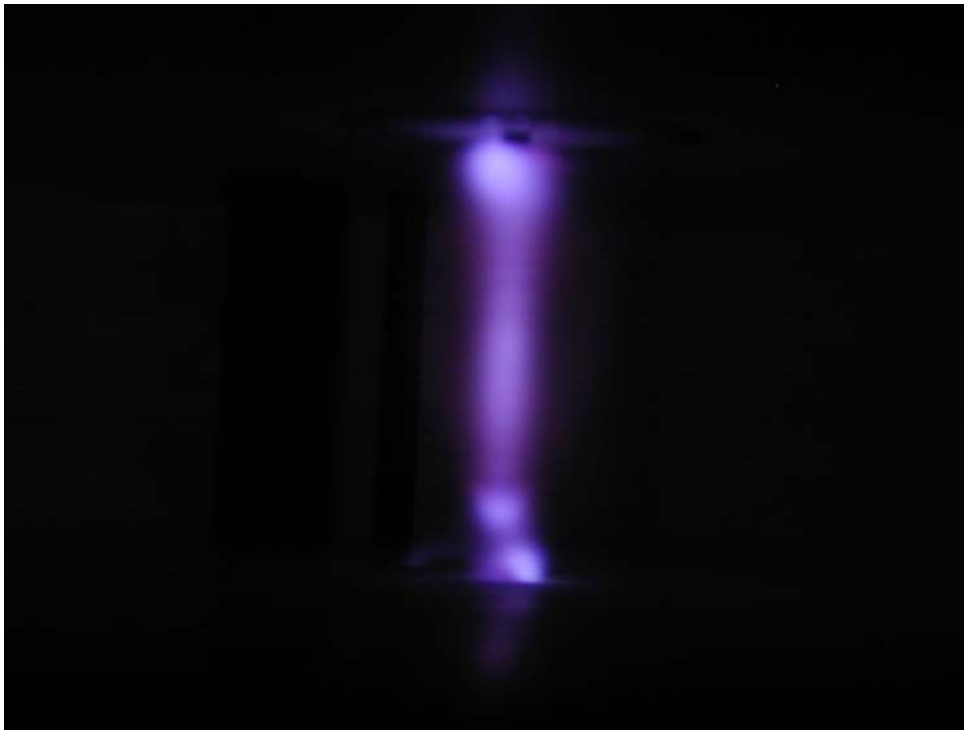

Figure 5.4(i) 9 Torr.

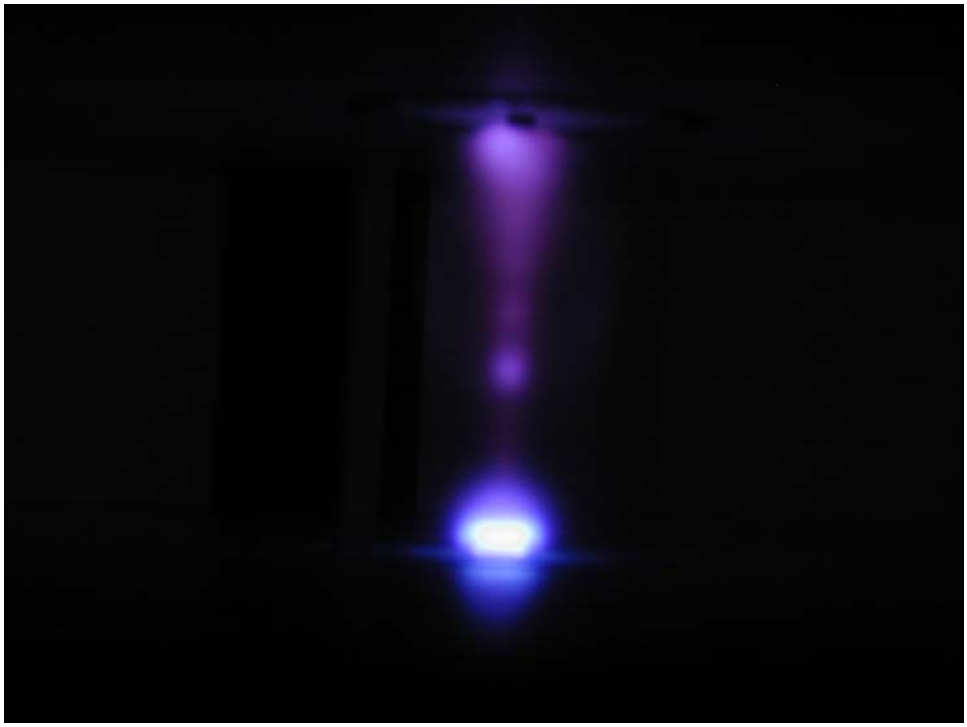

Figure 5.4(j) 10 Torr.

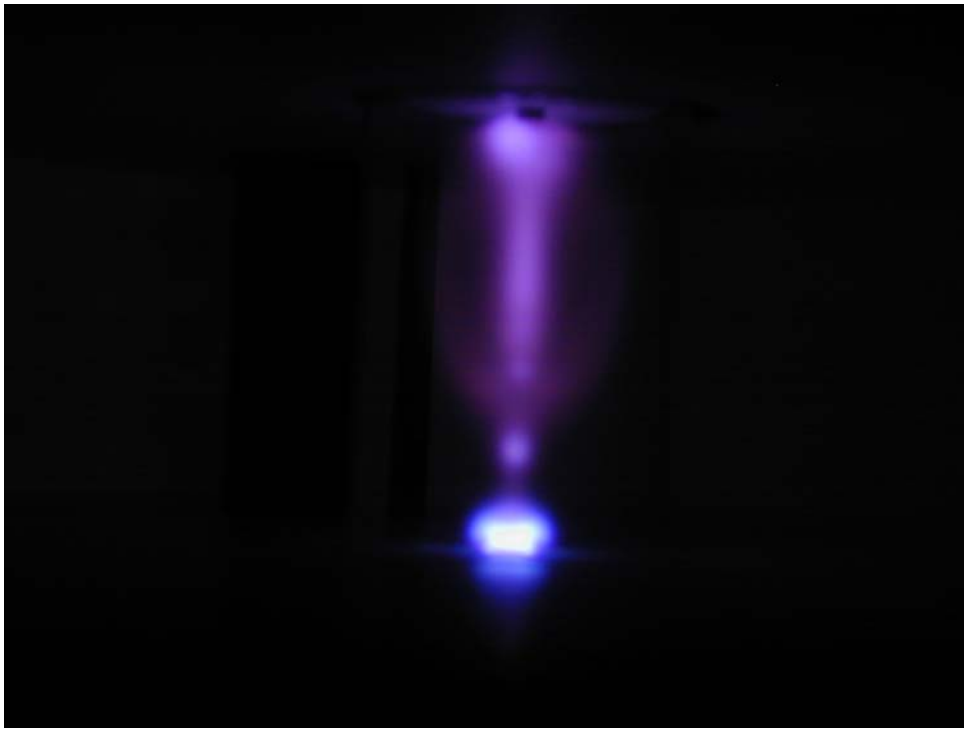

Figure 5.4(k) 15 Torr.

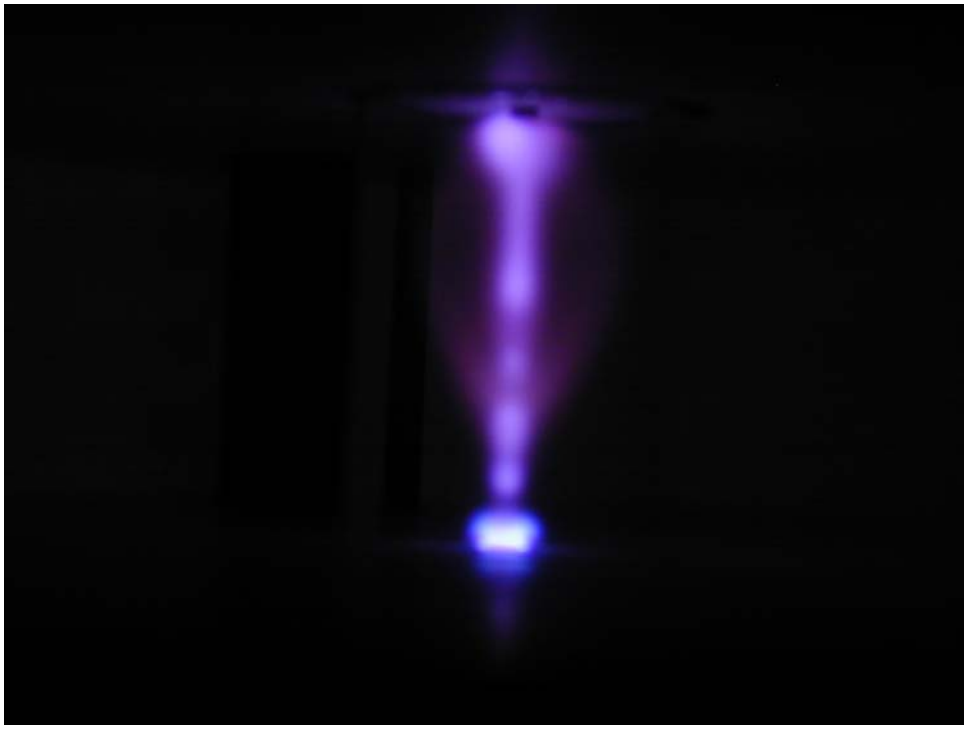

Figure 5.4(l) 20 Torr.

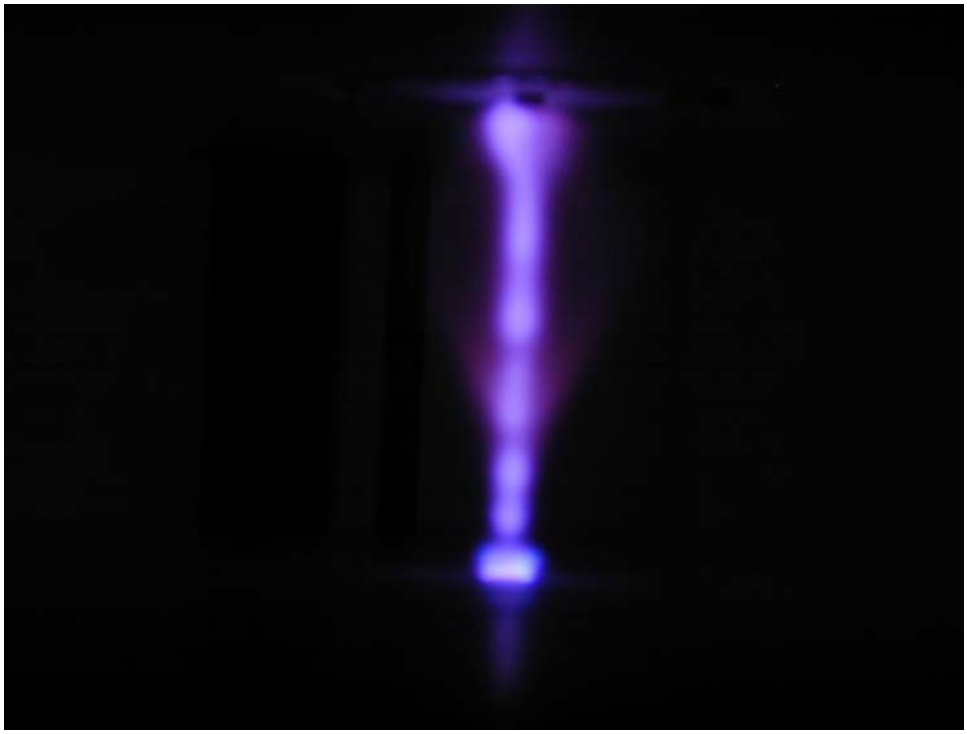

Figure 5.4(m) 25 Torr.

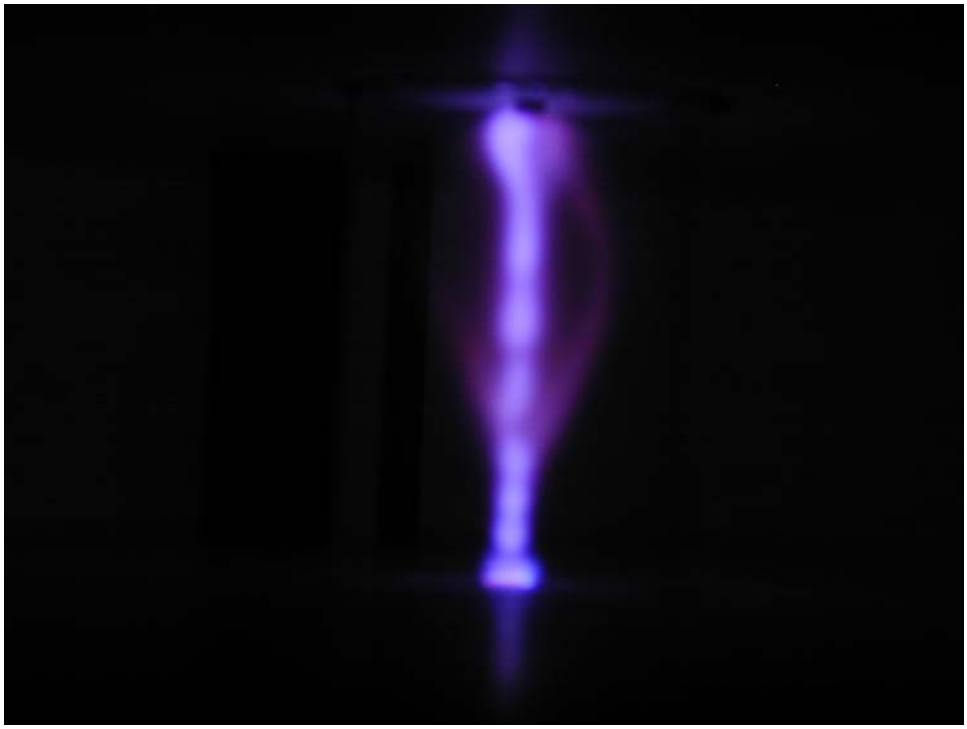

Figure 5.4(n) 30 Torr.

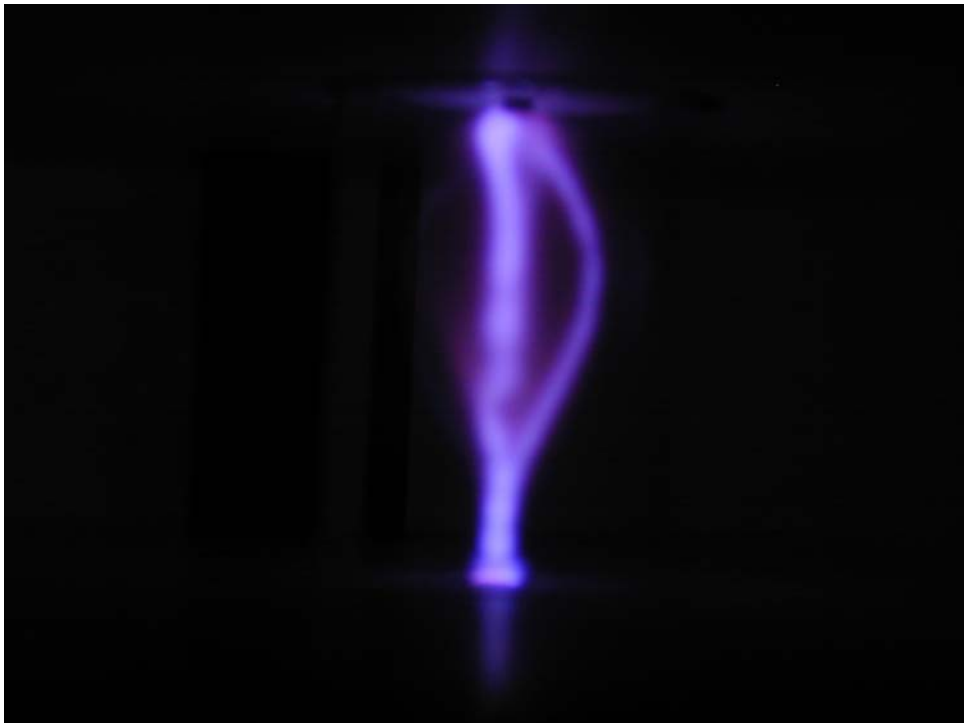

Figure 5.4(o) 35 Torr.

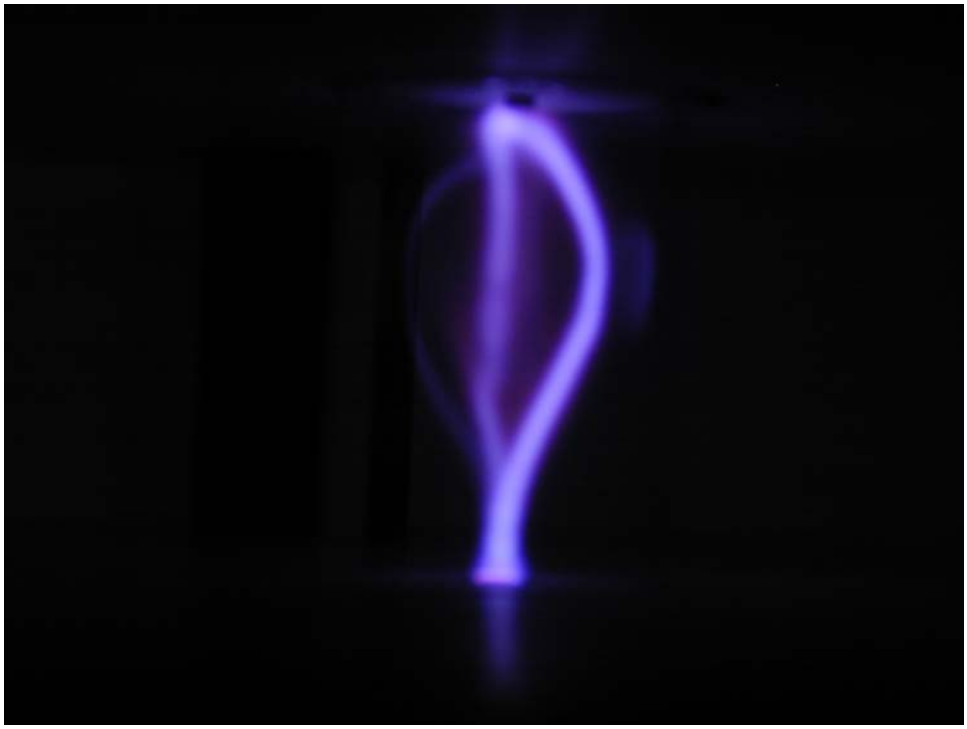

Figure 5.4(p) 40 Torr.

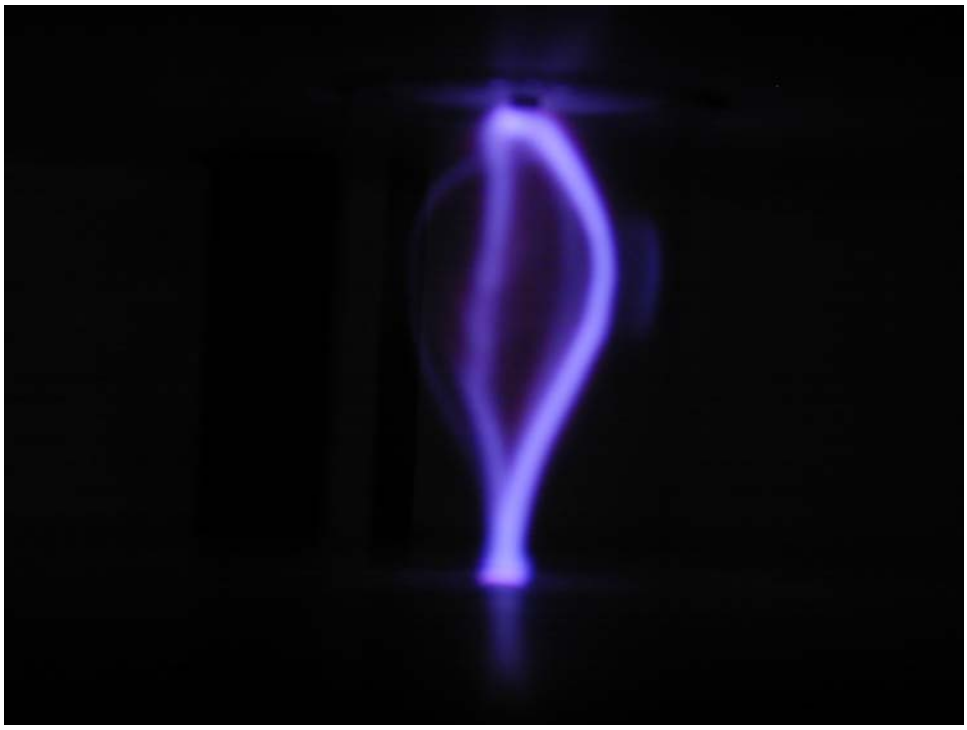

Figure 5.4(q) 45 Torr.

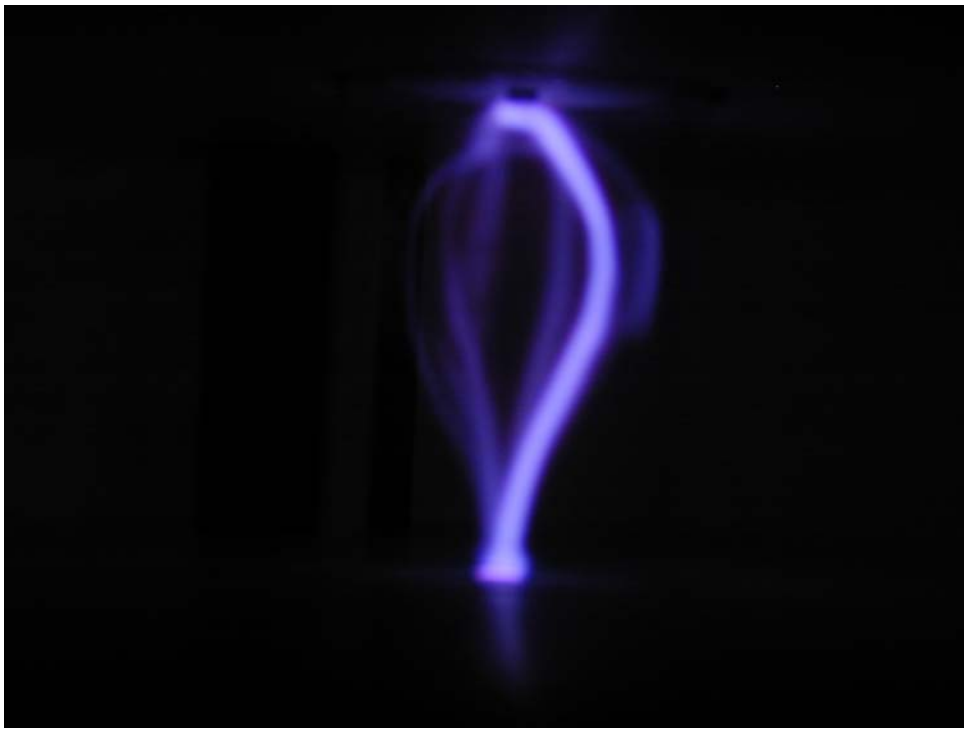

Figure 5.4(r) 50 Torr.

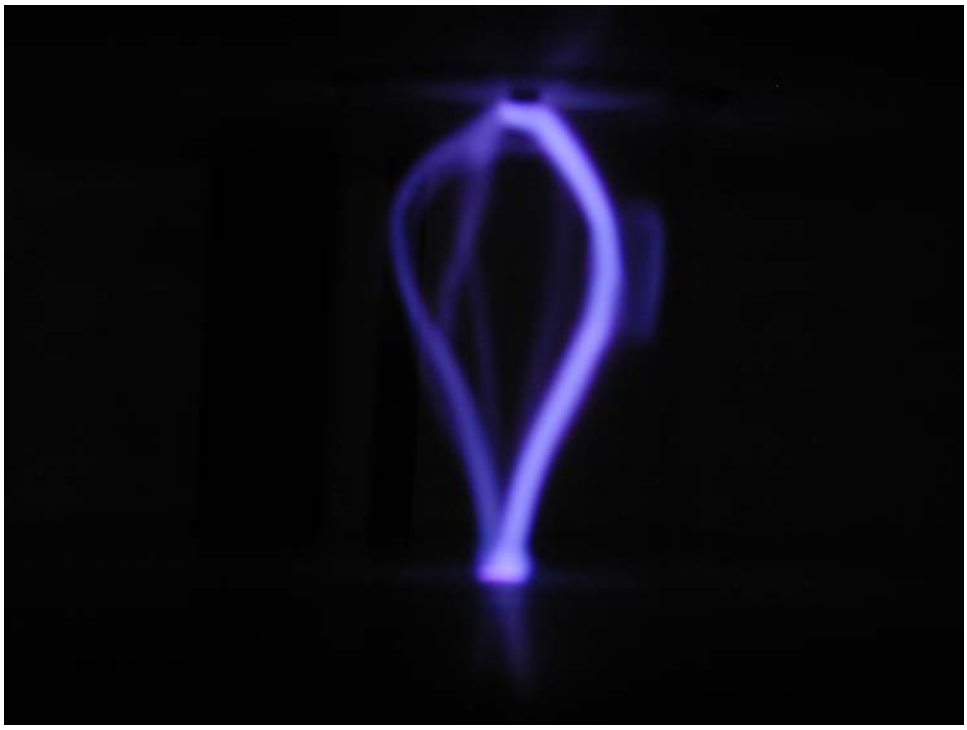

Figure 5.4(s) 55 Torr.

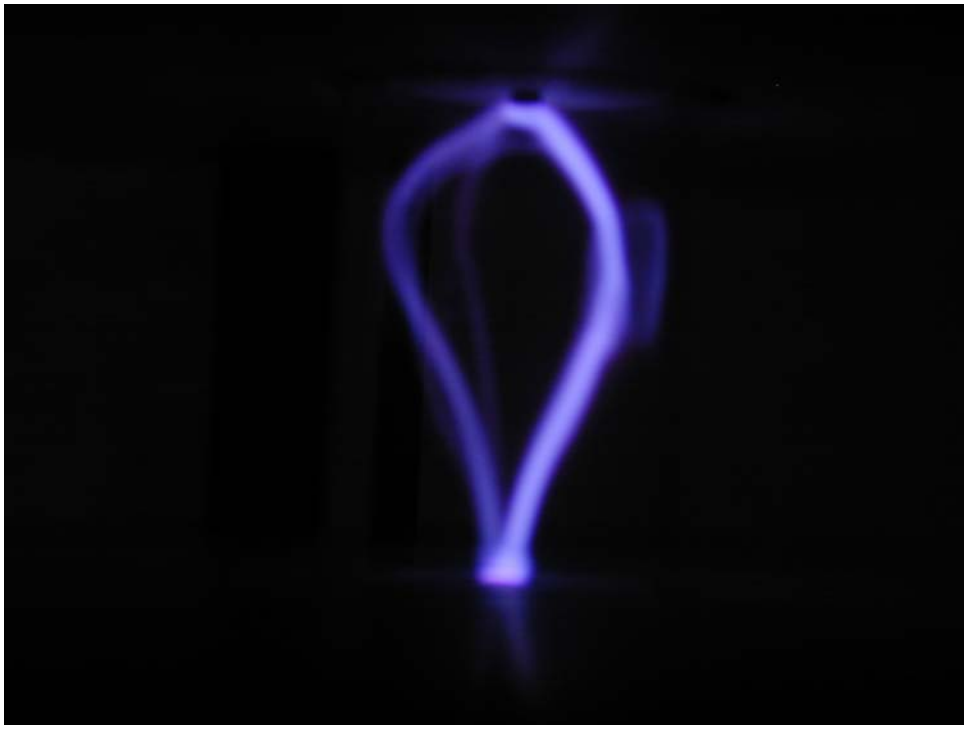

Figure 5.4(t) 60 Torr.

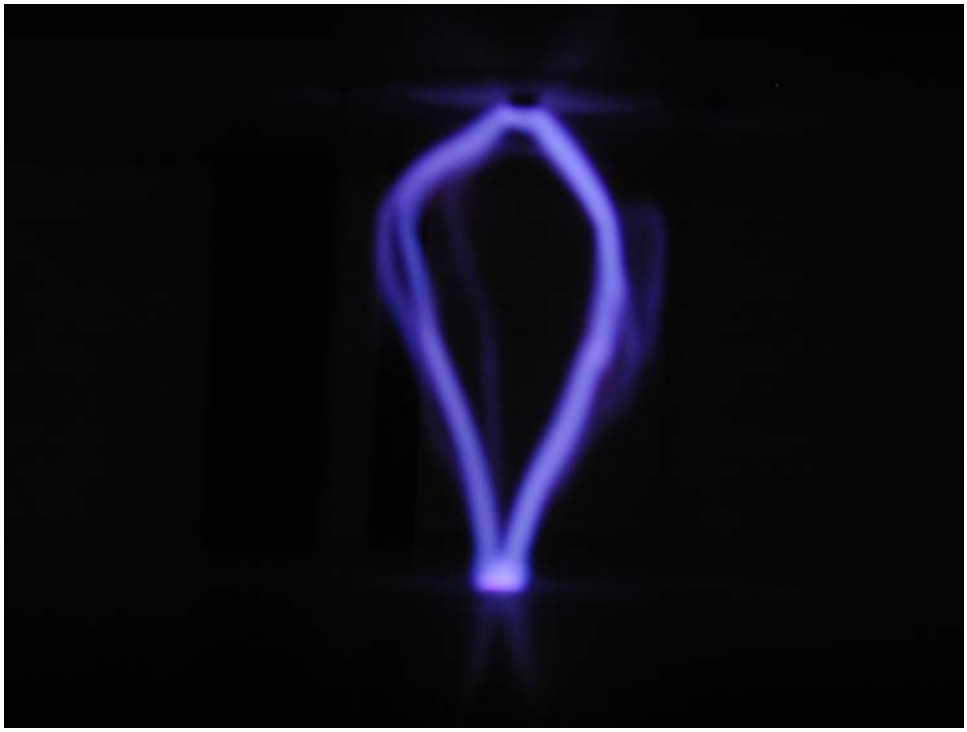

Figure 5.4(u) 65 Torr.

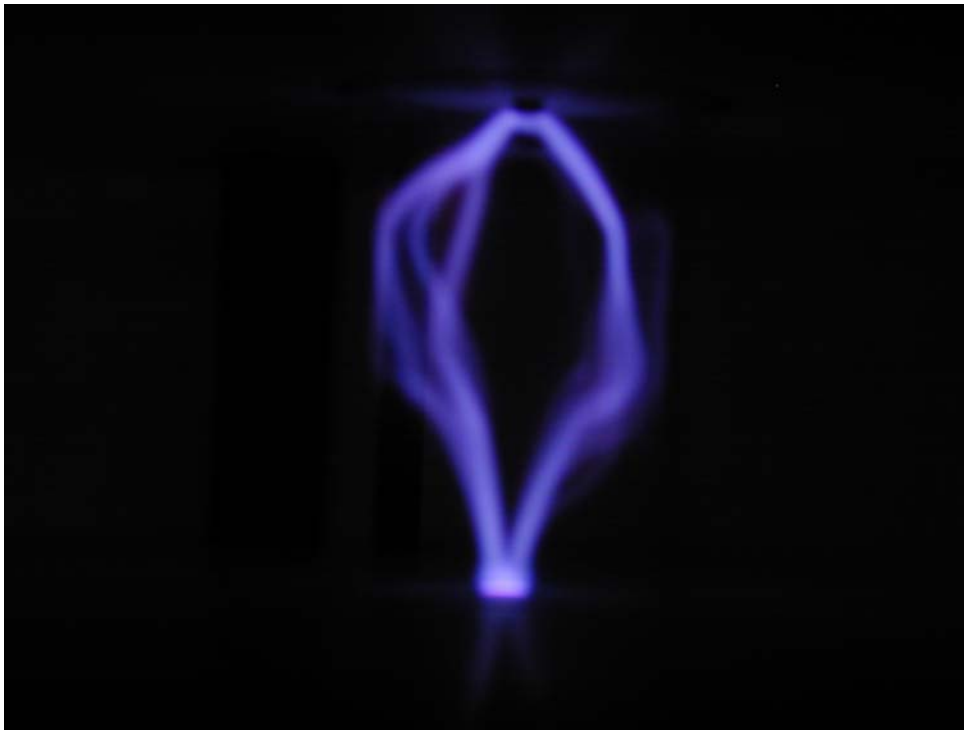

Figure 5.4(v) 70 Torr.

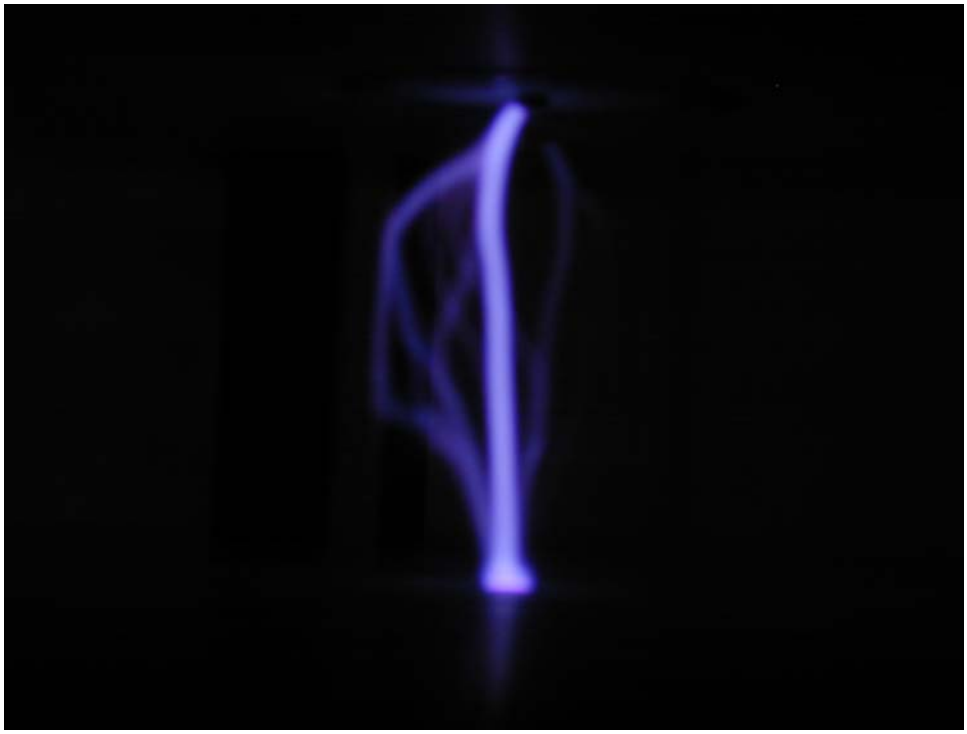

Figure 5.4(w) 75 Torr.

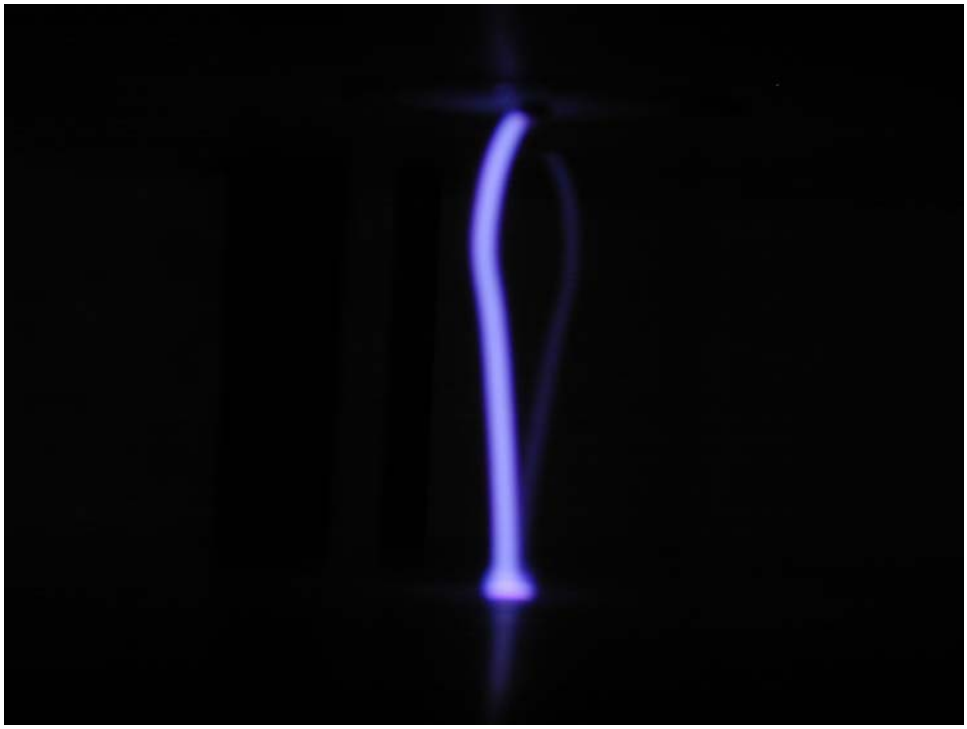

Figure 5.4(x) 80 Torr.

Figures 5.5 A 90% argon and 10% xenon discharges at different pressures with a constant applied 2000-V pulse at 1000 Hz.

(a) 1 Torr
(b) 2 Torr
(c) 3 Torr
(d) 4 Torr
(e) 5 Torr
(f) 6 Torr
(g) 7 Torr
(h) 8 Torr
(i) 9 Torr
(j) 10 Torr
(k) 15 Torr
(l) 20 Torr
(m) 50 Torr
(n) 110 Torr

Figure 5.5(a) 1 Torr.

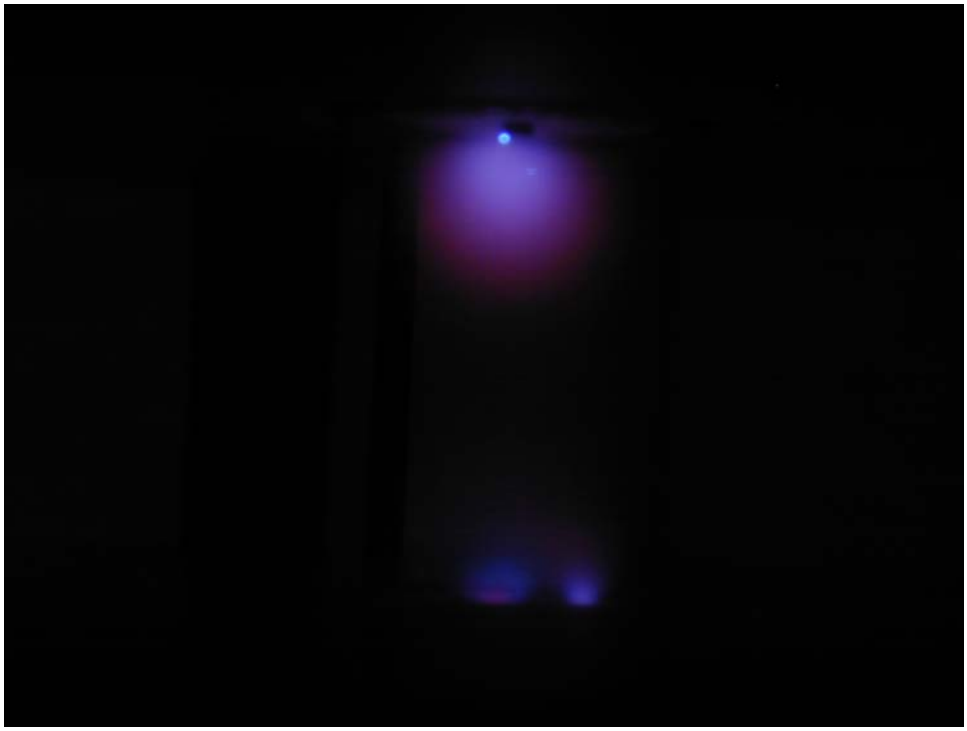

Figure 5.5(b) 2 Torr.

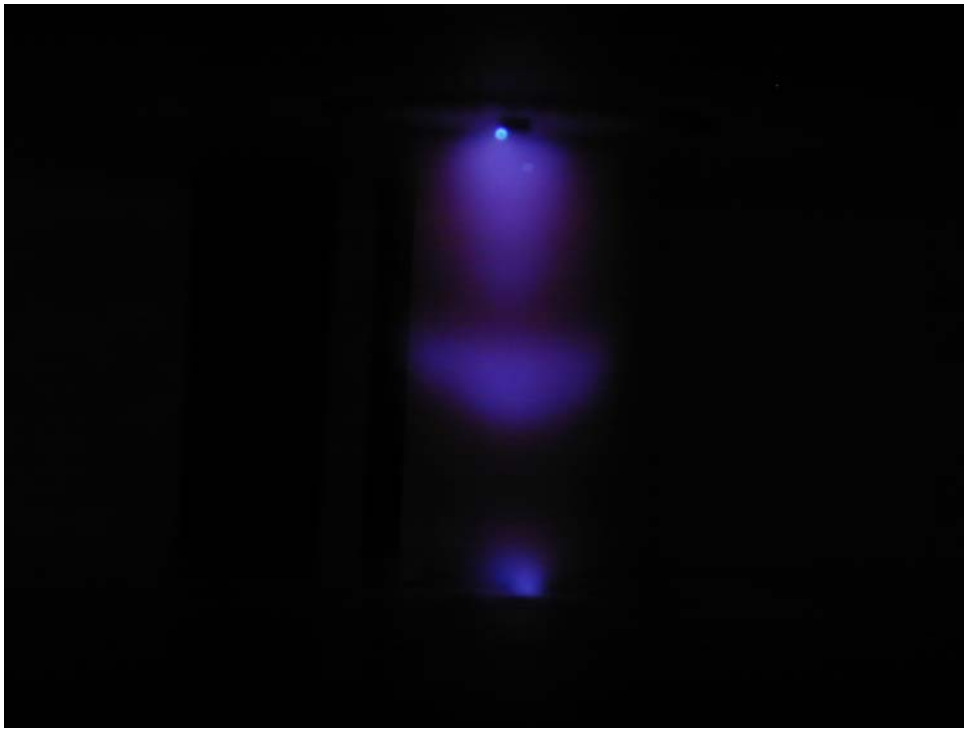

Figure 5.5(c) 3 Torr.

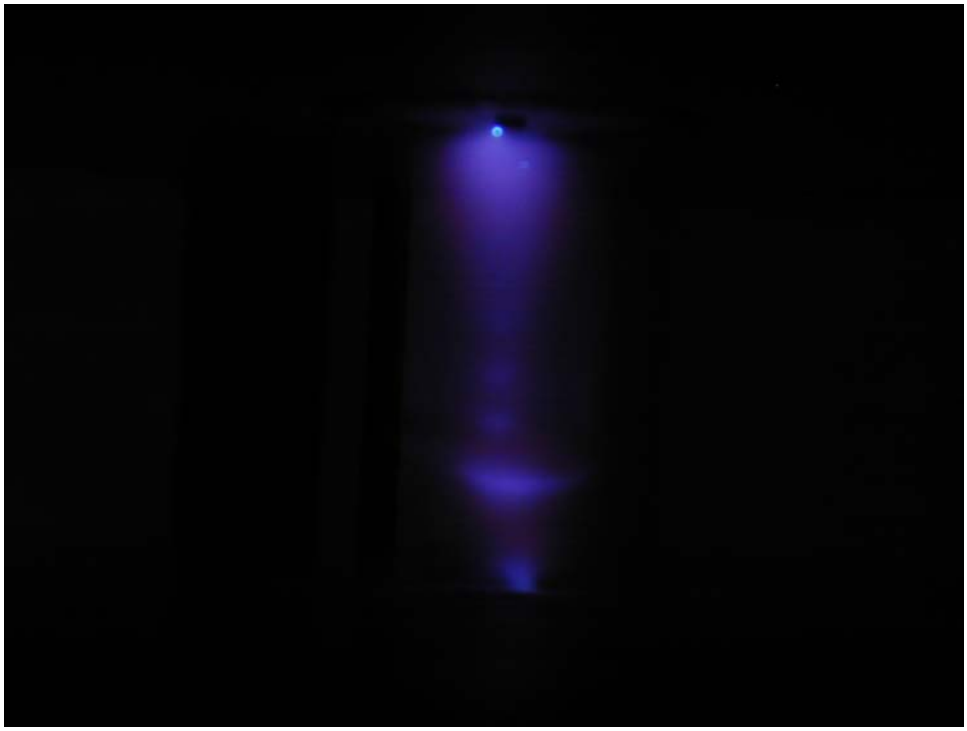

Figure 5.5(d) 4 Torr.

Figure 5.5(e) 5 Torr.

Figure 5.5(f) 6 Torr.

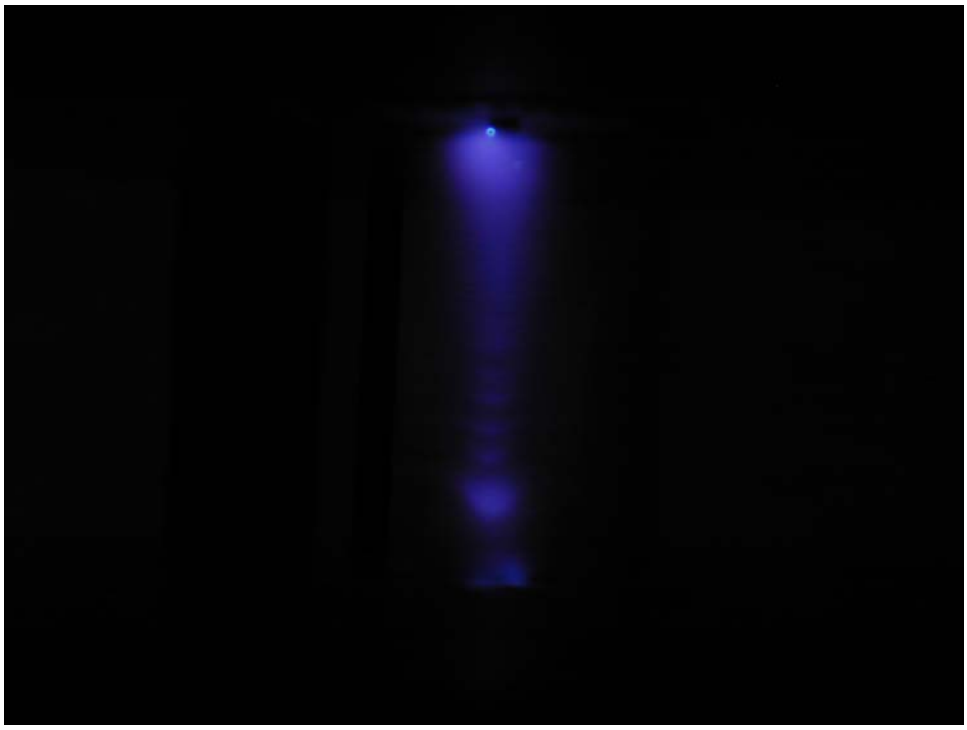

Figure 5.5(g) 7 Torr.

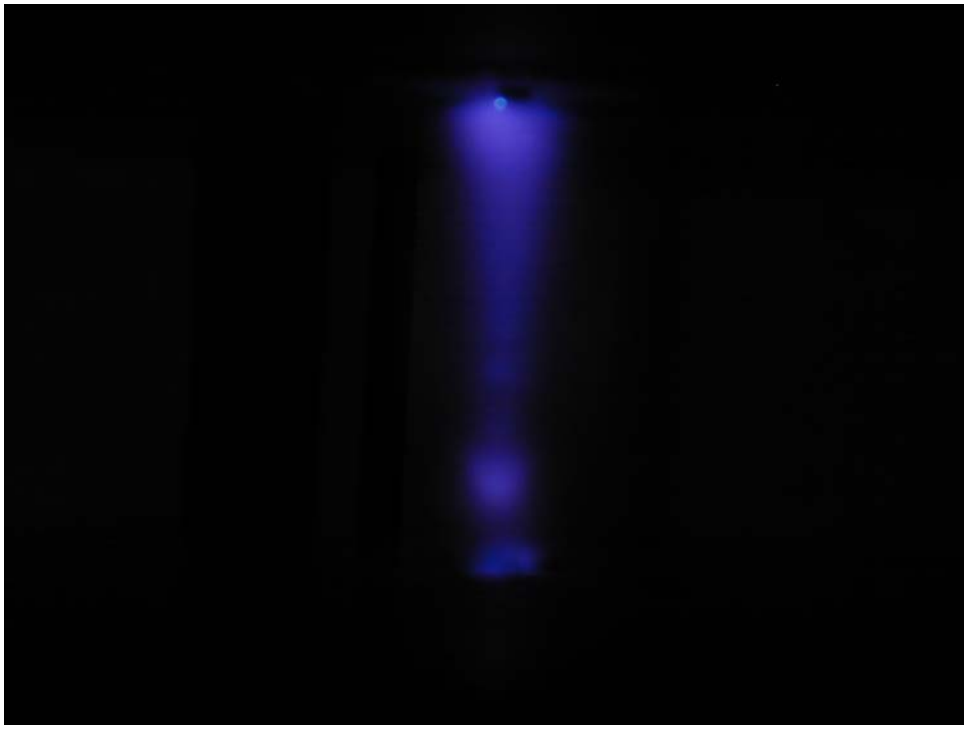

Figure 5.5(h) 8 Torr.

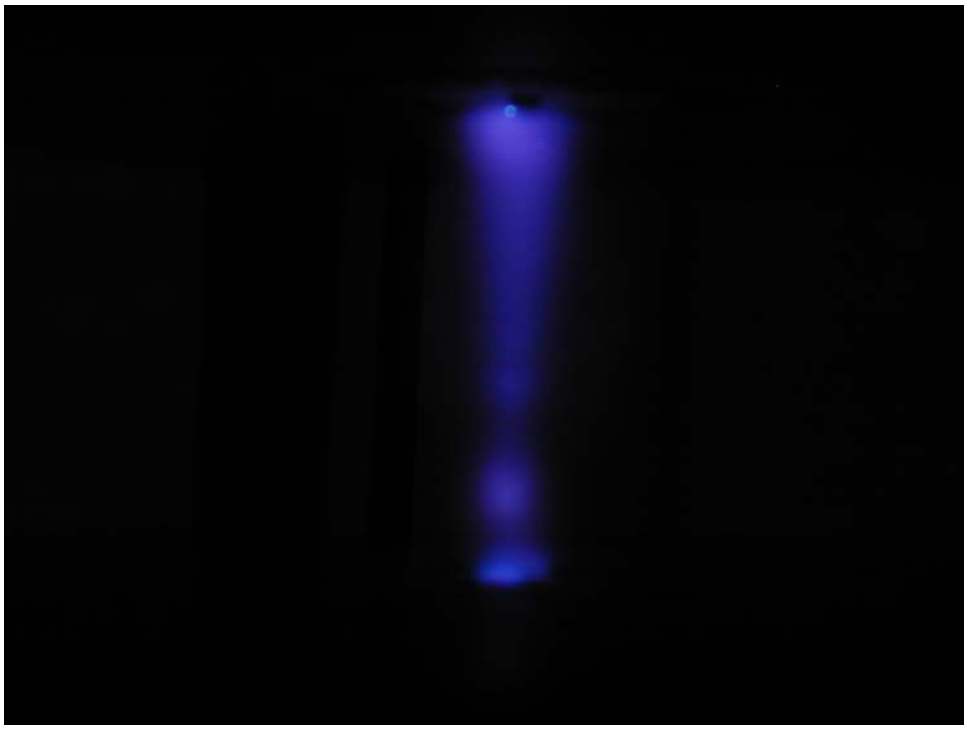

Figure 5.5(i) 9 Torr.

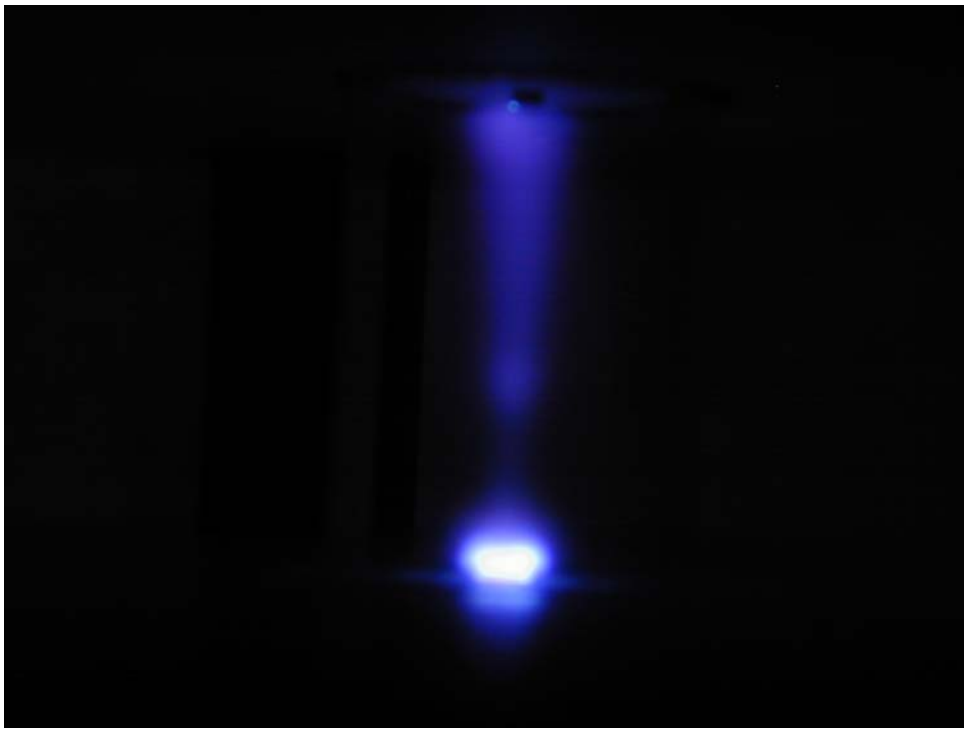

Figure 5.5(j) 10 Torr.

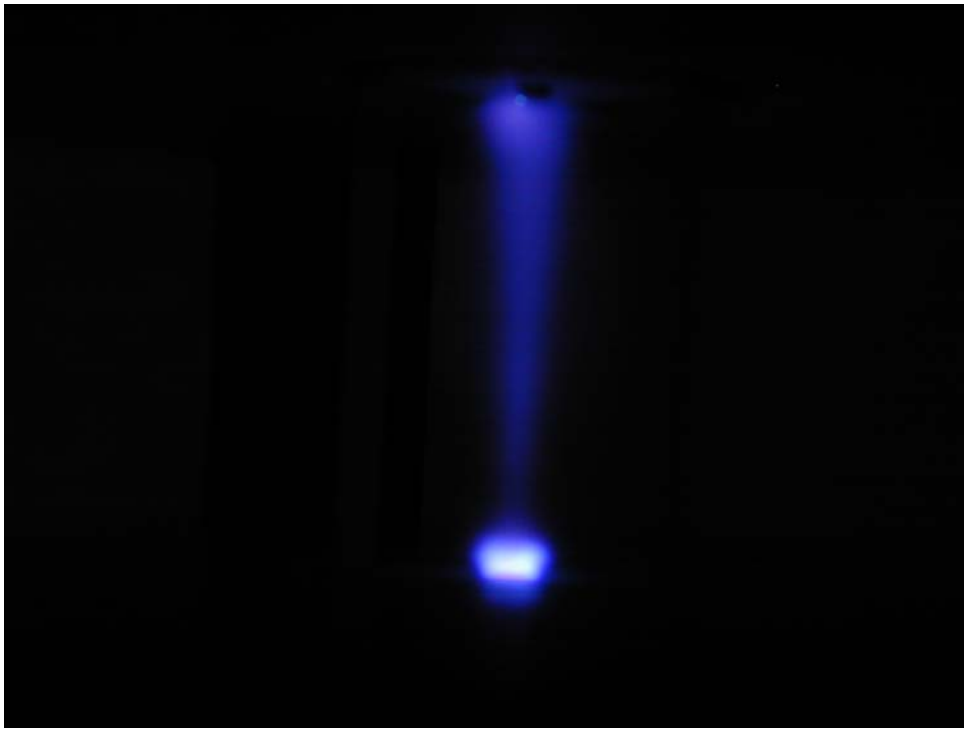

Figure 5.5(k) 15 Torr.

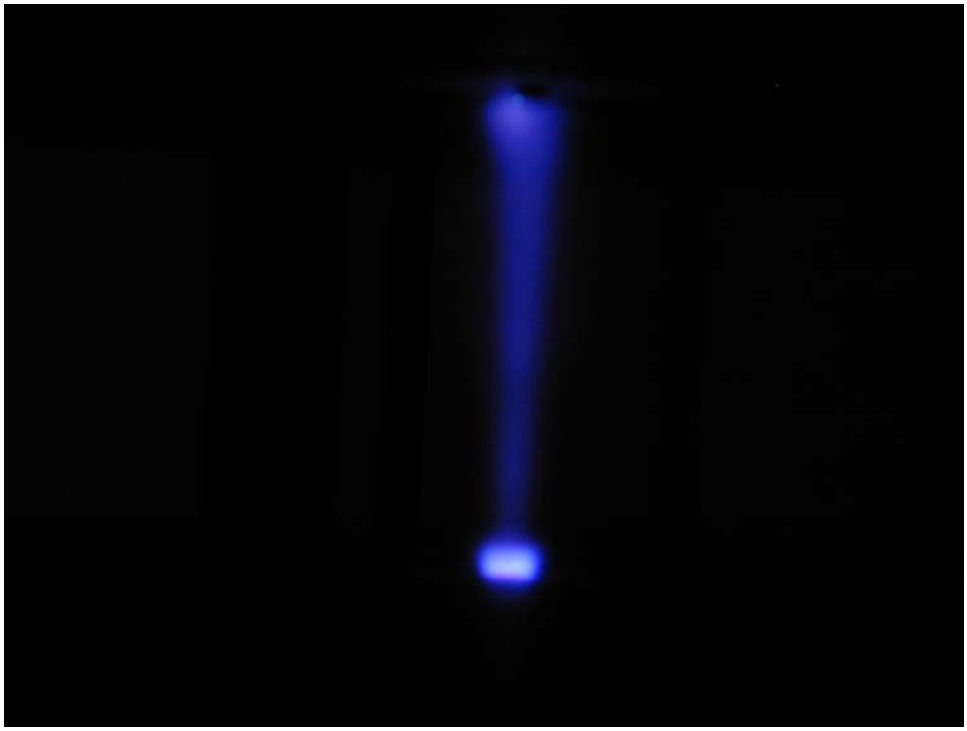

Figure 5.5(l) 20 Torr.

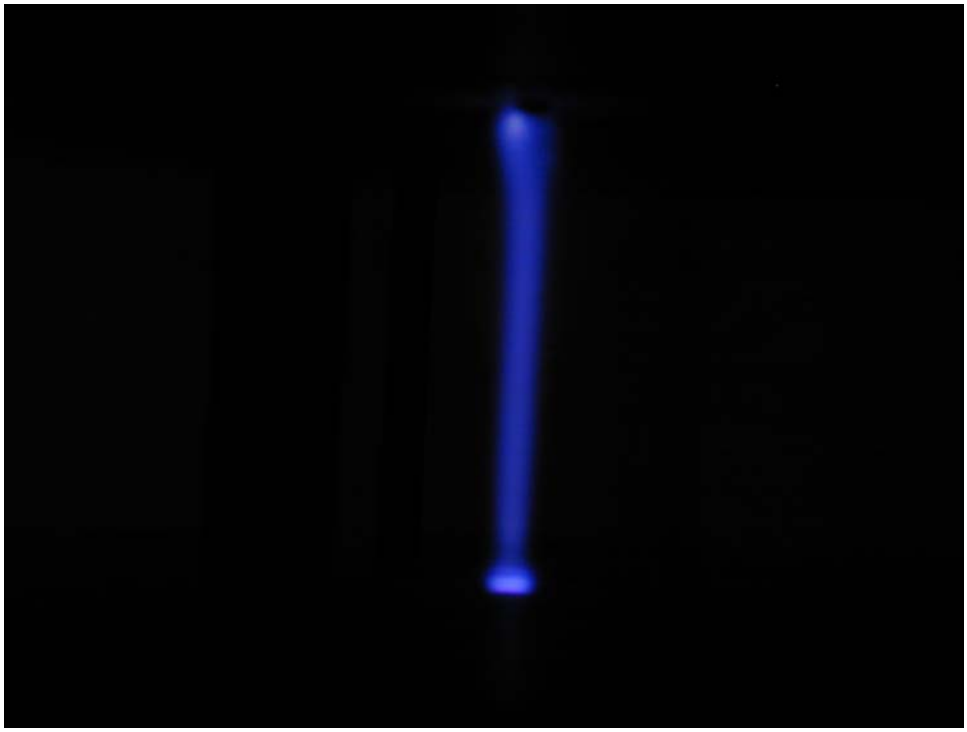

Figure 5.5(m) 50 Torr.

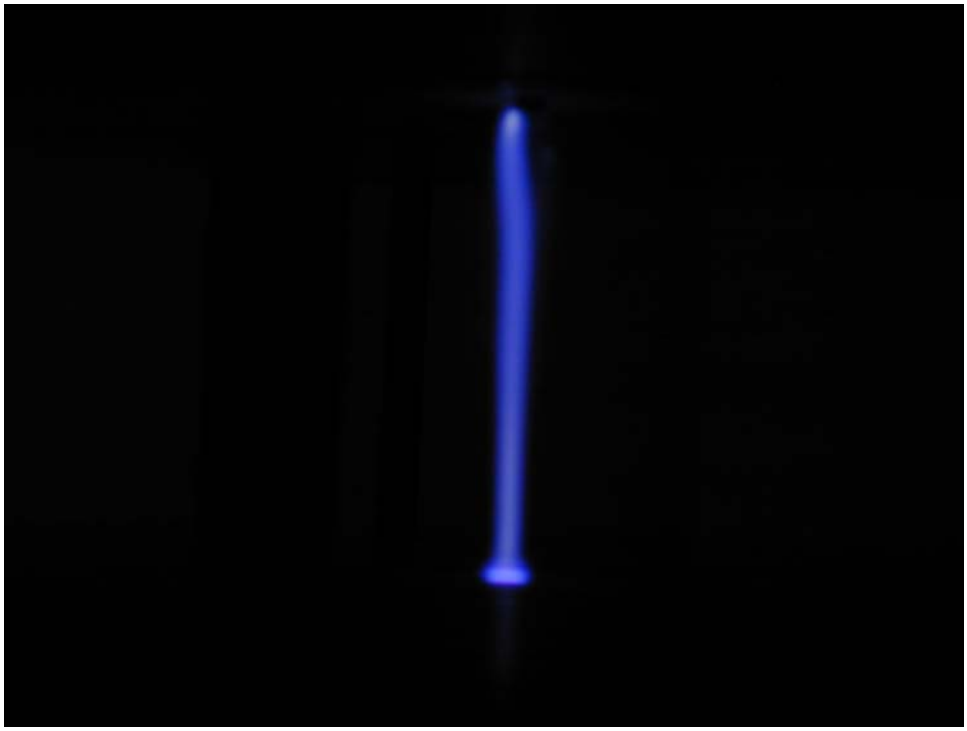

Figure 5.5(n) 110 Torr.

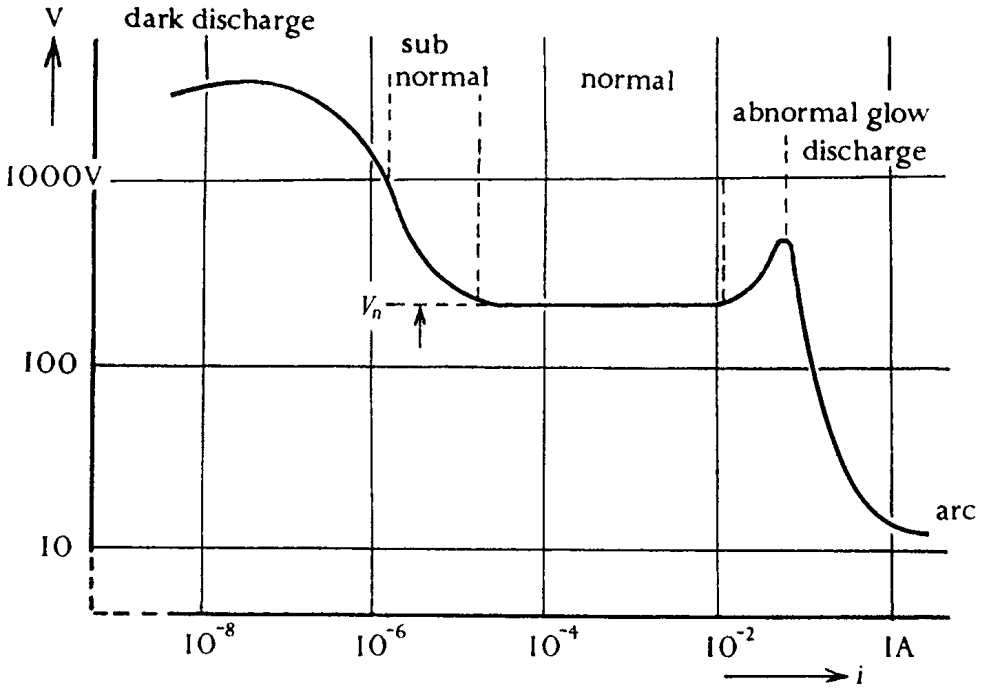

Figure 5.6 Classifications of discharges as defined by voltage-current Characteristics.[3] The three general regions are identified as the dark discharge, the glow discharge, and the arc discharge.

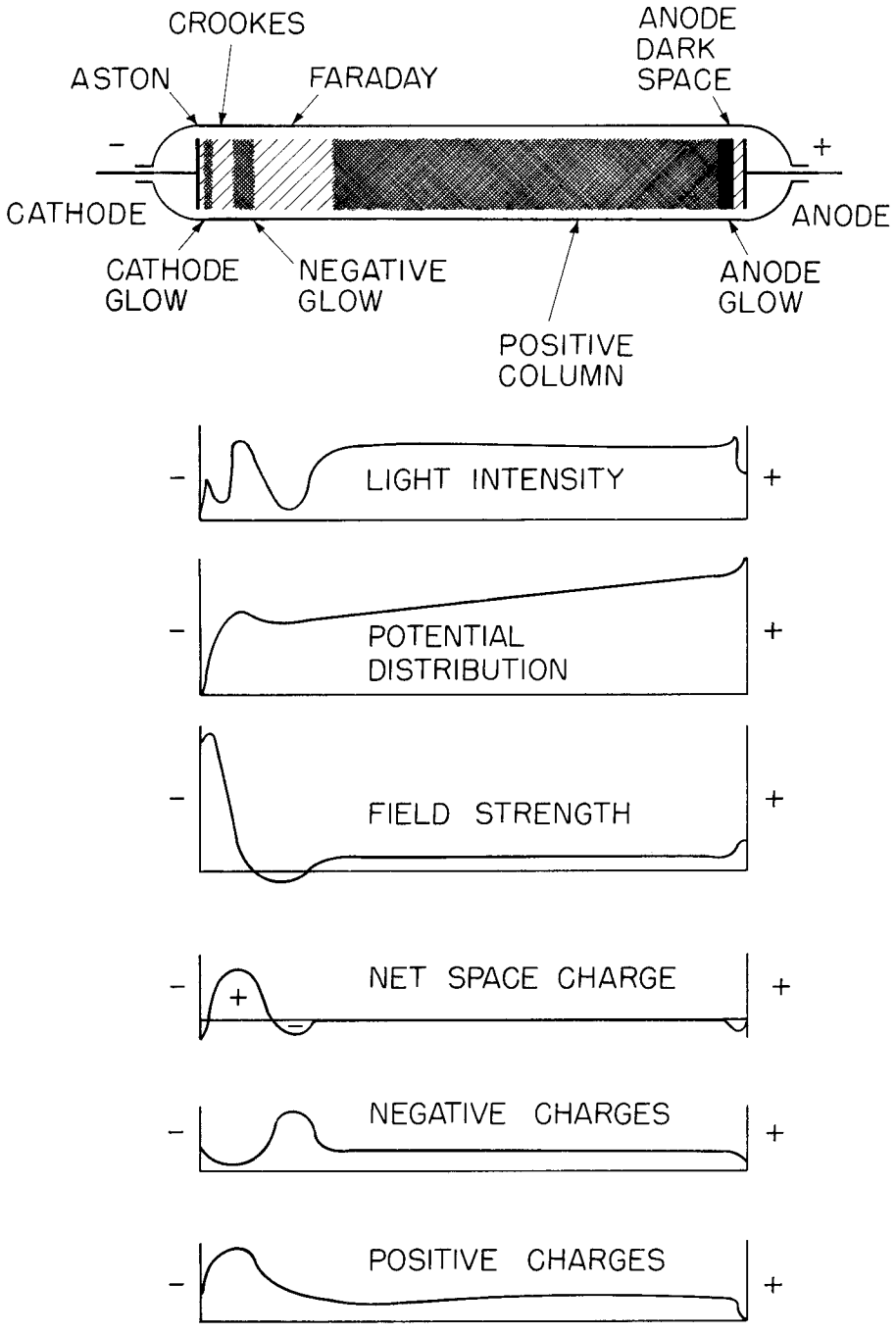

Figure 5.7 Classification of the glow discharge.[4]

5.4 References

1. H. L. Witting, "Acoustic resonances in cylindrical high-pressure arc discharges," Journal of Applied Physics **49** (5), 2680 (1978).

2. J. Zhou, L. Ma, and Z. Qian, "A novel method for testing acoustic resonance of HID lamps," *IEEE APEC '99. Fourteenth Annual Applied Power Electronics Conference and Exposition Conference Proceedings* vol. 1, 1999, p. 480.

3. A. von Engel, *Ionized Gases* (Clarendon Press, Oxford, 1955).

4. S. C. Brown, *Basic Data of Plasma Physics* (MIT Press, Cambridge, 1959).

5. B. Chapman, *Glow Discharge Processes* (John Wiley & Sons, New York, 1980).

6. J. D. Cobine, *Gaseous Conductors: Theory and Engineering Applications* (Dover, New York, 1958).

7. M. A. Lieberman and A. J. Lichtenberg, *Principles of Plasma Discharges and Materials Processing* (John Wiley & Sons, New York, 1994).

8. B. E. Cherrington, *Gaseous Electronics and Gas Lasers* (Pergamon Press, Oxford, 1979).

9. D. N. Ruzic (private communication, 2002).

10. D. L. Dempsey, T. W. Glover, C. M. Kurt, S. J. Koelfgen, G. M. Smayling, and K. A. Smith, "Image of a gaseous discharge in microgravity," IEEE Transactions on Plasma Science **27** (1), 42 (1999).

6. CONCLUSIONS

The goal of this thesis was to investigate basic processes using rare gas mixtures so that optimum starting strategies can be developed for metal halide high intensity discharge lamps. An experimental apparatus was fabricated to simulate an idealized metal halide lamp. This data was taken to provide insight into starting mechanisms as well as to provide a means of validating the code LAMPSIM.

Breakdown measurements on this apparatus were conducted at various pulse repetition frequencies (0.005-1000 Hz), voltage pulses (up to 2000 V), pressures (0.5 – 110 Torr), and argon/xenon compositions, and with various ground planes. It was found that the mean breakdown time is reflective of the rate at which electrons are being created, and is dependent upon E/N and capacitive effects.

Lower breakdown times are achieved by lowering pressure, increasing voltage and pulse repetition frequencies, and by closer placement of ground planes. It was also found that in argon/xenon mixtures, a small percentage (5-10%) of xenon lowers the breakdown times. Lower breakdown times essentially enable lowering the necessary applied voltage and breaking down at higher pressures, leading to reduced sputtering and faster warm restart periods.

Photographs of the discharges were also taken as another means of archiving the behavior of this apparatus. Systematic behaviors from these studies provide insight into the physics of the discharge and pose the challenge for future codes to simulate these fine details.

APPENDIX A: ARGON CROSS SECTIONS

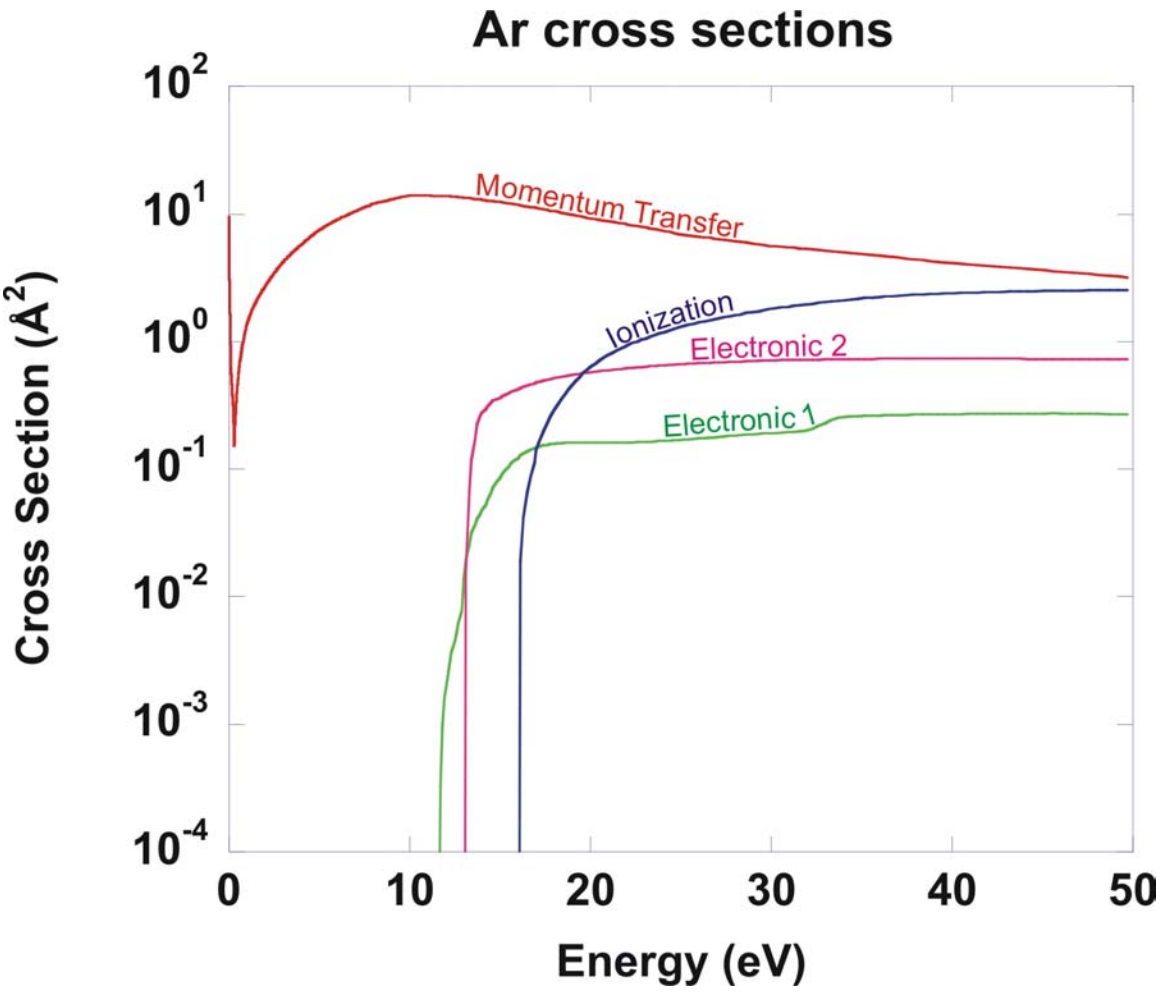

Figure A.1 Argon cross sections for momentum transfer,[1] Ionization,[2] and the two electronic states.[3]

A.1 References

1. M. Hayashi, Nagoya Institute of Technology Report No. IPPJ-AM-19 (1981).

2. D. Rapp and P. Englander-Golden, "Total cross sections for ionization and attachment in gases by electron impact. I. Positive ionization," Journal of Chemical Physics **43** (5), 1464 (1965).

3. K .Tachibana, "Excitation of the $1s_5$,$1s_4$, $1s_3$, and $1s_2$ levels of argon by low-energy electrons," Physical Review A **34** (2), 1007 (1986).

APPENDIX B: XENON CROSS SECTIONS

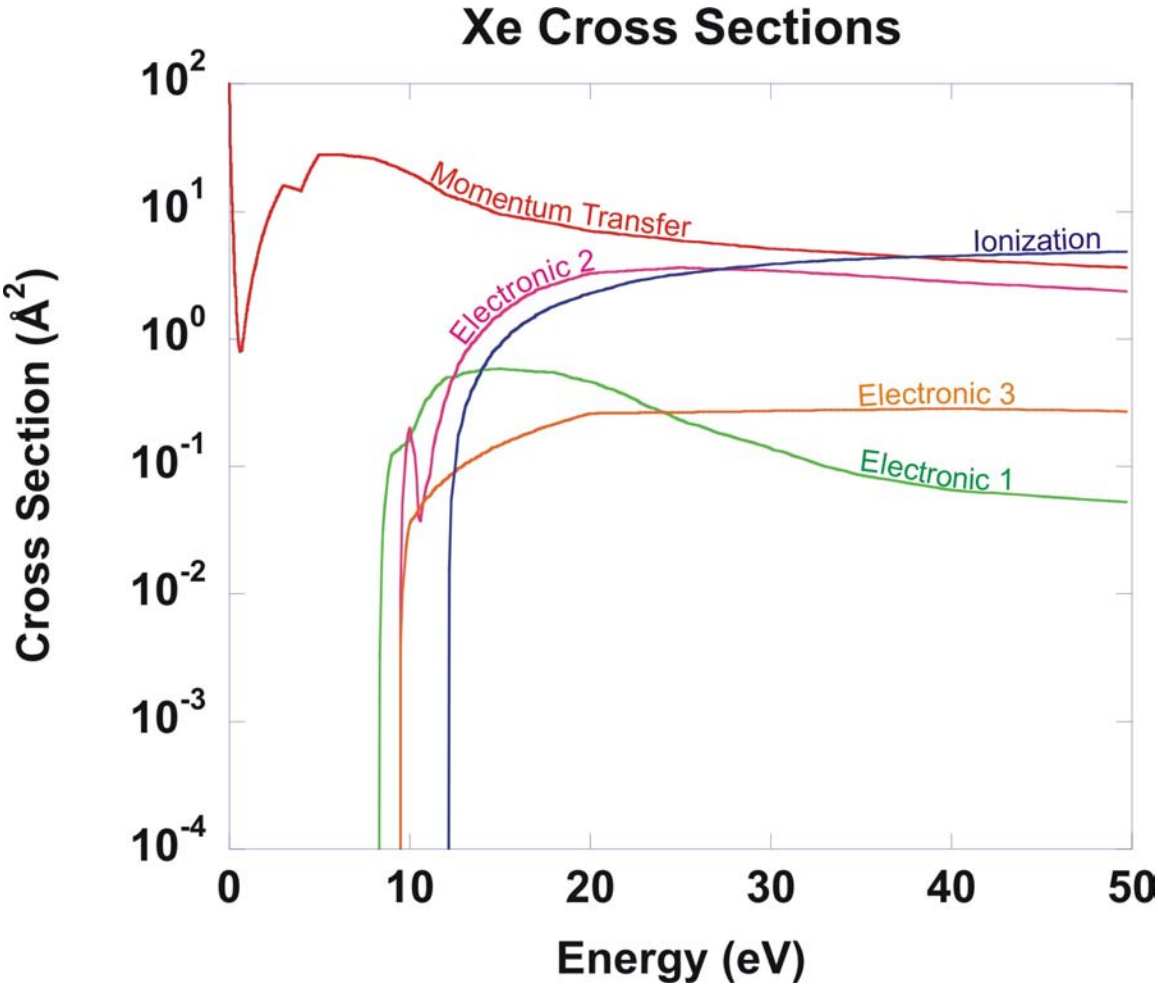

Figure B.1 Xenon cross sections for momentum transfer,[1] ionization,[2] and the three electronic states.[3-5]

B.1 References

1. M. Hayashi, Nagoya Institute of Technology Report No. IPPJ-AM-19 (1981).

2. D. Rapp and P. Englander-Golden, "Total cross sections for ionization and attachment in gases by electron impact. I. Positive ionization," Journal of Chemical Physics **43** (5), 1464 (1965).

3. N. J. Mason and W. R. Newell, "Total cross section for metastable excitation in the rare gases," Journal of Physics B: Atomic and Molecular Physics **20** (6), 1357 (1987).

4. M. Hayashi, "Determination of electron-xenon total excitation cross-sections, from threshold to 100 eV, from experimental values of Townsend's α," Journal of Physics D: Applied Physics **16** (4), 581 (1983).

5. T. Y. Suzuki, Y. Sakai, B. S. Min, T. Takayanagi, K. Wakiya, and H. Suziki, "Measurement of cross sections and oscillator strengths for Xe by electron impact," Physical Review A **43** (11), 5867 (1991).

APPENDIX C: KINETICS OF ARGON/XENON MIXTURES

C.1 Argon Reaction Mechanisms

Electron Impact Reactions

Reaction	Rate Coefficient[a]	Ref.
$e + Ar \rightarrow Ar^* + e$	$1.0 \times 10^{-11} T_e^{0.75} \exp(-11.6/T_e)$	8
$e + Ar \rightarrow Ar^{**} + e$	$5.0 \times 10^{-12} T_e^{0.5} \exp(-13.3/T_e)$	8
$e + Ar \rightarrow Ar^+ + e + e$	$4.0 \times 10^{-12} T_e^{0.5} \exp(-15.8/T_e)$	8
$e + Ar^* \rightarrow Ar^+ + e + e$	$1.0 \times 10^{-10} T_e^{3} \exp(-4.16/T_e)$	8
$e + Ar^{**} \rightarrow Ar^+ + e + e$	$1.41 \times 10^{-7} T_e^{0.61} \exp(-4.0/T_e)$	9
$e + Ar_2^* \rightarrow Ar_2^+ + e + e$	$6.78 \times 10^{-8} T_e^{0.7} \exp(-5.25/T_e)$	9
$e + Ar^* \rightarrow Ar^{**} + e$	$2.0 \times 10^{-7} T_e \exp(-13.3/T_e)$	8
$e + Ar^* \rightarrow Ar + e$	$1.0 \times 10^{-11} T_e^{0.75}$	7
$e + Ar^{**} \rightarrow Ar + e$	$5.0 \times 10^{-12} T_e^{0.5}$	7
$e + Ar^{**} \rightarrow Ar^* + e$	$2.0 \times 10^{-7} T_e$	7
$e + Ar_2^+ \rightarrow Ar^* + Ar$	$6.00 \times 10^{-7} T_e^{-0.67}$	8
$e + Ar_2^+ \rightarrow Ar^{**} + Ar$	$8.00 \times 10^{-8} T_e^{0.5}$	7
$e + Ar_2^* \rightarrow Ar + Ar + e$	1.00×10^{-9}	7
$e + Ar^+ \rightarrow Ar^*$	$4.00 \times 10^{-13} T_e^{-0.5}$	b
$e + e + Ar^+ \rightarrow Ar^* + e$	$5.00 \times 10^{-27} T_e^{-4.5}\ cm^6 s^{-1}$	b
$e + Ar^+ + Ar \rightarrow Ar^* + Ar$	$1.0 \times 10^{-26}\ cm^6 s^{-1}$	10

Heavy particle interactions

$Ar^+ + Ar \rightarrow Ar + Ar^+$	4.60×10^{-10}	b
$Ar^* + Ar + Ar \rightarrow Ar_2^* + Ar$	1.14×10^{-32} cm^6s^{-1}	7
$Ar^{**} + Ar \rightarrow Ar^* + Ar$	1.0×10^{-10}	7
$Ar^+ + Ar + Ar \rightarrow Ar_2^+ + Ar$	2.50×10^{-31} cm^6s^{-1}	7
$Ar_2^* \rightarrow Ar + Ar$	6.00×10^7 s^{-1}	7
$Ar^* \rightarrow Ar$	1.00×10^1 s^{-1}	b
$Ar^* + Ar^* \rightarrow Ar^+ + Ar + e$	5.0×10^{-10}	7
$Ar_2^* + Ar_2^* \rightarrow Ar_2^+ + Ar + Ar + e$	5.00×10^{-10}	7

Absorption[c]

$Ar^{**} + \phi \rightarrow Ar^+ + e$	3.5×10^{-18}	7
$Ar_2^* + \phi \rightarrow Ar_2^+ + e$	1.4×10^{-17}	7
$Ar_2^+ + \phi \rightarrow Ar^+ + Ar$	3.5×10^{-17}	7

[a]Rate coefficients have unit of cm^3s^{-1} unless noted otherwise.

[b]Estimated.

[c]Rate coefficients have units of cm^2.

C.2 Xenon Reaction Mechanisms

Electron Impact Reactions

Reaction	Rate Coefficient[a]	Ref.
$e + Xe \rightarrow Xe^* + e$	$1.2 \times 10^{-8} T_e^{0.72} \exp(-8.36/T_e)$	7
$e + Xe \rightarrow Xe^{**} + e$	$2.8 \times 10^{-8} T_e^{0.725} \exp(-9.73/T_e)$	7
$e + Xe^* \rightarrow Xe^{**} + e$	$2.71 \times 10^{-6} T_e^{0.71} \exp(-0.63/T_e)$	8
$e + Xe \rightarrow Xe^+ + e + e$	$3.47 \times 10^{-8} T_e^{0.72} \exp(-12.13/T_e)$	7
$e + Xe^* \rightarrow Xe^+ + e + e$	$7.85 \times 10^{-8} T_e^{0.71} \exp(-3.77/T_e)$	7
$e + Xe^{**} \rightarrow Xe^+ + e + e$	$2.15 \times 10^{-7} T_e^{0.71} \exp(-2.40/T_e)$	7
$e + Xe_2^* \rightarrow Xe_2^+ + e + e$	$9.75 \times 10^{-8} T_e^{0.705} \exp(-3.40/T_e)$	7
$e + Xe^* \rightarrow Xe + e$	$1.2 \times 10^{-8} T_e^{0.72} \exp(-8.36/T_e)$	7
$e + Xe^{**} \rightarrow Xe^* + e$	$2.71 \times 10^{-6} T_e^{0.71}$	8
$e + Xe^{**} \rightarrow Xe + e$	$2.8 \times 10^{-8} T_e^{0.725} \exp(-9.73/T_e)$	7
$e + Xe_2^+ \rightarrow Xe^* + Xe$	$0.37 \times 10^{-7} T_e^{-0.5}$	b
$e + Xe_2^+ \rightarrow Xe^{**} + Xe$	$2.0 \times 10^{-7} T_e^{-0.5}$	7
$e + Xe \rightarrow Xe^{***} + e$	d	13
$e + Xe^* \rightarrow Xe^{***} + e$	$0.02 \times 10^{\left(-4.88/T_e^{0.36} - 1.81/T_e^{0.51}\right)}$	7
$e + Xe^{**} \rightarrow Xe^{***} + e$	$10^{\left(-4.88/T_e^{0.36} - 1.81/T_e^{0.51}\right)}$	7
$e + Xe^{***} \rightarrow Xe^+ + e + e$	$2.15 \times 10 e^{-7} T_e^{0.71} \exp(-2.4/T_e)$	7
$e + Xe^{***} \rightarrow Xe^{**} + e$	$5.50 \times 10^{-7} T_e^{0.79} \exp(-2.00/T_e)$	b
$e + Xe^{***} \rightarrow Xe^* + e$	$10^{\left(-4.88/T_e^{0.36} - 1.81/T_e^{0.51}\right)}$	7

$e + Xe^{***} \rightarrow Xe + e$	d	13
$e + Xe_2^+ \rightarrow Xe^{***} + Xe$	$3.33 \times 10^{-7} T_e^{-0.5}$	b

Heavy particle interactions

$Xe^+ + Xe \rightarrow Xe + Xe^+$	3.60×10^{-10}	b
$Xe^* + Xe + Xe \rightarrow Xe_2^* + Xe$	$5.00 \times 10^{-32}\ cm^6 s^{-1}$	7
$Xe^{**} + Xe + Xe \rightarrow Xe_2^* + Xe$	$5.00 \times 10^{-32}\ cm^6 s^{-1}$	b
$Xe_2^* \rightarrow Xe + Xe$	$6.00 \times 10^7\ s^{-1}$	7
$Xe^* \rightarrow Xe$	$3.96 \times 10^6\ s^{-1}$	b
$Xe^{**} \rightarrow Xe^*$	$0.50 \times 10^7\ s^{-1}$	b
$Xe^{**} \rightarrow Xe$	$1.50 \times 10^7\ s^{-1}$	7
$Xe^* + Xe^* \rightarrow Xe^+ + Xe + e$	5.00×10^{-10}	7
$Xe_2^* + Xe_2^* \rightarrow Xe_2^+ + Xe + Xe + e$	3.5×10^{-10}	11
$Xe_2^* + Xe \rightarrow Xe + Xe + Xe$	2.7×10^{-13}	11
$Xe^{**} + Xe^{**} \rightarrow Xe^+ + Xe + e$	5.00×10^{-10}	b
$Xe^{***} + Xe \rightarrow Xe_2^+ + e$	2.00×10^{-10}	7
$Xe^+ + Xe + Xe \rightarrow Xe_2^+ + Xe$	$2.50 \times 10^{-31}\ cm^6 s^{-1}$	7
$Xe^{***} + Xe + Xe \rightarrow Xe_2^* + Xe$	$5.00 \times 10^{-32}\ cm^6 s^{-1}$	b
$Xe^{***} \rightarrow Xe$	$5.49 \times 10^6\ s^{-1}$	b
$Xe^{***} \rightarrow Xe^{**}$	$1.50 \times 10^7\ s^{-1}$	7
$Xe^{**} \rightarrow Xe^{***}$	$0.50 \times 10^7\ s^{-1}$	b
$Xe^{***} + Xe^{***} \rightarrow Xe^+ + Xe + e$	5.0×10^{-10}	b

	Absorption[c]	
$Xe^{***} + \phi \rightarrow Xe^{+} + e$	1.8×10^{-18}	7
$Xe^{**} + \phi \rightarrow Xe^{+} + e$	5.0×10^{-18}	7
$Xe^{*} + \phi \rightarrow Xe^{+} + e$	6.0×10^{-20}	7
$Xe_2^{+} + \phi \rightarrow Xe^{+} + Xe$	2.5×10^{-17}	7
$Xe_2^{*} + \phi \rightarrow Xe_2^{+} + e$	1.4×10^{-17}	7

[a]Rate coefficients have unit of cm^3s^{-1} unless noted otherwise.

[b]Estimated.

[c]Rate coefficients have units of cm^2.

[d]Rate coefficients can be calculated from the cross section given in reference.

C.3 Additional Reactions for Argon/Xenon Mixtures

Electron Impact Reactions

Reaction	Rate Coefficient[a]	Ref.
$e + ArXe^+ \rightarrow Xe^{**} + Ar$	$1.00 \times 10^{-7} T_e^{0.5}$	12
$e + ArXe^* \rightarrow Xe + Ar + e$	1.00×10^{-9}	7
$e + ArXe^* \rightarrow ArXe^+ + e + e$	$4.00 \times 10^{-10} T_e^3$	7

Heavy particle interactions

$Ar^* + Xe \rightarrow Ar + Xe^*$	2.10×10^{-10}	12
$Ar^* + Xe \rightarrow Ar + Xe^{**}$	2.10×10^{-10}	7
$Ar^{**} + Xe \rightarrow Ar + Xe^+ + e$	2.00×10^{-10}	7
$Ar^+ + Xe \rightarrow Ar + Xe^+$	4.30×10^{-13}	7
$Xe^* + Xe + Ar \rightarrow Xe_2^* + Ar$	$2.30 \times 10^{-32}\ cm^6 s^{-1}$	7
$Xe^{**} + Xe + Ar \rightarrow Xe_2^* + Ar$	$2.30 \times 10^{-32}\ cm^6 s^{-1}$	b
$Xe^{**} + Ar \rightarrow Xe^* + Ar$	1.10×10^{-11}	7
$Xe^+ + Xe + Ar \rightarrow Xe_2^+ + Ar$	$2.00 \times 10^{-31}\ cm^6 s^{-1}$	7
$Ar^* + Ar + Xe \rightarrow Ar_2^* + Xe$	$1.10 \times 10^{-32}\ cm^6 s^{-1}$	b
$Ar^+ + Ar + Xe \rightarrow Ar_2^+ + Xe$	$2.00 \times 10^{-31} cm^6 s^{-1}$	b
$Ar^* + Xe + Xe \rightarrow Xe_2^* + Ar$	$1.00 \times 10^{-33}\ cm^6 s^{-1}$	b
$Ar_2^+ + Xe \rightarrow Xe^+ + Ar + Ar$	1.0×10^{-9}	9
$Ar^* + Xe \rightarrow ArXe^*$	5.00×10^{-11}	7
$Ar_2^* + Xe \rightarrow Xe^* + Ar + Ar$	2.4×10^{-10}	7

$Ar_2^* + Xe \rightarrow ArXe^* + Ar$	5.00×10^{-11}	7
$Ar^+ + Xe + Ar \rightarrow ArXe^+ + Ar$	$1.00 \times 10^{-31}\ cm^6s^{-1}$	7
$Ar_2^+ + Xe + Ar \rightarrow Xe^+ + Ar + Ar + Ar$	$1.00 \times 10^{-29}\ cm^6s^{-1}$	7
$Ar^+ + Xe + Xe \rightarrow ArXe^+ + Xe$	$1.00 \times 10^{-31}\ cm^6s^{-1}$	b
$ArXe^+ + Xe \rightarrow Xe^+ + Ar + Xe$	5.00×10^{-10}	7
$ArXe^+ + Xe \rightarrow Xe_2^+ + Ar$	1.00×10^{-11}	7
$ArXe^* + Xe \rightarrow Xe_2^* + Ar$	1.00×10^{-10}	7
$ArXe^* \rightarrow Ar + Xe$	$5.00 \times 10^7 s^{-1}$	7
$Xe^+ + Ar + Ar \rightarrow ArXe^+ + Ar$	$1.00 \times 10^{-31}\ cm^6s^{-1}$	7
$Xe^* + Ar + Ar \rightarrow ArXe^* + Ar$	$1.00 \times 10^{-33}\ cm^6s^{-1}$	7
$Xe^{***} + Xe + Ar \rightarrow Xe_2^* + Ar$	$2.30 \times 10^{-32}\ cm^6s^{-1}$	b
$Xe^{***} + Ar \rightarrow Xe^{**} + Ar$	1.0×10^{-11}	7

Absorption[c]

$ArXe^* + \phi \rightarrow ArXe^+ + e$	1.5×10^{-17}	7
$ArXe^+ + \phi \rightarrow Xe^+ + Ar$	1.5×10^{-17}	7

[a]Rate coefficients have unit of cm^3s^{-1} unless noted otherwise.

[b]Estimated.

[c]Rate coefficients have units of cm^2.

C.4 Figures

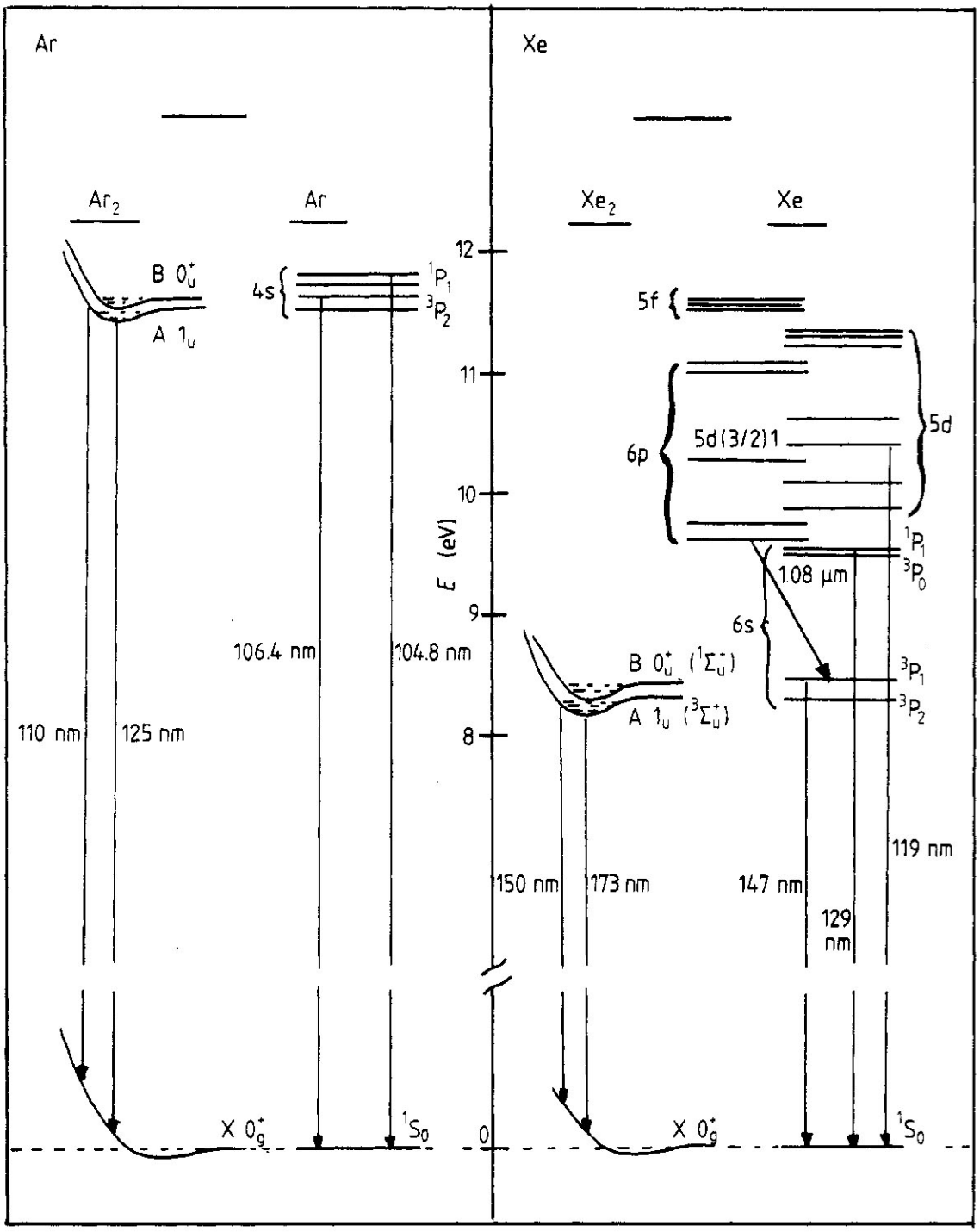

Figure C.1 Schematic energy-level diagram of atomic and molecular states of argon and xenon. The main radiative transitions are also indicated. Diagram from Brunet et al.[6]

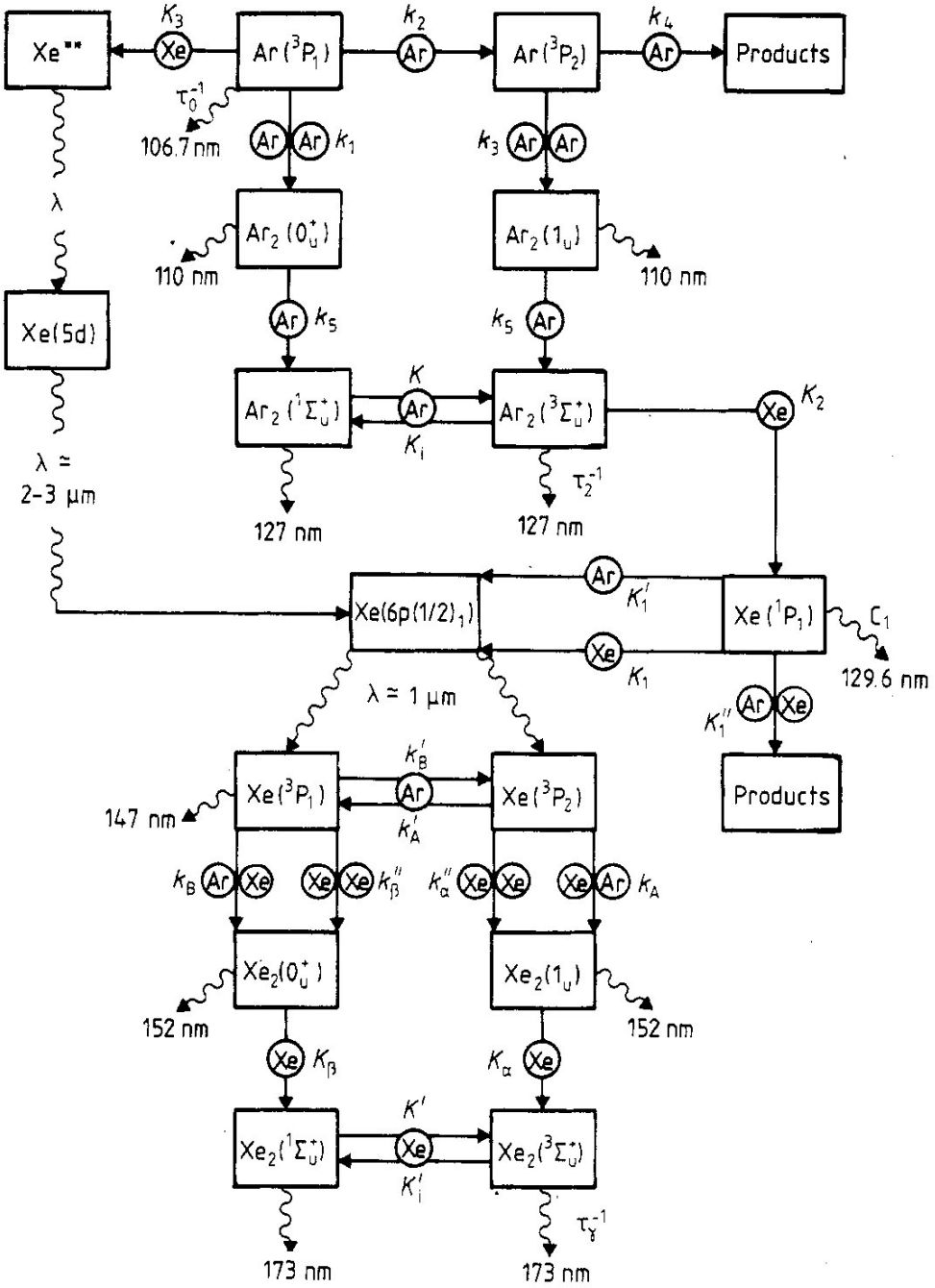

Figure C.2 Kinetic scheme of the energy transfers in Ar/Xe mixtures. The resonant and metastable states of xenon are formed by two competitive paths, from the molecular state $Ar_2(^3\Sigma_u^+)$ via the $Xe(^1P_1)$ state or from the $Ar(^3P_1)$ level via radiative transitions from the highly excited Xe** levels. In Ar/Xe mixtures, the radiative molecular states of Xe_2* are formed by two-body heteronuclear collisions. Diagram from Brunet et al.[6]

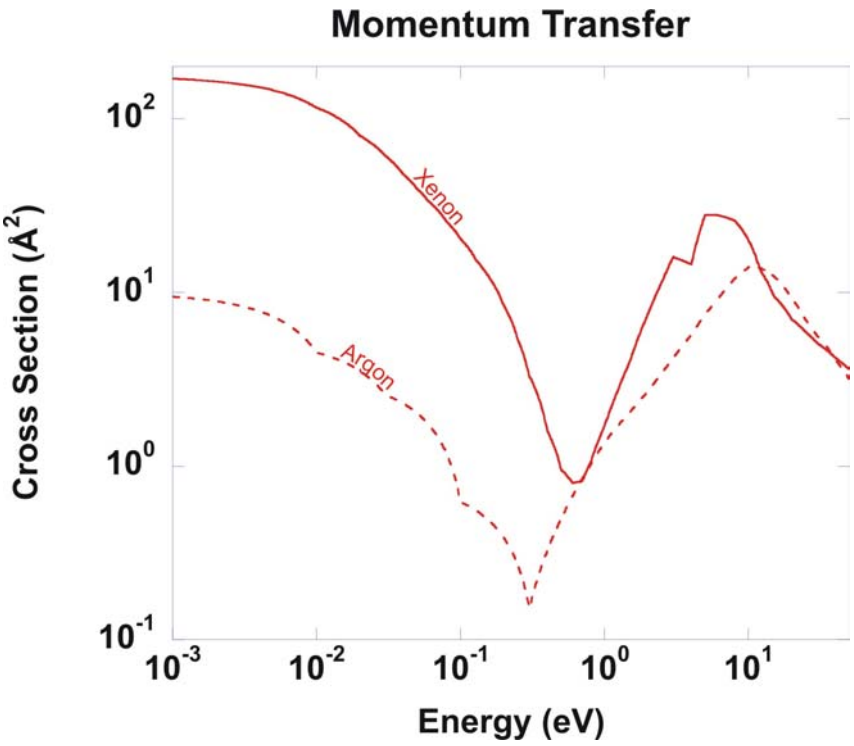

Figure C.3 Comparison of momentum transfer cross sections for argon and xenon.[1]

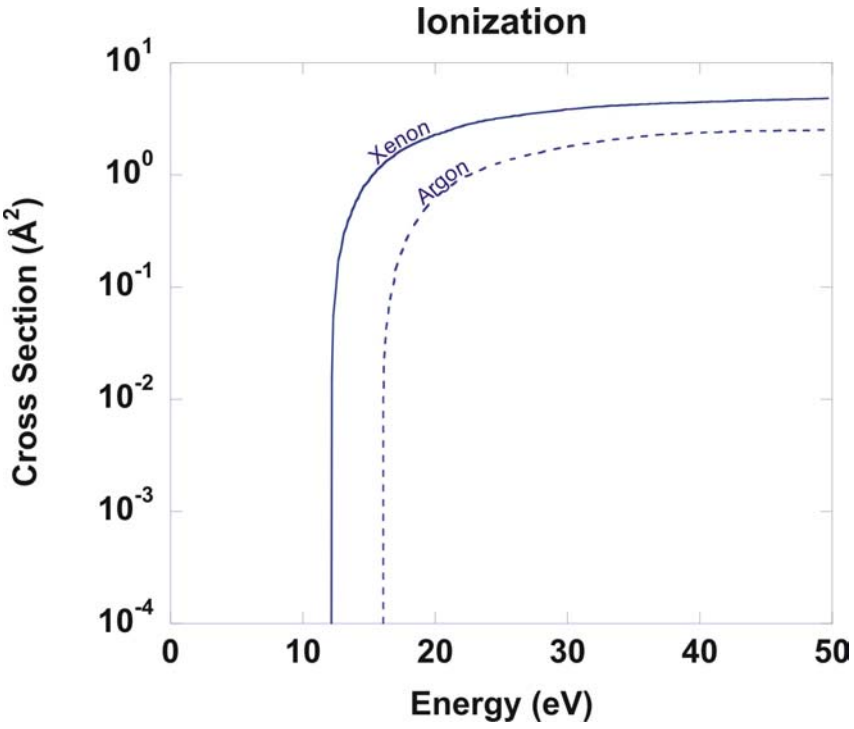

Figure C.4 Comparison of ionization cross sections for argon and xenon.[2]

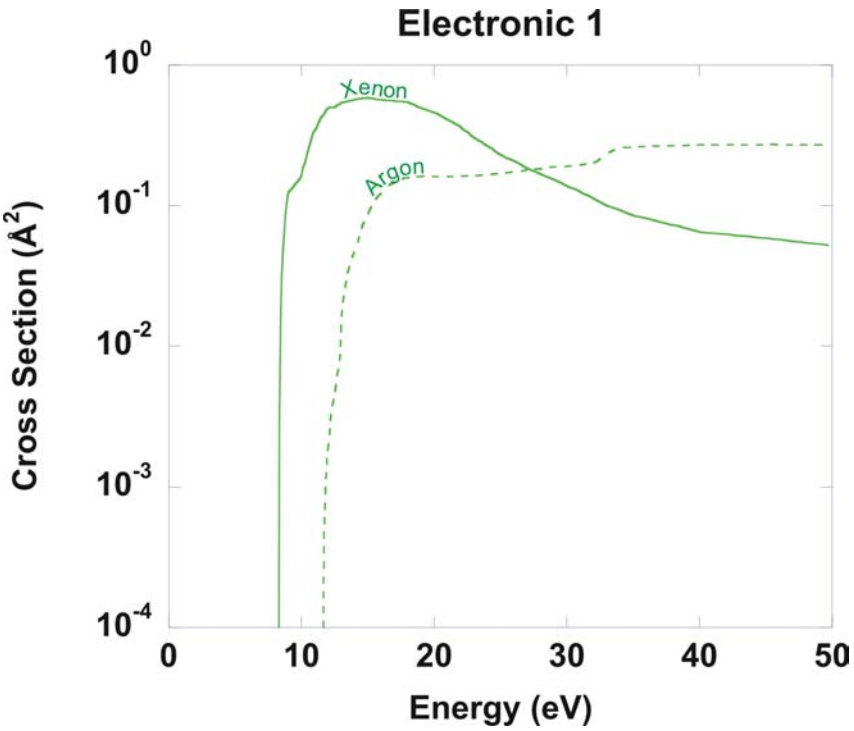

Figure C.5 Comparison of electronic 1 cross sections for argon[3] and xenon.[4]

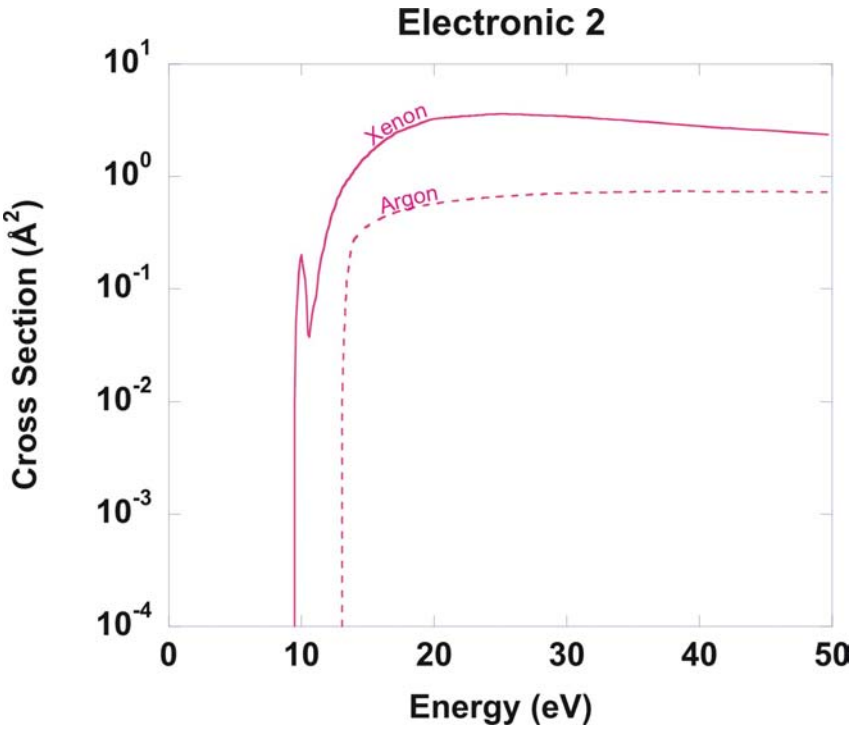

Figure C.6 Comparison of electronic 2 cross sections for argon[3] and xenon.[5]

C.5 References

1. M. Hayashi, Nagoya Institute of Technology Report No. IPPJ-AM-19 (1981).

2. D. Rapp and P. Englander-Golden, "Total cross sections for ionization and attachment in gases by electron impact. I. Positive ionization," Journal of Chemical Physics **43** (5), 1464 (1965).

3. K .Tachibana, "Excitation of the $1s_5$,$1s_4$, $1s_3$, and $1s_2$ levels of argon by low-energy electrons," Physical Review A **34** (2), 1007 (1986).

4. N. J. Mason and W. R. Newell, "Total cross section for metastable excitation in the rare gases," Journal of Physics B: Atomic and Molecular Physics **20** (6), 1357 (1987).

5. M. Hayashi, "Determination of electron-xenon total excitation cross-sections, from threshold to 100 eV, from experimental values of Townsend's α," Journal of Physics D: Applied Physics **16** (4), 581 (1983).

6. H. Brunet, A. Birot, H. Dijols, J. Galy, P. Millet, and Y. Salamero, "Spectroscopic and kinetic analysis of the VUV emissions of argon and argon-xenon mixtures: II. Energy transfer in Ar-Xe mixtures," Journal of Physics B : Atomics and Molecular Physics **15** (17), 2945 (1982).

7. T. H. Johnson, H. E. Cartland, T. C. Genoni, and A. M. Hunter, "A comprehensive kinetic model of the electron-beam-excited xenon chloride laser," Journal of Applied Physics **66** (12), 5707 (1989).

8. J. W. Shon, "Modeling of high pressure rare gas lasers: Kinetics and plasma chemistry," Master's thesis, University of Illinois at Urbana-Champaign, 1994.

9. N. Nishida, T. Takashima, F. K. Tittel, F. Kannari, and M. Obara, "Theoretical evaluation of a short-pulse electron-beam-excited XeF ($B \rightarrow X$) laser using a low-pressure, room-temperature $Ar/Xe/F_2$ gas mixture," Journal of Applied Physics **67** (9), 3932 (1990).

10. B. K. Min, H. Y. Choi, S. H. Lee, and H. S. Tae, "New combination of four-component gas He-Ne-Xe-Ar high efficiency plasma display panel," Journal of Vacuum Science and Technology **19** (1), 7 (2001).

11. G. Bekefi, *Principles of Laser Plasmas* (Wiley-Interscience, New York, 1976).

12. F. Kannari, A. Suda, M. Obara, and T. Fujioka, "Theoretical simulation of electron-beam-excited xenon-chloride (XeCl) lasers," IEEE Journal of Quantum Electronics **QE-19** (10), 1587 (1983).

13. T. Y. Suzuki, Y. Sakai, B. S. Min, T. Takayanagi, K. Wakiya, and H. Suziki, "Measurement of cross sections and oscillator strengths for Xe by electron impact," Physical Review A **43** (11), 5867 (1991).